Title

TPX2 Regulation of Spindle Architecture

Author

Pena, Guadalupe Elizabeth

Publication Date

2024

Peer reviewed|Thesis/dissertation

TPX2 Regulation of Spindle Architecture

by

Guadalupe Elizabeth Pena

A dissertation submitted in partial satisfaction of the

requirements for the degree of

Doctor of Philosophy

in

Molecular and Cell Biology

in the

Graduate Division

of the

University of California, Berkeley

Committee in charge:

Professor Rebecca Heald, Chair

Professor Matthew Welch

Professor Eva Nogales

Professor Daniel Fletcher

Summer 2024

TPX2 Regulation of Spindle Architecture

Abstract

TPX2 Regulation of Spindle Architecture

by

Guadalupe Elizabeth Pena

Doctor of Philosophy in Molecular and Cell Biology

University of California, Berkeley

Professor Rebecca Heald, Chair

A bipolar spindle functions to segregate chromosomes during cell division in all eukaryotes, yet spindle size and microtubule organization vary dramatically across different species and cell types. Targeting protein for Xklp2 (TPX2) is one candidate factor for modulating spindle architecture through its roles in branching microtubule nucleation, activation of the mitotic kinase Aurora A, and association with the kinesin-5 (Eg5) motor.

Xenopus egg extracts provide an ideal system to study the role of TPX2 in defining spindle architecture since in vitro reactions combining metaphase-arrested extracts and sperm nuclei recapitulate meiotic spindle assembly and can be biochemically manipulated. Here, we characterize a conserved nuclear localization sequence (NLS) motif, 123-KKLK-126, in *X. laevis* TPX2, which regulates astral microtubule formation and spindle pole morphology in *Xenopus* egg extracts. Addition of recombinant TPX2 with this sequence mutated to AALA dramatically increased spontaneous formation of microtubule asters and recruitment of phosphorylated Aurora A, Eg5 and pericentrin to meiotic spindle poles.

TPX2 is frequently overexpressed in aggressive human cancers, and it is not well understood how overexpression of TPX2 affects spindle assembly and function. We analyzed the spindle morphology of human cell lines and showed that cells over-expressing the oncogene MYC and TPX2 possess shorter spindles with increased TPX2 localization at spindle poles. These results indicate that TPX2 alters spindle length and morphology in cancer cells, which may contribute their ability to divide despite MYC-induced mitotic stress and are consistent with previous observations in *Xenopus* egg extract showing that high levels of TPX2 shrink meiotic spindles.

We propose that TPX2 is a lynchpin spindle assembly factor that contributes to the recruitment and activity of microtubule nucleation factors, regulating spindle size and generating distinct spindle architectures.

Acknowledgments

There are so many people I would love to thank and acknowledge. First and foremost, I would like to thank Rebecca Heald for being such an incredible mentor and for her unwavering support throughout this project. Thank you for always being my loudest cheerleader and scientific guide over these last seven years. Other advisors I would like to thank are my committee members Matt Welch, Eva Nogales, and Dan Fletcher. Thank you for your invaluable discussions and continual support from my qualification exam to my final thesis meeting.

I would like to thank Xiao Zhou for being my first friend/mentor in the lab and for sharing his knowledge and project with me. I also have immense gratitude for Kelly Miller who was and still is one my dearest friends. Thank you for your support, science wisdom, and friendship. I will dearly miss our regular lunch outings and conversations about our kids and family. Thank you also to Coral Zhou, for mentoring me in the ways of proper and rigorous biochemistry. Your friendship and support throughout these last several years has had a profound impact on my success and completion of this project. To Chris Brownlee, Romain Gibeaux, Mina Sun, Ambika Nadkarni, Clotilde Cadart, Helena Cantwell, Xiao Liu, Gabe Cavin-Mesa, Maiko Kitaoka, Elizabeth Early, and Khansaa Maar, thank you for your kindness, friendship, and your scientific advice. To Lupe Coy, thank you for being such a wonderful friend, for sharing invaluable life advice and for keeping our lab running smoothly. To other fellow postdocs, graduate students, undergraduates, and lab managers I have overlapped with, Cordell Clarke, Megan Onyendo, Tracy Luo, Hilda Cabrera, Jon Sulit, Christine Wan, Gillian Oaks, Anu Mukherjee and Martin Liu, I am grateful to have gotten to know you all and thank you for our many conversations and laughs.

Too my parents Eduardo and Adela, if it were not for your many sacrifices, I would not be where I am at today. Thank you for always supporting me, helping with our many moves and for your unquestionable love of my Chabelita. To my loving siblings Eddy and Jenny, thank you for always listening to me complain and for showing up no matter what the circumstance.

Finally, I would love to thank my husband, Jose for supporting and believing in me unconditionally every day of this long journey. From endless rides to the lab to working long hours so that our family was provided for. I am incredibly indebted to the sacrifices you have made not just for me but for our family.

Dedication

To my dearest children, Isabela and José Jr., and my beloved husband, José,

This achievement is not just mine but ours. I happily dedicate this work with all my heart to you guys.

As a first-generation college student, I have walked through challenging paths and defied expectations. Through the ups and downs, it has always been your unconditional love and support illuminating the way.

This Ph.D. not only represents years of hard work and dedication but also a future filled with possibilities for our family.

May this accomplishment be a guiding light for you and future generations, reminding them that the boldest dreams are achievable, even when the paths seem challenging.

Con mucho amor y cariño,

Mamá

Table of Contents

List of Figures

Chapter 1: Introduction

A bipolar spindle composed of microtubules and many associated proteins functions to attach to chromosomes at their kinetochores, bi-orient them, and accurately segregate them to daughter cells during cell division in all eukaryotes. While the spindle carries out this function universally, its architecture varies dramatically across species and in different cell types. We strive to elucidate mechanisms establishing spindle morphology and to determine how structural changes affect spindle function.

Spindle Components and Assembly

Microtubules, Building Blocks of the Spindle

Microtubules (MTs) are cytoskeletal polymers comprised of αβ-tubulin heterodimers. Tubulin heterodimers self-assemble longitudinally in the presence of GTP to generate protofilaments that laterally associate to form a hollow tube with a diameter of ~ 25nm (Chrétien *et al.*, 1992; Downing and Nogales, 1998). The asymmetrical nature of αβ-tubulin heterodimers generate a polar filament with distinct dynamic properties at each end. The fast-growing end is called the plus-end while the slower-growing end is called the minus-end (Desai and Mitchison*, 1997).

MTs are highly dynamic and can exist in either a growing, polymerizing state or a shrinking, depolymerizing state. Switching stochastically between these two states defines a behavior known as dynamic instability (Mitchison and Kirschner, 1984a, 1984b). During polymerization, αβ-tubulin heterodimers bound to GTP add to the growing plus-end of a MT. As the MT grows, GTP in β-tubulin subunits is hydrolyzed within the lattice producing a “GTP cap” that stabilizes the MT (Carlier, 1982; Mitchison and Kirschner, 1984a; Erickson and O’Brien, 1992; Howard and Hyman, 2009; Brouhard and Rice, 2018). However, if GTP hydrolysis catches up to the end of the MT, the GTP cap is lost, and the MT undergoes a “catastrophe,” converting to a depolymerizing state. The depolymerizing MT can recover if the GTP cap is re-established in a “rescue” event and transitions back to a polymerizing state (Figure 1.1, (Mitchison and Kirschner, 1984a; Helmke *et al.*, 2013).

Figure 1.1

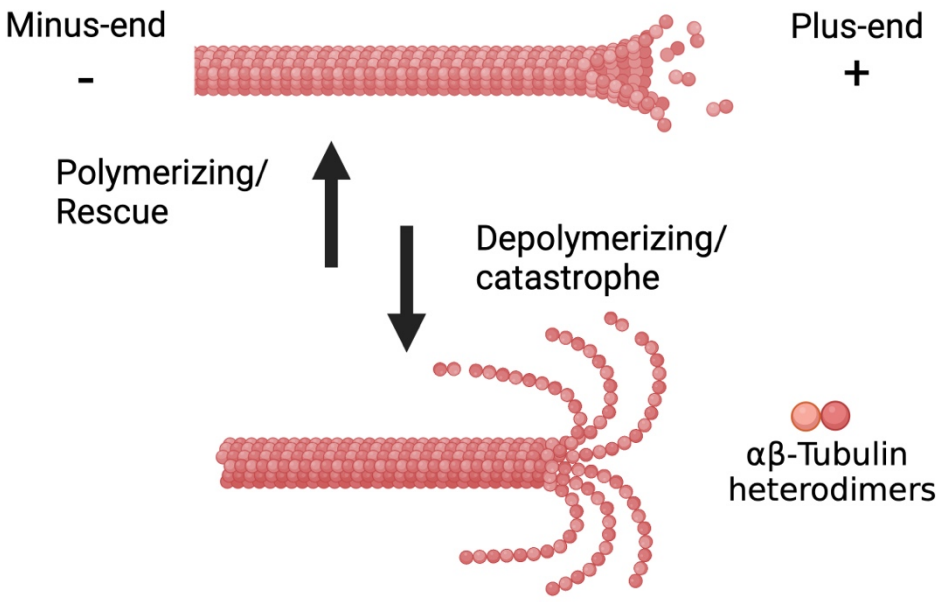

Figure 1.1: MT Dynamics
Polarized MT protofilaments grow by adding GTP-bound αβ-tubulin heterodimers to the plus-end. When the GTP hydrolysis rate is slower than the polymerization rate, a GTP cap is formed that stabilizes the MT. When GTP hydrolysis catches up to the end, the MT undergoes a catastrophe and depolymerizes. The GTP cap can be recovered and rescue MT growth. Adapted from (Helmke and Heald, 2014) with BioRender.com.

Microtubule Organizing Center: The Centrosome
After discovering dynamic instability, the first proposed mechanism for spindle assembly involving centrosomes was proposed. Duplicated centrosomes were predicted to be the primary source of MT nucleation, which could form a bipolar array in cells as nucleated MTs underwent periods of growth and shrinkage, "searching" for a kinetochore to "capture" and biorient chromosomes within the spindle. (Holy and Leibler, 1994). Evidence for the "search and capture" model was first observed in newt lung cells (Hayden *et al.*, 1990). When present in cells, centrosomes are the main MTOCs. Centrosomes consist of two centrioles surrounded by a dense protein matrix called the pericentriolar material (PCM). Centrosomes rapidly expand their PCM during mitosis, which is essential for spindle assembly (Woodruff *et al.*, 2014). This process, known as centrosome maturation, is initiated by mitotic kinases Aurora A and PLK1, which phosphorylate core PCM scaffolds such as Centrosomin (Cnn), Pericentrin (PCNT), and CEP192 (Kinoshita *et al.*, 2005; Lee and Rhee, 2011; Conduit *et al.*, 2014; Joukov *et al.*, 2014; Joukov and Nicolo, 2018). As key PCM components, PCNT, CEP192, AKAP450, and CDK5RAP2 contribute to recruitment of ring complexes that contain the γ-tubulin isoform (γ-TuRC), (Moritz *et al.*, 1995; Zheng *et al.*, 1995; Takahashi *et al.*, 2002; Zimmerman *et al.*, 2004; Fong *et al.*, 2008; Zhu *et al.*, 2008). Embedded γ-TuRCs stabilize the minus-ends of MTs and function as templates for MT polymerization (Kollman *et al.*, 2010, 2011). However, computational modeling indicated that without a

bias of MT growth towards chromosomes, the “search and rescue” model on its own was insufficient to assemble a spindle within a typical timescale (Wollman *et al.*, 2005).

Although centrosomes provide a dominant pathway for MT nucleation in most cells, evidence demonstrates that they are not essential for bipolar spindle assembly. One landmark discovery supporting this idea was the generation of bipolar spindles around DNA-coated beads that assemble mitotic chromatin in *Xenopus* egg extract (Heald *et al.*, 1996). When centrosomes are ablated in human cells, a spindle can still form, demonstrating support for an alternative centrosome-independent pathway for spindle assembly (Khodjakov *et al.*, 2000). This evidence, along with the existence of acentrosomal spindles in oocytes and fly mutants lacking centrioles all indicated that centrosomes were not essential for bipolar spindle assembly (Basto *et al.*, 2006; Schuh and Ellenberg, 2007).

Chromatin-Mediated MT Nucleation

The generation of bipolar spindles from chromatin coated beads lacking kinetochores and centrosomes in *Xenopus* egg extract elucidated an alternative MT self-organizing pathway of spindle assembly (Heald *et al.*, 1996). Around condensed chromosomes, chromatin bound RCC1, the guanosine nucleotide exchange factor for the small GTPase Ran, converts RanGDP to RanGTP. The localization of RCC1 and slow GTP hydrolysis rate establishes a local gradient of active RanGTP surrounding chromatin (Bischoff and Ponstingl, 1991; Kalab *et al.*, 2002). Interestingly, experiments by various groups using mutants of Ran demonstrated its essential role in driving spindle assembly and how constitutively active Ran leads to aberrant ectopic MT nucleation (Carazo-Salas *et al.*, 1999; Kalab *et al.*, 1999; Ohba *et al.*, 1999; Wilde and Zheng, 1999; Zhang *et al.*, 1999). Remarkably, RCC1-coated glass beads are also sufficient to generate spindles in *Xenopus* egg extract by establishing a RanGTP gradient in the absence of DNA (Halpin *et al.*, 2011).

Within the RanGTP gradient, RanGTP releases spindle assembly factors (SAFs) sequestered by the karyopherin protein complex of importin α and β. Importin-α binds cargos, including SAFs through a nuclear localization signal (NLS) within the protein (Fried and Kutay, 2003). Both the RanGTP gradient and release of importin bound cargos could be visualized in *Xenopus* egg extract using fluorescence resonance energy transfer (FRET) probes and disruption of either gradient affected spindle assembly or maintenance (Kalab *et al.*, 2002). After release from the inhibitory interaction with importins, SAFs become active to mediate MT nucleation and organization around chromatin (Kalab and Heald, 2008). To this day, investigations are underway to elucidate how SAFs precisely carry out spindle assembly. One Ran-regulated cargo, Targeting Protein for Xklp2, TPX2, is a prominent SAF whose role in mediating MT nucleation and branching has broadened our understanding of how MTs are nucleated downstream of RanGTP.

The chromosome passenger complex (CPC) is an alternative chromatin-mediated MT nucleation pathway independent of RanGTP. The CPC comprises four protein components: INCENP, survivin, borealin/Dasra, and Aurora B kinase (Ruchaud *et al.*,

2007; Carmena *et al.*, 2012). Work in *Xenopus* egg extract has proposed that the CPC can stabilize MTs near chromosomes by suppressing the activity of MT-destabilizing proteins such as MCAK and Op18/Stathmin through Aurora B-dependent phosphorylation (Budde *et al.*, 2001; Ohi *et al.*, 2004; Sampath *et al.*, 2004). Enrichment of CPC components on chromatin beads can induce MT nucleation when RanGTP is not present in *Xenopus* egg extract, supporting the idea that MT polymerization is promoted by two different pathways near chromatin (Maresca *et al.*, 2009).

MT Nucleation from Kinetochores

From the original "search and capture" model (Mitchison and Kirschner, 1984a), it was proposed that growing MTs emanating from the centrosome searched for kinetochores to form the mitotic spindle and facilitate segregation. However, several early *in vitro* studies from the 1970s had reported that kinetochores from isolated chromosomes or lysed mitotic cells could initiate MT polymerization when incubated with purified tubulin (McGill and Brinkley, 1975; Snyder and McIntosh, 1975; Telzer *et al.*, 1975; Gould and Borisy, 1978). In budding yeast during early mitosis, MT nucleation from kinetochores has also been observed, but these MTs are short-lived and do not persist to become part of the metaphase spindle (Kitamura *et al.*, 2010). More recent work using RPE-1 cells and bovine oocytes lacking centrosomes found that the fibrous corona, a transient outer-kinetochore meshwork, could nucleate MTs to function as an alternative MTOC (Wu *et al.*, 2023). Although kinetochore-mediated nucleation may play a prominent role in systems lacking centrosomes, it remains unknown whether kinetochores themselves nucleate or recruit nucleated MTs (Renda and Khodjakov, 2023).

Branching MT Nucleation

MT branching occurs when a new MT is polymerized off a pre-existing MT lattice. This idea of MT branching was first postulated after visualizing growing MT plus-ends with fluorescently labeled EB1 that initiated within the spindle at sites away from centrosomes and chromatin, as well as localization of γ-tubulin throughout the spindle (Lajoie-Mazenc *et al.*, 1994; Tirnauer *et al.*, 2004; Lüders *et al.*, 2006; Mahoney *et al.*, 2006). In *Drosophila* cells, it was discovered that an 8-member complex named Augmin was required to target γ-tubulin to spindle MTs but not centrosomes (Goshima *et al.*, 2008). Depletion or knockdown of Augmin in vertebrates and *Drosophila* caused a severe loss of spindle MTs and other defects in chromosome segregation and spindle bipolarity (Goshima *et al.*, 2008; Lawo *et al.*, 2009). Other proteins required for MT branching are XMAP215 and TPX2. XMAP215 is also a MT polymerase that has been shown to directly bind γ-TuRC to cooperatively nucleate MTs *in vitro* (Thawani *et al.*, 2018). TPX2 is capable of forming co-condensates with tubulin on pre-existing MTs to facilitate MT nucleation and enhance MT branching rates in *Xenopus* egg extracts (King and Petry, 2020). The nucleation of MTs by branching allows spindles to rapidly amplify the number of MTs while maintaining their polarity and increasing the rate of spindle assembly (Kraus *et al.*, 2023a).

Motor Proteins Organizing MTs

One of the main plus-end directed motors in the spindle is the homotetrameric kinesin-5 or Eg5 (Cole *et al.*, 1994). Eg5 crosslinks and slides antiparallel MTs outward (Eckerdt

et al., 2008; Ma *et al.*, 2011) and bundles parallel MTs at spindle poles (Helmke and Heald, 2014). Eg5 is essential for generating spindle bipolarity and separating spindle poles by sorting and bunding MTs (Kashlna *et al.*, 1996; Walczak *et al.*, 1998; Kapitein *et al.*, 2005). In *Xenopus* egg extract, pharmacological inhibition of Eg5 causes bipolar spindles to collapse into a monopolar structure (Kapoor *et al.*, 2000). However, in human cells, Eg5 is not important to maintain bipolarity once the spindle is formed due to the redundant activity of kinesin-12, HKlp2 (Kollu *et al.*, 2009; Vanneste *et al.*, 2009). Eg5 also contributes to poleward MT flux by continuously sliding MT outwards towards the poles (Helmke *et al.*, 2013).

Minus end-directed motor proteins help interconnect MTs from centrosomes and kinetochores to achieve the pole-focused-diamond shape of the spindle. The primary minus end-directed MT motors are dynein and kinesin-14 motors. Dynein is essential for focusing MTs into a single pole in the presence or absence of centrosomes (Heald *et al.*, 1996, 1997). Pole coalescence by dynein is depends on the transport and activation of the spindle pole protein NuMA, which is driven by dynein interacting with the dynactin complex (Merdes *et al.*, 2000). Inhibition of Dynein perturbs the formation of a focused poles in spindles assembled from DNA-coated beads in *Xenopus* egg extract (Heald *et al.*, 1996). Several other motor proteins are transported to the spindle poles in a dynein-dependent manner, including kinesin-like Protein Xklp2 and Eg5 (Wittmann *et al.*, 1998; Uteng *et al.*, 2008).

Kinesin-14 family members include Ncd, HSET, and XCTK2. Mutation of Ncd, the *Drosophila* homolog, causes spindle pole defects and overall spindle instability (Hatsumi and Endow, 1992; Endow *et al.*, 1994; Matthies *et al.*, 1996; Endow and Komma, 1997). Inhibition of XCTK2 in *Xenopus* spindles compromises spindle pole formation only in spindles generated in the absence of centrosomes (Walczak *et al.*, 1998). Overall, motor proteins play an integral role in spindle formation and maintenance by physically transporting MTs and localizing MT effectors.

Microtubule Populations of the Spindle

There are several different types of MTs that comprise the metaphase spindle. The first and likely most crucial variety are kinetochore MTs, also termed k-fibers. Kinetochore fiber MTs in vertebrates are comprised of a dense bundle of ~ 30-40 MTs that extend from poles to kinetochores (Biggins and Walczak, 2003; Cleveland *et al.*, 2003). K-fiber MTs attach end on at each of the two kinetochores of a duplicated chromosome, bi-orienting them and ensuring that one copy is targeted to each spindle pole (Helmke *et al.*, 2013).

A second population consists of dynamic astral MTs. Astral MTs radiate from centrosomes to capture kinetochores and help position the spindle properly by interacting with the cell cortex (Hayden *et al.*, 1990; Forth and Kapoor, 2017).

The third population of MTs includes non-kinetochore microtubules (nK-MTs) also known as interpolar MTs. nK-MT make up the bulk of MTs in the *Xenopus* spindle and

overlapping arrays span from pole to pole making them the most abundant MT population (Dumont and Mitchison, 2009).

Figure 1.2

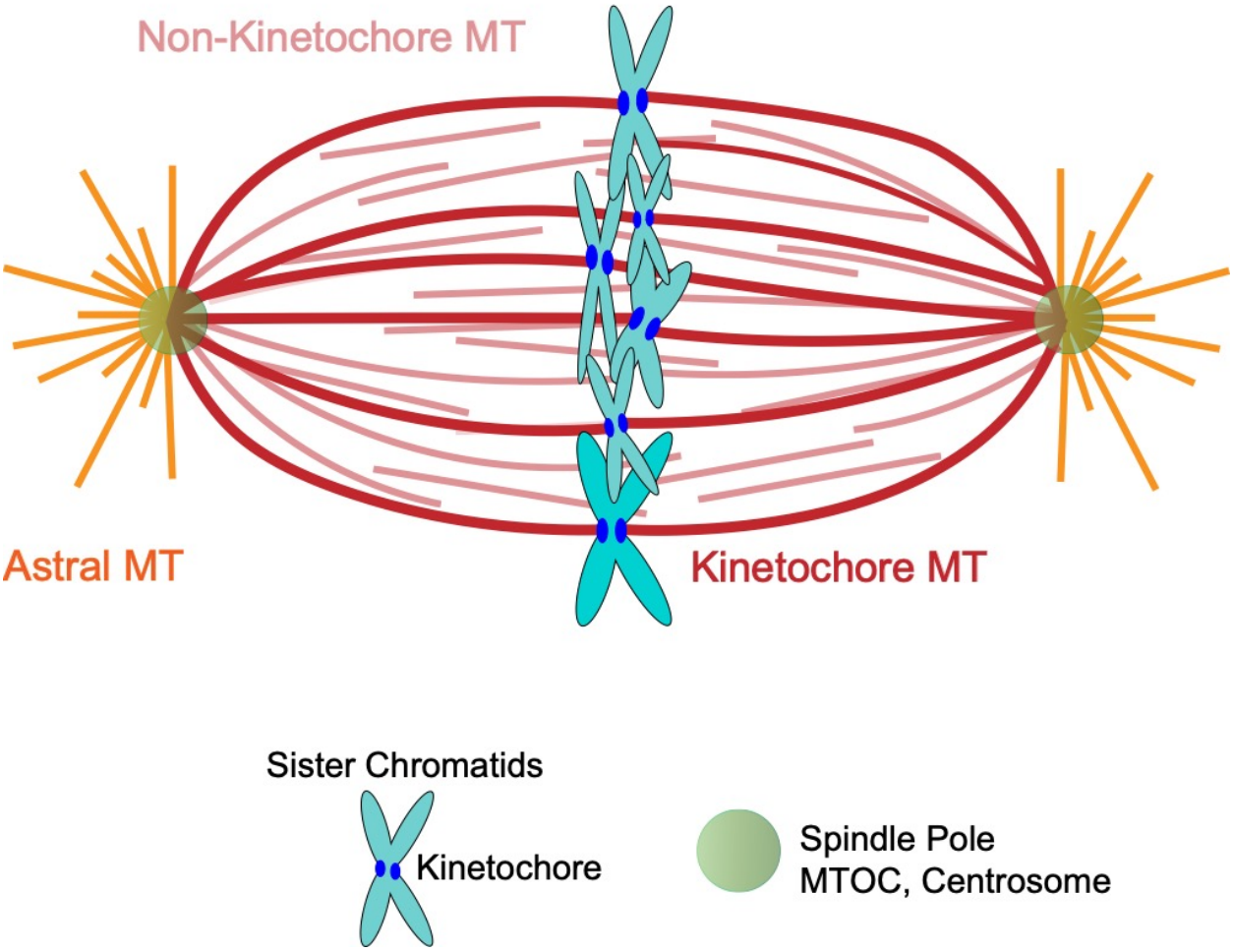

Figure 1.2: MT populations in the spindle
Three populations of MTs present in the metaphase spindle. Astral MTs emanate from spindle poles to help anchor and position the spindle. Kinetochore MTs attach to kinetochores on duplicated chromosomes and biorient them to target one sister chromatid to each pole. Non-kinetochore MTs are found throughout the spindle and make up a majority of the MTs present in spindles.

Phase separation in the Spindle
Liquid-liquid phase separation (LLPS) is a concentration-dependent phenomenon in which macromolecules undergo de-mixing and partition from a single phase into two phases that can spatially restrict cellular components in membrane-less compartments (Hyman *et al.*, 2014; Banani *et al.*, 2017; Shin and Brangwynne, 2017; Holehouse and Pappu, 2018). LLPS is driven by weak, multivalent interactions and often involves proteins that lack folded structure and are intrinsically disordered (Dignon *et al.*, 2020).

When present in cells, centrosomes are the main MTOC. When entering mitosis, centrosomes rapidly expand their PCM, which is essential for spindle assembly and MT nucleation (Woodruff *et al.*, 2014). *In vitro* and theoretical studies propose that LLPS can trigger centrosome assembly (Zwicker *et al.*, 2014; Woodruff *et al.*, 2017). The coiled-coil PCM protein SPD-5 from *C. elegans* can form spherical condensates that recruit XMAP215 and TPX2 homologs *in vitro* and in *C. elegans* embryos. Notably, *in vitro*, these condensates can also concentrate tubulin (Woodruff *et al.*, 2017). Recent work in human cells showed that endogenously tagged PCNT, a key PCM scaffold, could undergo phase separation which supports this idea of LLPS driving centrosome assembly (Jiang *et al.*, 2021). GFP-PCNT condensates formed in human cells were found to be enriched with other PCM components such as γ-tubulin, CEP215, CEP192, and endogenous PCNT (Jiang *et al.*, 2021). Phase separation plays a role in the recruitment and concertation of PCM proteins at the centrosome, but whether it plays a role in activating γ-TuRC to nucleate MTs is not understood.

The spindle matrix is predicted to be a non-MT-based material that engulfs the spindle apparatus to balance motor forces and regulate spindle assembly factors (Zheng, 2010). BugZ, a protein component of the spindle matrix, has been shown to undergo LLPS. BugZ facilitates spindle assembly via MT nucleation by co-condensing with tubulin and activating the mitotic kinase Aurora A (Jiang *et al.*, 2015; Huang *et al.*, 2018). Similarly to BugZ, the spindle assembly factor, TPX2 has also been shown to undergo LLPS and drive MT nucleation and branching by co-condensing with tubulin (King and Petry, 2020) which will be discussed in detail in a later section.

Phase separation has also been observed at the inner kinetochore. The chromosomal passenger complex (CPC) is localized to the inner kinetochore and exists in a phase-separated state driven by its borealin subunit. *In vitro*, purified borealin with additional CPC components, such as survivin, and the 58 N-terminal a.a of INCENP, can form liquid droplets that nucleate MTs. This observation implies that the CPC may regulate MT formation near chromosomes by an alternative mechanism (Trivedi *et al.*, 2019). CPC regulation of MT nucleation at the kinetochore is typically attributed to its inhibition of the MT depolymerase MCAK (Sampath *et al.*, 2004)

Although phase separation does not have a well-defined biological function, it highlights the biochemical interactions that facilitate rapid association of the many components needed to form the spindle.

The Model System of *Xenopus* Egg Extract

Xenopus egg extracts provide an ideal *in vitro* system that recapitulates many morphological changes associated with cell division, making it ideal to study spindle assembly in biologically active undiluted cytoplasm (Desai *et al.*, 1998). This cell-free extract is biochemically manipulable, allowing for techniques including protein depletion, addition, and inhibition. This ability to manipulate specific components during the cell cycle has led to significant insight into numerous mechanisms including those driving spindle assembly and chromosome condensation.

Freshly made extract remains in a metaphase-arrested state due to the activity of cytostatic factor (CSF) present in unfertilized *Xenopus* oocytes which arrests them in metaphase of meiosis II (Tunquist and Maller, 2003). Sperm nuclei can then be added to CSF-arrested *Xenopus* egg extract to induce meiotic spindle assembly around unreplicated chromosomes that lack functional kinetochores. The extract can also be cycled into interphase by the addition of calcium, which causes cyclin degradation leading to the formation of nuclei and DNA replication. Subsequent addition of CSF extract to the reaction cycles it back into metaphase of the cell cycle, triggering spindle assembly (Maresca and Heald, 2006).

Xenopus extracts are typically made from eggs of the African clawed frog, *Xenopus laevis*. However, extracts can also be prepared from various other *Xenopus* species, one of which is *Xenopus tropicalis*. Spindles generated in both extracts using the same DNA have a distinct morphological appearance. *X. tropicalis* spindles are significantly shorter than *X. laevis* spindles and contain more stable kinetochore fibers (Brown *et al.*, 2007; Loughlin *et al.*, 2011). One contributing factor to the shorter observed *X. tropicalis* spindles is the presence of a more active MT-severing protein p60 katanin, which harbors a mutation that prevents inhibitory phosphorylation (Loughlin *et al.*, 2011). High-resolution microscopy of both *X. laevis* and *X. tropicalis* spindles also showed that *X. laevis* spindles are more densely packed with highly bundled MTs extending in a tiled array across the entire spindle. In contrast, *X. tropicalis* spindles lack MT density in the spindle midzone (Helmke and Heald, 2014). In the same study, biochemical analysis revealed that varying levels and a sequence difference in the key SAF, TPX2, was responsible for the morphological differences between *X. laevis* and *X. tropicalis* spindles. Using the biochemical tractability of *Xenopus* egg extract as a powerful tool, we can continue to elucidate the underlying mechanisms regulating spindle architecture.

The Many Roles of Microtubule Associated Protein, TPX2, During Spindle Assembly

*Discovery of **T**arget **P**rotein for **X**klp**2** **(TPX2)***
Target **P**rotein for **X**klp**2**, TPX2 was initially discovered as a novel microtubule associated protein (MAP) required for targeting the plus-end directed motor Xklp2 (kinesin-12) to MTs (Wittmann *et al.*, 1998, 2000). TPX2, which bound MTs with high affinity, localized to spindle poles in a dynein-dependent manner during mitosis and maintained a nuclear localization during interphase. When spindles were formed in

Xenopus egg extracts depleted of TPX2, they were able to assemble a MT array but displayed several pole defects and a lower MT density. In spindle reactions carried out with 5-10-fold molar excess of TPX2, the percentage of bipolar structures was significantly decreased. Instead, monopolar half spindles with increased MT density and ring-like poles formed. Additionally, when excess TPX2 was added to *Xenopus* egg extract reactions, the formation of ectopic MT asters was induced, indicating a possible role in MT nucleation (Wittmann *et al.*, 2000).

TPX2 is a RanGTP-Regulated Cargo

RanGTP plays a central role in the chromatin-mediated MT nucleation pathway by establishing a gradient around condensed chromosomes and releasing SAF inhibited by the protein complex of importin α and β (Karsenti and Vernos, 2001; Fried and Kutay, 2003; Rieder, 2005).TPX2 was first established as a key SAF driving chromatin-mediated nucleation when TPX2-depleted *Xenopus* extracts could not form MT aster structures in the presence of a constitutively active Ran mutant, RanQ69L (Gruss *et al.*, 2001). The addition of recombinant TPX2 protein to TPX2-depleted *Xenopus* extracts rescued MT aster formation which in turn could be suppressed by the introduction of recombinant importin-α (Gruss *et al.*, 2001).

Importin-α recognizes cargos like SAFs by recognizing and binding a nuclear localization signal (NLS) within the protein. NLSs are characterized by clusters of basic residues termed “monopartite” (MP) or “bipartite” (BP). A MP NLS is characterized by a short consensus sequence of K(K/R)X(K/R) (Hodel *et al.*, 2001). Immunoprecipitation and crystal structures of a truncated *X. laevis* TPX2 bound to importin-α demonstrated interaction through two NLS motifs located at 284-KRKH-287 (NLS1) and 327-KMIK-330 (NLS2) (Schatz *et al.*, 2003; Giesecke and Stewart, 2010). More recent *in vitro* binding experiments using full-length X. laevis TPX2 identified an additional NLS located upstream of the previously established NLSs located at 123-KKLK-126 (Safari *et al.*, 2021).

MT Nucleation Stimulated by TPX2 Co-condensation with Tubulin

Many proteins that can undergo liquid-liquid phase separation (LLPS) exhibit characteristics that include intrinsically disordered regions and domains that can facilitate multivalent interaction with other proteins (Alberti *et al.*, 2019). TPX2 is predicted to be a highly intrinsically disordered protein with little secondary structure. The N-terminal half of the protein is highly disordered and has been shown to be dispensable for MT branching nucleation while the C-terminal half which is more structured can replace full-length TPX2 protein and induce MT branching nucleation (Petry *et al.*, 2013; Alfaro-Aco *et al.*, 2017; King and Petry, 2020).

In vitro experiments using truncated variants of *X. laevis* TPX2 incubated with purified tubulin showed that the N-terminus (a.a. 1-480) could co-condense with tubulin at low and high concentrations. TPX2 was also shown to preferentially co-condense with tubulin on nucleated MTs at a physiologically relevant concentration in *Xenopus* egg extract (King and Petry, 2020). To induce MT branching, TPX2 must first accumulate on MTs to recruit augmin and, therefore γ-TuRCs (Song *et al.*, 2018; Thawani *et al.*, 2018;

Alfaro-Aco *et al.*, 2020). The ability to co-condense with tubulin on pre-existing MT suggests a mechanism whereby TPX2 can concentrate tubulin, which could serve as an efficient MT branching point (King and Petry, 2020).

TPX2 Targeting and Activation of the Mitotic Kinase Aurora A

The mitotic kinase Aurora A plays many essential roles in mitosis. First, Aurora A drives centrosome maturation and separation during the G2/M transition by initiating rapid recruitment of PCM components to expand and increase MT nucleation at centrosomes (Palazzo *et al.*, 1999; Hannak *et al.*, 2001; Nigg, 2001; Berdnik and Knoblich, 2002; Joukov and Nicolo, 2018; Magnaghi-Jaulin *et al.*, 2019). This increase in MT nucleation at the centrosome is stimulated by targeting γ-TuRCs to the PCM (Tillery *et al.*, 2018). Besides regulating centrosome maturation, Aurora A is also essential for the timely entry into mitosis and proper spindle formation (Barr and Gergely, 2007; Lindqvist *et al.*, 2009). Activation and targeting of Aurora A to spindle poles by TPX2 triggers phosphorylation of targets such as NEDD1 to promote MT nucleation by γTuRC (Garrett *et al.*, 2002; Kufer *et al.*, 2002; Bayliss *et al.*, 2003; Eyers *et al.*, 2003; Tsai *et al.*, 2003; Sardon *et al.*, 2008; Pinyol *et al.*, 2013; Scrofani *et al.*, 2015). The N-terminal domain (a.a 1-39 in *Xenopus*, a.a. 1-43 in humans) of TPX2 can activate Aurora A by binding and allosterically activating Aurora A by protecting a phosphorylation site located in the activation loop at T295, in *Xenopus* (T288 in human) while also promoting autophosphorylation (Kufer *et al.*, 2002; Bayliss *et al.*, 2003; Eyers and Maller, 2004; Zorba *et al.*, 2014). MT nucleation by the Aurora A/TPX2 complex is activated through both centrosomal and chromatin pathways (Joukov and Nicolo, 2018). Although TPX2 plays a central role in MT branching nucleation, the role of Aurora A in this process has not been well characterized (Petry *et al.*, 2013; Alfaro-Aco *et al.*, 2017; Joukov and Nicolo, 2018). Overexpression of both TPX2 and Aurora A is common in many human cancers and perturbing their interaction is an attractive target for cancer therapies (Asteriti *et al.*, 2010; Joukov and Nicolo, 2018; Orth *et al.*, 2018).

TPX2 binding with the kinesin-5 motor Eg5

Interaction with the kinesin-5 motor Eg5 is mediated by the last 35 amino acids in the C-terminal domain of TPX2 (Eckerdt *et al.*, 2008). Interaction with Eg5 is required to localize TPX2 to the spindle poles in a dynein-dependent manner (Ma *et al.*, 2010). Deletion of the Eg5 binding domain in TPX2 prevents localization of Eg5 to spindle MTs in human cells and prevents TPX2 localization in meiotic *Xenopus* spindles suggesting that this interaction is required for the proper localization of both proteins (Ma *et al.*, 2011; Helmke and Heald, 2014). Besides being essential for Eg5 localization, the C-terminal end of TPX2 alone is sufficient to inhibit *in vitro* MT-MT gliding by Eg5 (Ma *et al.*, 2011). Additional *in vitro* work using *Xenopus* egg extract has shown that the 35 a.a C-terminal domain of TPX2 is essential for inducing MT branching nucleation. However, if Eg5 activity is inhibited by pharmacological agents, branching MT nucleation can still occur (Alfaro-Aco *et al.*, 2017).

MT Binding and Stabilization by TPX2

Full-length TPX2 was first visualized binding to MT in *Xenopus* egg extracts (Wittmann *et al.*, 2000). *In vitro* work using both full-length and truncated variants of hTPX2

showed that the central region of TPX2 lacking both Aurora A and Eg5 binding domains was sufficient to bind to MTs directly. This same study also concluded that hTPX2 preferentially bound to the growing end of MTs to help stabilize MT intermediates and increased overall MT lifetime (Roostalu *et al.*, 2015). Several other *in vitro* studies support this finding of MT stabilization by showing that TPX2 binding can reduce the rate of MT catastrophe events (Wieczorek *et al.*, 2015; Reid *et al.*, 2016). Using high-resolution cryo-EM, a truncated hTPX2 (a.a. 274-270) was visualized bound to stable GMPCPP-MTs and displayed interactions across the tubulin dimer interface. These interactions are predicted to bridge adjacent tubulin protofilaments and allow MT nucleation before MT tube closure (Zhang *et al.*, 2017). The lack of secondary structure and overall disorder of TPX2 make it challenging to elucidate how the protein and its multiple domains simultaneously interact with binding partners including tubulin.

TPX2 in Spindle Architecture

Although there is substantial knowledge and evidence characterizing TPX2's role in modulating MT nucleation in an organization during spindle assembly, it remains unknown how the regulation of TPX2 influences spindle morphology. Many studies both *in vitro* and *in vivo*, have provided in depth characterizations of the different functional domains in TPX2. However, there is no interconnected model showing how all these domains interact and regulate the activity of the full-length protein.

Studies in *C. elegans* and human cells have shown that significantly shorter spindles are produced when the interaction of TPX2 and Aurora A is perturbed by TPX2 knockdown (Özlü *et al.*, 2005; Bird and Hyman, 2008; Greenan *et al.*, 2010). This has also been observed in *Drosophila* when TPX2 homolog, ssp1, is knocked down via RNAi (Goshima *et al.*, 2007; Goshima, 2011). Studies using a pharmacological inhibitor of Aurora A have shown a reduction in MT nucleation and decreased spindle formation in *Xenopus* egg extracts and human cells (Asteriti *et al.*, 2014; Huang *et al.*, 2018; Nadkarni and Heald, 2021). It is likely that the decreased spindle size viewed in studies employing knock-down strategies of TPX2 is due to reduced MT density between spindle poles caused by reduced Aurora A activation (Kufer *et al.*, 2002; Pinyol *et al.*, 2013; Magnaghi-Jaulin *et al.*, 2019).

Previously, we showed that distinct spindle architectures observed between two closely related frogs were caused by varying levels of TPX2. *Xenopus tropicalis* egg extract was discovered to contain 3-fold more TPX2 than *Xenopus laevis* egg extract and increasing *X. laevis* TPX2 levels to those of *X. tropicalis* significantly reduced spindle length. Increasing levels of TPX2 led to more recruitment of Eg5 which shifted MT density from the center of the spindle to the poles. Additionally, when *X. tropicalis* TPX2 was added to *X. laevis* spindle reactions, it increased ectopic MT aster formation and the number of astral MT present at spindle poles. The cause of this enhanced MT nucleation activity was a deletion of a 7-a.a. sequence, 619-LSGSIVQ-625, in *X. tropicalis* TPX2 (Helmke and Heald, 2014). This 7-a.a. sequence is located just upstream of the C-terminal Eg5 binding domain (Δ7) and was also shown to increase the MT branching nucleation activity of *X. laevis* TPX2 when deleted (Alfaro-Aco *et al.*,

2017). Yet, how this 7 a.a deletion regulates TPX2 interacting with Eg5 and other proteins to coordinate MT nucleation and organization is still not well understood.

In Chapter 2, we will present the characterization of a conserved nuclear localization sequence (NLS) motif, 123KKLK126 in *X. laevis* TPX2, which regulates astral MT formation and spindle pole morphology in *Xenopus* egg extract. Mutation of this conserved motif drives increased TPX2 interactions with Aurora A, Eg5 and pericentrin, and modulates binding to the regulatory karyopherin, importin-α. This increase in overall TPX2 activity provides insight into the consequences of TPX2 misregulation.

TPX2 Overexpression in Cancer

Consequent to the discovery of TPX2, overexpression TPX2 was detected in malignant cancer samples embedded in paraffin and in cell lines derived from small cell lung carcinomas (Heidebrecht *et al.*, 1997; Manda *et al.*, 1999). Since this observation, several studies found elevated levels of TPX2 across a variety of cancers and its presence in many aggressive malignant cancers (Castro *et al.*, 2007; Asteriti *et al.*, 2010; Neumayer *et al.*, 2014). Overexpression of TPX2 in human cancers is also used as a prognostic marker associated with worse outcomes in patients (Carter *et al.*, 2006; Ma *et al.*, 2006; Shigeishi *et al.*, 2009; Li *et al.*, 2010; Zou *et al.*, 2018; Jiang *et al.*, 2019; Koike *et al.*, 2022). It was recently shown that overexpression of the oncogene MYC can lead to chromosomal instability and errors in spindle assembly via its effects on MT nucleation and organization. Further analysis of the upregulated genes caused by MYC expression in mouse models and human breast cancers revealed a correlation between MYC and TPX2 expression (Rohrberg *et al.*, 2020). However, given TPX2's role in MT nucleation and organization, little is known about how overexpression of TPX2 modulates spindle architecture in cancer cells and will be further discussed in Chapter 3.

Chapter 2: Identification of a motif in TPX2 that regulates spindle architecture in *Xenopus* egg extracts

Introduction

During cell division, a dynamic, microtubule (MT)-based spindle forms to faithfully segregate duplicated chromosomes to daughter cells. Although the spindle performs this universal function in all eukaryotes, its architecture varies dramatically, both across species and in different cell types (Crowder *et al.*, 2015). For example, during meiosis, a small, diamond-shaped spindle in the egg segregates half of the maternal genome to a small polar body. Following fertilization, the first mitotic division occurs and is accompanied by dramatic changes in spindle size and architecture, with long astral MTs extending outward from the spindle poles. Such changes in spindle dimensions and architecture are likely to be critical for proper spindle function, but how they arise at the molecular level remains unclear.

One candidate factor for modulating astral MT density and organization is the MT-associated protein TPX2. Originally identified as the spindle *t*argeting *p*rotein for the *Xenopus* kinesin motor *X*klp*2* (Wittmann *et al.*, 2000), TPX2 is essential for spindle bipolarity, MT nucleation, stabilization and organization at spindle poles in multiple species and cell types (Schatz *et al.*, 2003; Brunet *et al.*, 2004; Tulu *et al.*, 2006), and its overexpression is common in a number of cancers (Asteriti *et al.*, 2010; Neumayer *et al.*, 2014). TPX2 is one of several spindle assembly factors (SAFs) containing nuclear localization sequence (NLS) motifs that mediate binding and inhibition by importins, which is locally derepressed in the vicinity of mitotic chromatin by RanGTP (Gruss *et al.*, 2001, 2002; Schatz *et al.*, 2003). TPX2 drives MT nucleation at least in part by recruiting and activating Aurora A kinase, which phosphorylates targets such as NEDD1 to promote MT nucleation via γTuRC (Garrett *et al.*, 2002; Kufer *et al.*, 2002; Bayliss *et al.*, 2003; Eyers *et al.*, 2003; Tsai *et al.*, 2003; Sardon *et al.*, 2008; Pinyol *et al.*, 2013; Scrofani *et al.*, 2015). In addition, the C-terminal domain of TPX2 interacts with the homotetrameric plus end–directed motor Eg5, which crosslinks and slides antiparallel MTs outward (Eckerdt *et al.*, 2008; Ma *et al.*, 2011) and bundles parallel MTs at spindle poles (Helmke and Heald, 2014). TPX2 binding to Eg5 inhibits its ability to slide MTs *in vitro* (Ma *et al.*, 2010, 2011; Gable *et al.*, 2012). More recently, it was discovered that TPX2 plays a key role in branching MT nucleation off the sides of existing MTs together with augmin that recruits γTuRC and the MT polymerase XMAP215 (Petry *et al.*, 2013; Song *et al.*, 2018; Thawani *et al.*, 2018; Travis *et al.*, 2022; Kraus *et al.*, 2023b). Both *in*

vitro and in the presence of *Xenopus* egg cytoplasm, TPX2 is capable of undergoing liquid-liquid phase separation (LLPS), forming co-condensates with tubulin that stimulate branching MT nucleation (King & Petry, 2020). However, whether and how TPX2 is regulated to generate different spindle MT architectures and the underlying mechanisms are poorly understood.

Xenopus egg extracts provide an ideal system to study the role of TPX2 in defining spindle architecture since *in vitro* reactions combining cytostatic factor (CSF) metaphase-arrested extracts and sperm nuclei recapitulate meiotic spindle assembly and can be biochemically manipulated. Here we show that addition of recombinant *X. laevis* or *X. tropicalis* TPX2 in which a high-affinity NLS motif, ^{123}KKLK^{126} (Safari *et al.*, 2021) is mutated to AALA caused dramatic changes in spindle architecture, MT polymerization, and astral MT growth, recruiting activated Aurora A, pericentrin, and Eg5 to spindle poles. *X. tropicalis* TPX2 possessed higher activity than the *X. laevis* protein, which was further enhanced by the NLS mutation. Interestingly, importin-α binding and recruitment to spindle poles occurred despite mutation of the NLS. We propose that TPX2-dependent association with multiple SAFs and importin-α promotes multivalent interactions that strongly enhance MT polymerization, branching, and bundling.

Results and Discussion

Mutating the 123-KKLK-126 motif *of X. laevis* and *X. tropicalis* TPX2 alters spindle pole morphology in *Xenopus* egg extracts

We showed previously that recombinant *X. laevis* and *X. tropicalis* TPX2 proteins produce distinct spindle architectures in egg extracts due to differences in TPX2 levels that affect spindle length and mid-zone organization, as well as a 7-aa deletion (Δ7) adjacent to the Eg5-binding domain in *X. tropicalis* TPX2 that was shown to stimulate astral MT growth and branching MT nucleation (Helmke and Heald, 2014)(add citation to the relevant Petry paper). Through further mutational analysis of *X. laevis* TPX2, we identified another sequence at 123-KKLK-126 that regulates MT polymerization in egg extract (Supplementary Figure 2.1). Previously identified as an NLS motif termed NLS3, this sequence is conserved in mammals and contributes to the high-affinity interaction between TPX2 and importin-α, which was shown to regulate TPX2 LLPS and co-condensation with tubulin (King and Petry, 2020; Safari *et al.*, 2021). However, the function of this motif in regulating TPX2 interactions with other SAFs and MT architecture in the spindle was unknown.

To probe the role of NLS3 during spindle assembly, wildtype (123-KKLK-126) and NLS3 mutant (123-AALA-126) GFP-tagged *X. laevis* and *X. tropicalis* TPX2 proteins were expressed in *E.coli*, purified, and added to *X. laevis* egg extract spindle assembly reactions at 100 nM, similar to the endogenous concentration and below the 200 nM needed to significantly reduce spindle length (Helmke and Heald, 2014). Both NLS3 mutants altered spindle morphology (Figure 2.1A), increasing the formation of ectopic

MT asters and disrupting focusing of MTs to generate “hollow” spindle poles (Figure 2.1B and C). The *X. tropicalis* proteins had a more dramatic effect compared to the *X. laevis* versions and were recruited more strongly to the spindle, especially the poles as revealed by line scan measurements of fluorescence intensity along the length of the spindle (Figure 2.1D). Addition of the NLS3 mutants further increased TPX2 localization and tubulin intensity relative to the wild type proteins. Thus, the *X. tropicalis* wildtype and NLS3 mutant proteins more strongly promoted MT polymerization activity compared to the *X. laevis* versions, consistent with previous work (Helmke and Heald, 2014) and highlighting the inhibitory effect of NLS3 on microtubule growth.

Figure 2.1

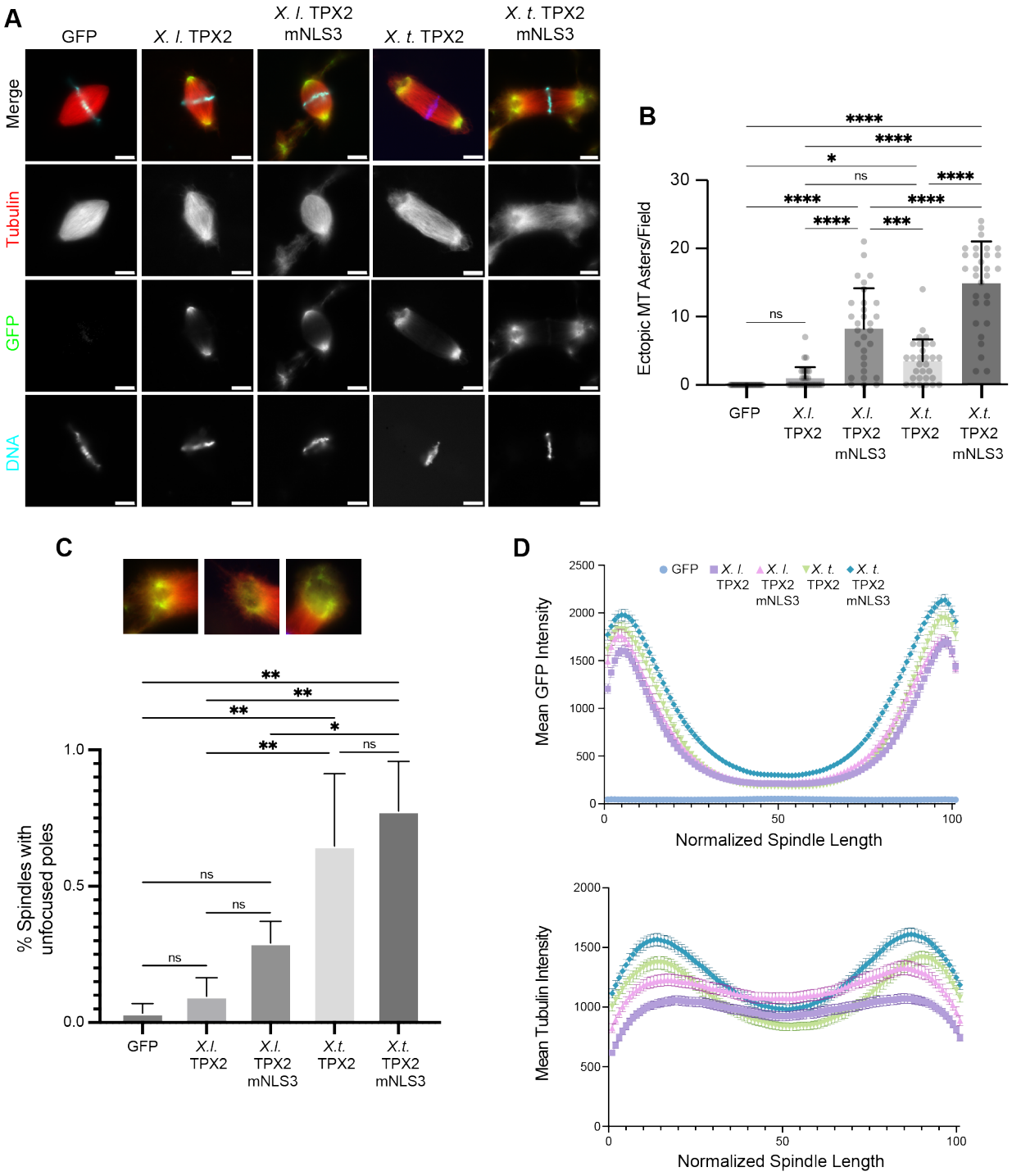

Figure 2.1: Addition of recombinant *X. laevis (X. l.)* and *X. tropicalis (X. t.)* mNLS3 TPX2 proteins modify spindle architecture in *Xenopus laevis* egg extract
(A) Immunostaining of spindle assembly reactions in the presence of 100 nm recombinant GFP or GFP-tagged TPX2 proteins. Spindle reactions were sedimented

onto coverslips before immunostaining as described in materials and methods. Scale bar = 10 μm. *X.t*. TPX2 mNLS3 image is taken from a larger field of view. (B) Quantification of ectopic MT asters induced by recombinant TPX2 proteins. For each condition, the number of ectopic asters were counted in 10 microscope fields, repeated in three separate extracts. (C) Percentage of spindles per condition which displayed unfocused pole defects. Total spindles analyzed for each condition, GFP n = 155, *X.l.* TPX2 n = 130, *X.l.* TPX2 mNLS3 n = 171, *X.t.* TPX2 n = 206, *X.t.* TPX2 mNLS3 n = 177. (D) Line scan quantification of mean GFP fluorescence (Top) and mean Tubulin (bottom). n = 3 different extracts, total spindles analyzed for each condition analyzed, GFP n = 150, *X.l.* TPX2 n = 127, *X.l.* TPX2 mNLS3 n = 163, *X.t.* TPX2 n = 206, *X.t.* TPX2 mNLS3 n = 174. Error bars = SEM. **** = $p<0.0001$, *** = $p<0.001$, ** = $p<0.01$, * = $p<0.1$, ns = not significant.

Xenopus TPX2 NLS3 mutants increase recruitment of activated Aurora A and pericentrin to spindle poles

We next investigated which known protein interactions of TPX2 were altered in the presence of NLS3 mutants to mediate changes in spindle morphology and ectopic MT aster formation. TPX2 binds and allosterically maintains activation of Aurora A by protecting a phosphorylation site located in the activation loop at T295 in *Xenopus* (T288 in humans) (Bayliss *et al.*, 2003; Eyers and Maller, 2004). Using a phospho-specific antibody, we quantified total phospho-Aurora A T295 (pT295-AurA) immunostaining on spindles generated in the presence of wildtype and NLS3 mutant *X. laevis* and *X. tropicalis* TPX2 proteins. Compared to GFP, addition of TPX2 proteins recruited and activated more Aurora A at spindle poles, with the *X. tropicalis* TPX2 NLS3 mutant showing the highest pT295-AurA staining relative to tubulin fluorescence (Figure 2.2A and B). Comparable differences in Aurora A activation were also detected biochemically by immunoprecipitating the recombinant proteins from egg extract reactions using a GFP antibody and probing Western blots with the pT295-AurA antibody (Figure 2.2C). To test whether the effects of the NLS3 mutant on MTs were mediated through kinase activation, we treated extracts with the Aurora A inhibitor Alisertib (MLN 8237), which was previously shown to diminish MTs emanating from sperm centrosomes and prevent spindle formation from Aurora A coated beads (Huang *et al.*, 2018; Nadkarni and Heald, 2021). However, although MT density in spindles decreased with inhibitor treatment, pT295-AurA staining was not entirely abolished (Supplementary Figure 2.3), and NLS3 TPX2 mutants still co-precipitated with reduced levels of active kinase in the presence of the drug (Figure 2.2D). Together, these results show that mutating the NLS3 motif increases TPX2 binding and activation of Aurora A at spindle poles which is at least in part responsible for the increased MT polymerization observed.

Figure 2.2

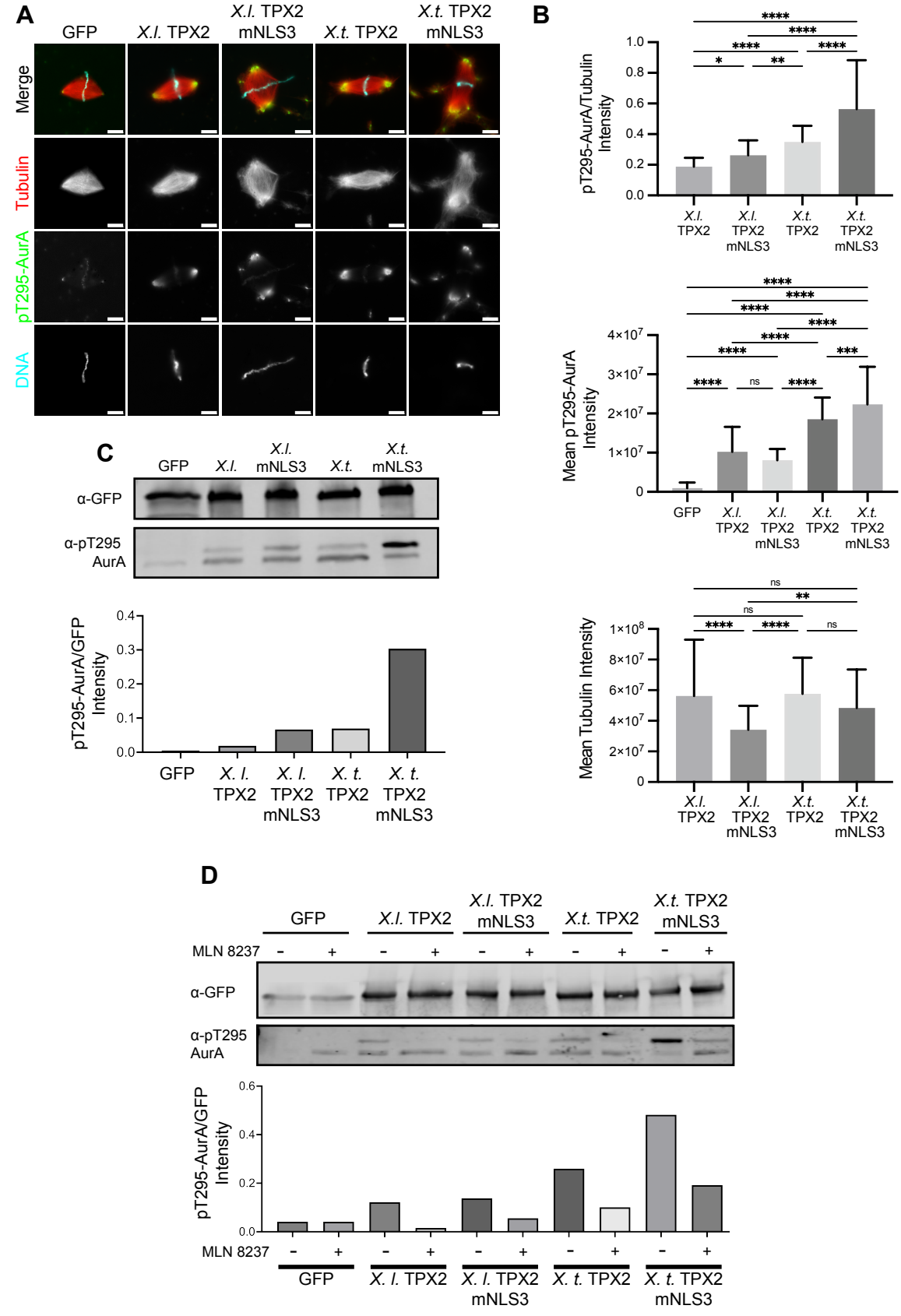
A
GFP
X.l. TPX2
X.l. TPX2 mNLS3
X.t. TPX2
X.t. TPX2 mNLS3
Merge
Tubulin
pT295-AurA
DNA
B
pT295-AurA/Tubulin Intensity
Mean pT295-AurA Intensity
Mean Tubulin Intensity
C
α-GFP
α-pT295 AurA
pT295-AurA/GFP Intensity
D
MLN 8237

Figure 2.2: *X. laevis* and *X. tropicalis* TPX2 NLS3 motif mutants increase levels of pAurora A recruited to the spindle relative to tubulin
(A) Immunostaining of spindle assembly reactions in *X. laevis* egg extracts in the presence of 100 nm recombinant GFP and GFP-tagged TPX2 proteins. Spindle reactions were sedimented onto coverslips before immunostaining. Scale bar = 10 μm. (B) Mean intensity measurements from bipolar spindles of recombinant TPX2/Tubulin fluorescence intensity ratio (Top), GFP fluorescence (middle), and Tubulin fluorescence (bottom). n = 3 different extracts, >27 spindles per biological replicate. Error bars indicate SD. One-way ANOVA results indicate significant differences between conditions (C) Immunoprecipitation of GFP and GFP-TPX2 proteins from CSF aster reactions with 500 nM protein added followed by immunoblot analysis using indicated antibodies. (D) Immunoprecipitation of GFP and GFP-TPX2 proteins from CSF aster reactions in the presence of DMSO or 1 μM MLN 8237. 500 nM protein was added for each condition followed by immunoblot analysis using indicated antibodies. **** = $p<0.0001$, *** = $p<0.001$, ** = $p<0.01$, * = $p<0.1$, ns = not significant.

In addition to inducing MT nucleation, Aurora A also regulates centrosome maturation and recruitment of pericentriolar material (PCM) (Magnaghi-Jaulin *et al.*, 2019). To investigate whether TPX2 NLS3 mutants also affected PCM assembly, we examined localization of pericentrin (PCNT), a core PCM component (Doxsey *et al.*, 1994). Quantification of PCNT immunostaining intensity on spindle poles revealed that, consistent with effects on Aurora A activation, the *X. tropicalis* NLS3 mutant recruited the highest levels of pericentrin, whereas tubulin intensity was not strongly affected (Figure 2.3). Overall, the effects of the NLS3 mutants on intensity were subtle. Like several PCM scaffold proteins, PCNT has been shown to undergo phase separation in human cells (Jiang *et al.*, 2021). In *C. elegans*, such condensates also contain XMAP215 as well as a TPX2-like protein (Woodruff *et al.*, 2017). It is tempting to speculate that the hollow pole phenotype observed when MT nucleation is stimulated by TPX2, particularly the *X. tropicalis* NLS3 mutant, is due to the formation of concentrically layered PCM proteins as well as SAFs that recruit soluble tubulin and drive MT assembly at the periphery, similar to what has been observed in acentrosomal mouse oocyte spindles (So *et al.*, 2019; Kraus *et al.*, 2023a). Further experiments are needed to examine the pole structures at higher resolution and the localization of other PCM and SAF proteins.

Figure 2.3

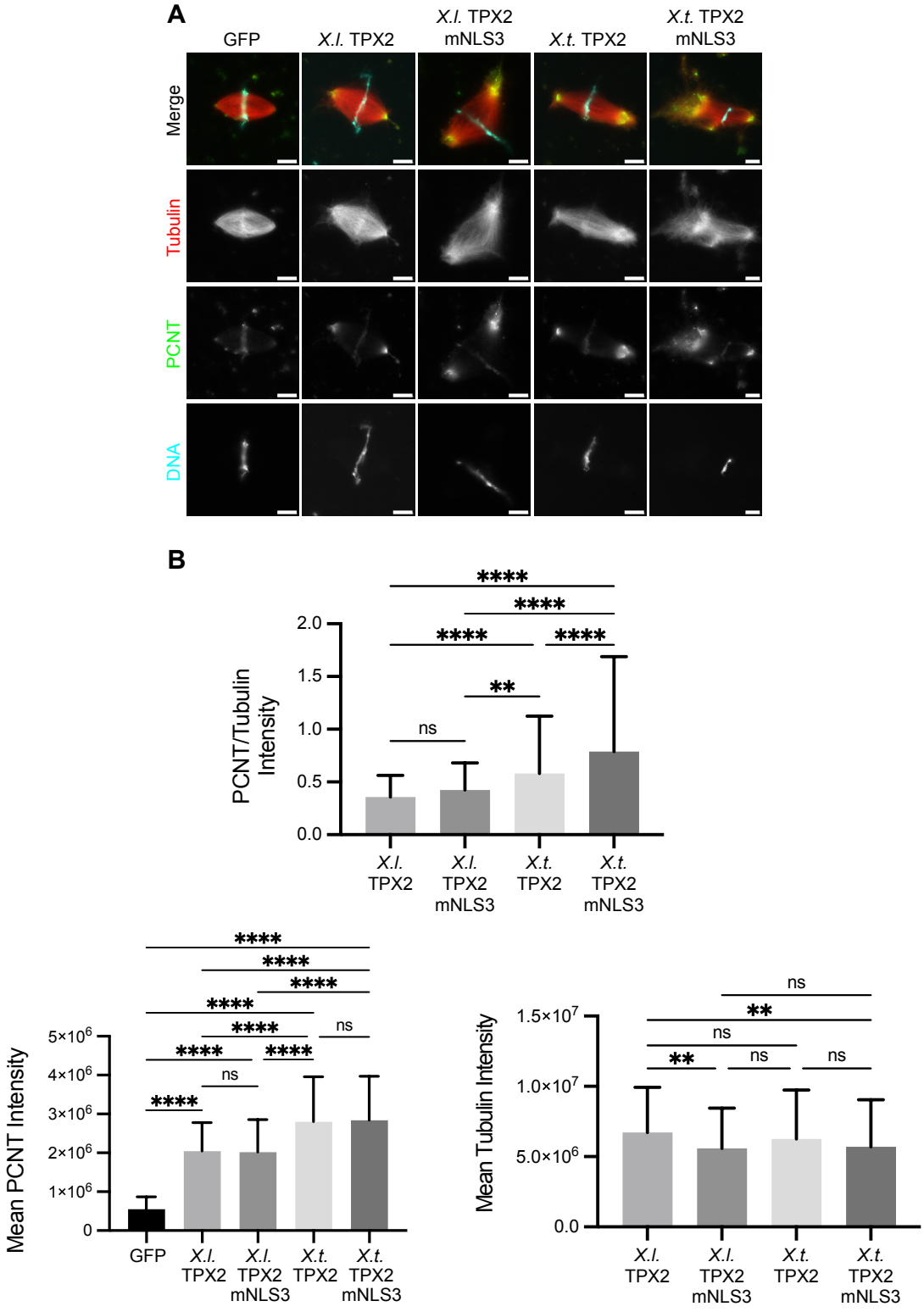
A
GFP
X.l. TPX2
X.l. TPX2 mNLS3
X.t. TPX2
X.t. TPX2 mNLS3
Merge
Tubulin
PCNT
DNA
B
PCNT/Tubulin Intensity
2.0
1.5
1.0
0.5
0.0
****
****
****
****
**
ns
X.l. TPX2
X.l. TPX2 mNLS3
X.t. TPX2
X.t. TPX2 mNLS3
Mean PCNT Intensity
5×10^6
4×10^6
3×10^6
2×10^6
1×10^6
0
****
****
****
****
****
****
ns
ns
GFP
X.l. TPX2
X.l. TPX2 mNLS3
X.t. TPX2
X.t. TPX2 mNLS3
Mean Tubulin Intensity
1.5×10^7
1.0×10^7
5.0×10^6
0.0
ns
**
ns
**
ns
ns
X.l. TPX2
X.l. TPX2 mNLS3
X.t. TPX2
X.t. TPX2 mNLS3

Figure 2.3:*X. tropicalis* TPX2 proteins recruit more pericentrin (PCNT) to spindle poles
(A) Immunostaining of spindle assembly reactions in *X. laevis* egg extracts in the presence of 100 nm recombinant GFP or GFP-tagged TPX2 proteins. Spindle reactions were sedimented onto coverslips before immunostaining for PCNT. Scale bar = 10 μm. *X.t*. TPX2 mNLS3 image is taken from a larger field of view. (B) Mean intensity measurements from spindle poles of GFP/Tubulin intensity ratio (Top), GFP fluorescence (bottom left), and Tubulin fluorescence (bottom right). n = 3 different extracts, >63 spindle poles per biological replicate. Error bars indicate SD. One-way ANOVA results indicate significant differences between conditions, **** = $p<0.0001$, ** = $p<0.01$, ns = not significant.

Xenopus wild type and NLS3 TPX2 mutants recruit both Eg5 and importin-α to spindles

An additional interacting protein of TPX2 is the class 5 kinesin-like motor protein Eg5 (Eckerdt *et al.*, 2008). Previously we showed that addition of recombinant TPX2 to *X. laevis* spindles increased the localization of Eg5 as well as MT bundling at spindle poles, altering spindle architecture (Helmke and Heald, 2014). This led us to test whether NLS3 mutants also affected Eg5 recruitment. Using immunostaining, we quantified total Eg5 intensity on spindles formed in the presence of each recombinant TPX2 protein, normalized to tubulin intensity, and observed that the *X. tropicalis* TPX2 NLS3 mutant increased Eg5 spindle recruitment relative to tubulin, whereas the *X. laevis* protein did not (Figure 2.4A and B). Interestingly, wildtype or mutant *X. tropicalis* TPX2 proteins recruited significantly more Eg5 to the spindle than the *X. laevis* proteins, indicating that *X. tropicalis* TPX2 binds more Eg5 (Figure 2.4B), which was corroborated by immunoprecipitation of the recombinant proteins from extract reactions and immunoblot analysis (Figure 2.4C). These findings indicate that the NLS3 motif acts additively to recruit Eg5 together with the previously identified deletion of a 7-a.a. sequence, 619-LSGSIVQ-625, in *X. tropicalis* TPX2. This 7-a.a. sequence is located just upstream of the C-terminal Eg5 binding domain (Δ7) (Helmke and Heald, 2014) and its deletion was shown to stimulate MT branching nucleation activity of *X. laevis* TPX2 (Alfaro-Aco *et al.*, 2017). Mechanistically, it remains unknown how these two regions of TPX2 that are hundreds of amino acids apart modulate its activity.

Figure 2.4

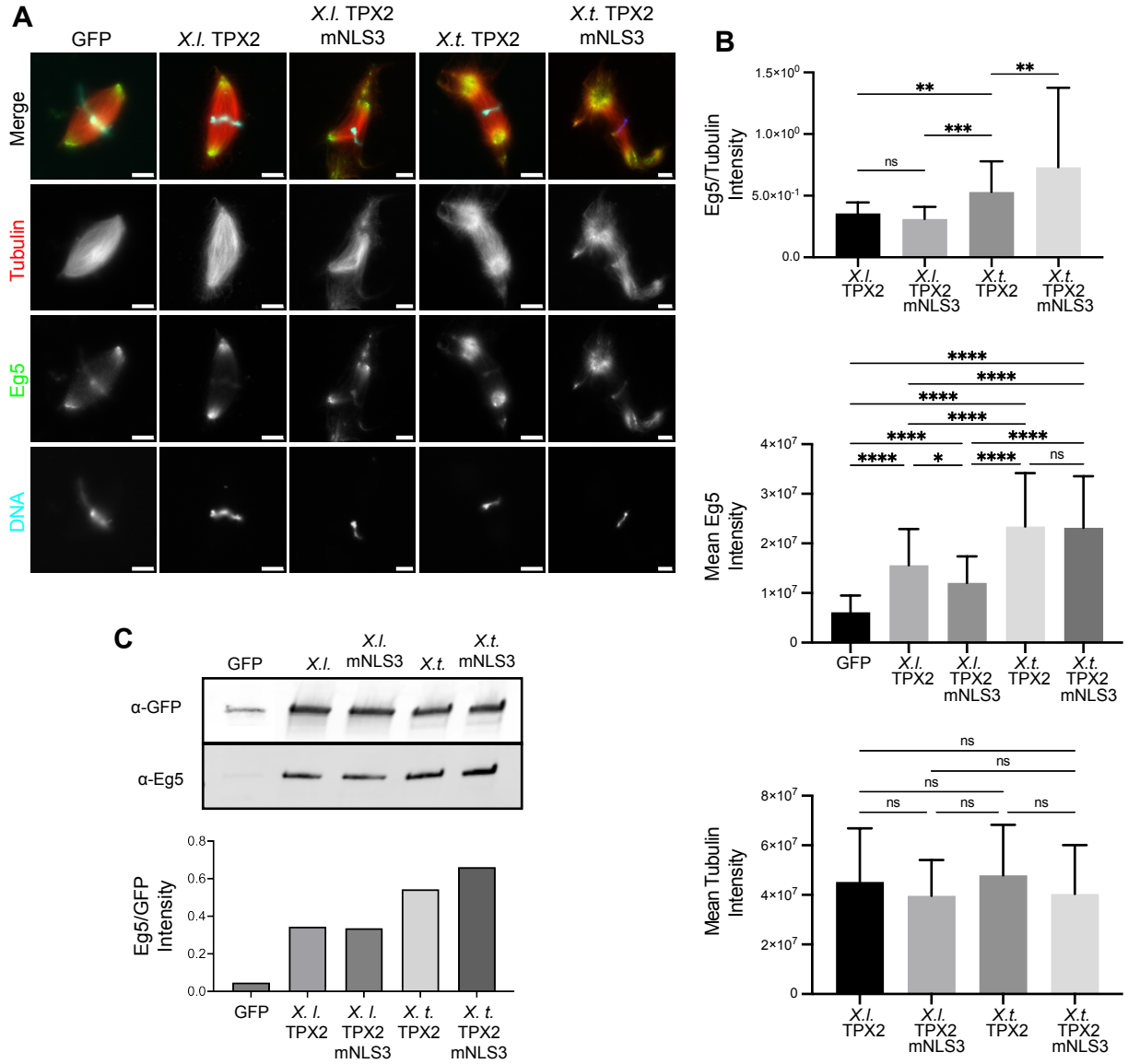

Figure 2.4: Increased recruitment of Eg5 to metaphase spindles upon addition of recombinant *X. tropicalis* wildtype and NLS3 mutant TPX2 proteins
(A) Immunostaining of spindle assembly reactions in *X. laevis* egg extracts in the presence of 100 nm recombinant GFP and GFP-tagged TPX2 proteins. Spindle reactions were sedimented onto coverslips before immunostaining for Eg5. Scale bar = 10 μm. *X.l.* TPX2 mNLS3 and *X.t.* TPX2 mNLS3 images are taken from a larger field of view. (B) Mean intensity measurements from whole spindles of GFP/Tubulin intensity ratios (Top) GFP fluorescence (middle) and Tubulin fluorescence (bottom. n = 3 different extracts, >23 spindles per biological replicate. Error bars indicate SD. One-way ANOVA results indicate significant differences between conditions, **** = p<0.0001, *** = p<0.001, ** = p<0.01, * = p<0.1, ns = not significant. (C) Immunoprecipitation of GFP

and GFP-TPX2 from CSF aster reactions supplemented with 500 nM recombinant protein followed by immunoblot analysis using indicated antibodies.

As a key Ran-regulated spindle assembly factor, TPX2 binds to importins and is released in the vicinity of mitotic chromosomes to stimulate MT polymerization and organization (Gruss *et al.*, 2001, 2002; Schatz *et al.*, 2003; Gruss and Vernos, 2004; Walczak and Heald, 2008; Cavazza and Vernos, 2016). Crystal structures of a truncated *X. laevis* TPX2 bound to importin-α demonstrated interaction through two NLS motifs located at 284-KRKH-287 (NLS1) and 327-KMIK-330 (NLS2) (Giesecke and Stewart, 2010). However, *in vitro* work measuring binding kinetics of TPX2 to importin-α showed that the NLS3 motif, 123-KKLK-126, alone confers a higher affinity for importin-α than the NLS1 and NLS2 sites do (Safari *et al.*, 2021). We therefore investigated the contribution of TPX2 NLS3 to importin-α spindle localization and binding in egg extract. Immunofluorescence and quantification of total importin-α intensity on spindles normalized to tubulin revealed that addition of *X. laevis* NLS3 mutant TPX2 slightly reduced importin-α recruitment compared wildtype, while the *X. tropicalis* TPX2 NLS3 mutant showed a slight increase in importin-α levels (Figure 2.5A and B). By immunoprecipitation and immunoblot analysis, we found that both *X. laevis* and *X. tropicalis* TPX2 NLS3 mutant proteins still bound to importin-α (Figure 2.5C), which is perhaps not surprising since NLS1 and NLS2 were intact

Figure 2.5

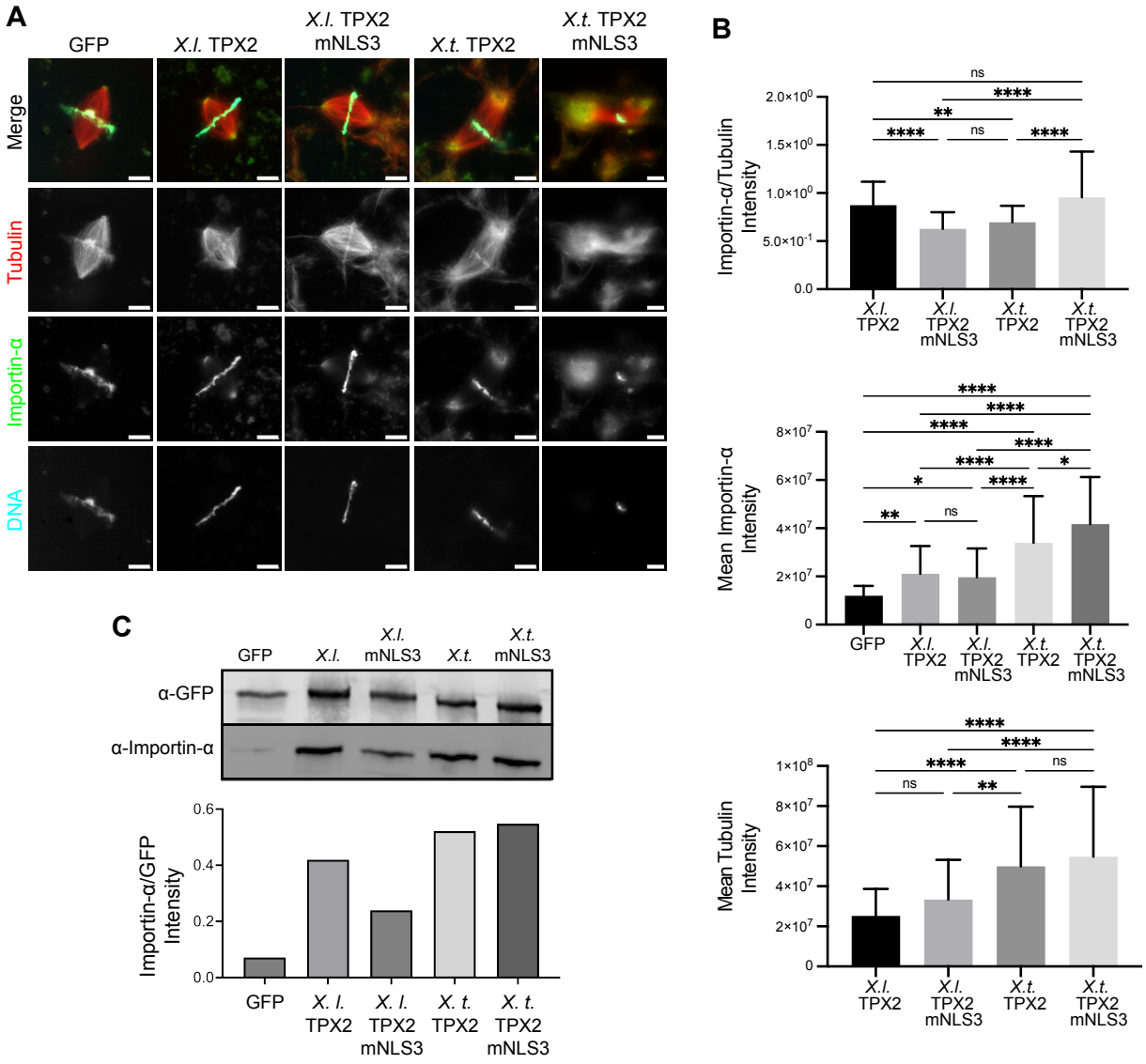

Figure 2.5: *X. laevis* and *X. tropicalis* TPX2 NLS3 mutants localize importin-α to spindle poles

(A) Immunostaining of spindle assembly reactions in *X. laevis* egg extracts in the presence of 100 nm recombinant GFP and GFP-tagged TPX2 proteins. Spindle reactions were sedimented onto coverslips before immunostaining for importin- α. Scale bar = 10 μm. *X.t.* TPX2 mNLS3 image is taken from a larger field of view. (B) Mean intensity measurements from bipolar spindles of GFP/Tubulin intensity ratio (Top), GFP fluorescence (middle), and Tubulin intensity ratio (bottom). n = 3 different extracts, >21 spindles per biological replicate. Error bars indicate SD. One-way ANOVA results indicate significant differences between conditions, **** = p<0.0001, ** = p<0.01, * = p<0.1, ns = not significant. (C) Immunoprecipitation of GFP and GFP-TPX2 from CSF

aster reactions supplemented with 500 nM recombinant protein followed by immunoblot analysis using indicated antibodies.

Previous work has shown how importin-α can spatially regulate the minus-end-directed kinesin motor, XCTK2, on spindle MTs (Ems-McClung *et al.*, 2004; Weaver *et al.*, 2015). Near the chromatin, XCTK2 is released from importins by RanGTP crosslinks MTs while also sliding both parallel and antiparallel MTs. At the spindle poles, XCTK2 MT crosslinking ability is selectively inhibited by importin-α, allowing for differential activity based on its location in the spindle (Ems-McClung *et al.*, 2004; Weaver *et al.*, 2015). Our results indicate that importin-α does not block TPX2 activity in the spindle. Furthermore, recruitment of importin-α by *X. tropicalis* TPX2 NLS3 mutant may suggest an alternative role for importin-α at spindle poles. *In vitro*, a truncated version of importin-α has been shown to enhance TPX2 condensation (Safari *et al.*, 2021). There is also evidence that importin-α isoforms can form dimers *in vitro* and simultaneously bind to a single cargo containing a bipartite NLS (Miyamoto and Oka, 2016; Matsuura, 2023). Given these findings, importin-α could enhance TPX2 activity at the spindle poles by functioning as a point of multivalency, facilitating interactions among various SAFs. Future experiments involving TPX2 mutants lacking all NLSs will inform how importin-α recruitment contributes to LLPS, MT polymerization and spindle pole morphology.

Overall, our study demonstrates that an NLS mutation and a small deletion in TPX2 produce a gain of function phenotype by increasing recruitment of several TPX2-interacting proteins to spindle poles, increasing PCM levels, Aurora A activation, and astral MT polymerization. We also highlight how comparison of TPX2 from even closely related frog species provides insight into how differences in TPX2 sequence affect spindle architecture. Whether and how TPX2 activity is regulated at the transition between oocyte meiosis and zygotic mitosis, remains an important open question. Nonetheless, this work supports the notion that TPX2 is a linchpin for spindle assembly. Further exploring its structure-function relationships and regulation will be key to unraveling the role of TPX2 in determining spindle architecture and how changes in MT organization affect the fidelity of chromosome segregation.

Material and Methods

Xenopus egg extract and spindle assembly reactions

All frogs were used and maintained following standard protocols established by the UC Berkeley Animal Care and Use Committee and approved in our Animal Use Protocol. Egg extracts from *X. laevis* were prepared as previously described (Hannak and Heald, 2006; Maresca and Heald, 2006). Briefly, eggs were dejellied and then fractionated in a Sorvall HB-6 rotor for 16 min at 10,200 rpm. The cytoplasmic layer was then isolated and supplemented with 10 µg/ml LPC, 20 µg/ml CytoB, 1× energy mix, and 0.3 µM rhodamine-labeled porcine tubulin. Spindle reactions contained 50 µl cytostatic-factor (CSF) metaphase-arrested extract and *X. laevis* sperm at a final concentration of 500 nuclei per µl. Recombinant protein and inhibitors were added before the start of spindle assembly reactions, which were carried out in a 18°C water bath and flicked every 10–15 min until spindle assembly was complete, approximately 45 min.

Protein Purification

Table 2.1 Proteins used in study

Name	***Description***	***Source***
X. l. TPX2	*6xHis-mGFP-XLTPX2-StrepII*	*This paper. Plasmids and genes sourced from in-house plasmids.*
X. l. TPX2 mNLS3	*6xHis-mGFP-XLTPX2-123-AALA-126-StrepII*	
X. t. TPX2	*6xHis-mGFP-XTTPX2-StrepII*	
X. t. TPX2 mNLS3	*6xHis-mGFP-XTTPX2-123-AALA-126-StrepII*	
GFP	*6xHis-mGFP-StrepII*	

6xHis-mGFP-StrepII and 6xHis-mGFP-TPX2-StrepII *X. laevis* and *X. tropicalis* proteins were cloned into the pHAT2 vector (Addgene #112583) using NEBuilder HiFi DNA Assembly Master Mix (NEB #E2621). Proteins were transfected into Rosetta2 (DE3) pLysS *E. coli* cells (QB3 Berkeley Macro Lab) and grown to an OD of ~0.35 at 37°C and then moved to 16°C until an OD of 0.5-0.7 was reached. Protein expression was induced with 750 nM Isopropyl ß-D-1-thiogalactopyranoside (IPTG) and carried out for 5-8 hours at 27°C. Cells were pelleted, resuspended in lysis buffer (50 mM Hepes, 20 mM Imidazole, 750 mM NaCl, 5 mM MgCl2, 25 mM sucrose, pH 7.75) containing 3 µM Avidin (Thermo Fisher # A887) 200 µM phenylmethylsulfonyl fluoride (PMSF), 10 µg/ml LPC, 5 mM β-mercaptoethanol (βME), cOmplete™ EDTA-free Protease Inhibitor tablet (Roche #11873580001), 10 µg/ml DNase I (Roche #10104159001) and flash frozen to be stored in -80°C for purification the following day. After thawing, resuspended cells were supplemented with Bug Buster protein reagent (Millipore #70584-3) before being sonicated. Lysate was centrifugated in a Sorvall SS-34 fixed

angle rotor for 30 min at 4°C. Cleared lysate was flowed over pre-equilibrated HisPur™ Ni-NTA Resin (Thermo Fisher #88223) in a gravity column. The column was washed with 2x with 5 CV. Protein was eluted using lysis buffer with 0.5 M imidazole then underwent buffer exchange using via Sephadex G-25 in PD-10 Desalting Columns (Cytiva #17085101) into strep buffer (50 mM Hepes, 75 mM NaCl, 5 mM MgCl2, 25 mM sucrose, 5 mM EDTA, pH 7.75) containing 200 µM phenylmethylsulfonyl fluoride (PMSF), 10 µg/ml LPC, 5 mM β-mercaptoethanol (βME), cOmplete™ EDTA-free Protease Inhibitor tablet (Roche #11873580001). Eluant was then run over a pre-equilibrated Strep-Tactin®XT 4Flow® high capacity resin (IBA # 2-5030-010) gravity column. The column was washed 3x with 2 column volumes and protein eluted using strep elution buffer (50 mM Hepes, 75 mM NaCl, 5 mM MgCl2, 50 mM arginine, 50 mM glutamate, 25 mM sucrose, 50 mM Biotin, pH 7.75). Eluant was concentrated using Amicon® Ultra Centrifugal Filter (Millipore #UFC9100) then buffer exchanged into XB buffer (10 mM Hepes, 2 mM MgCl2, 1 mM CaCl2, 10% w/v sucrose, pH 7.75) using Zeba spin desalting column (Thermo Fisher #87766).

Immunofluorescence of spindles in egg extracts

Spindle reactions were fixed and processed for immunofluorescence as described in (Hannak and Heald, 2006). 50 µl reactions were fixed with a spindle dilution buffer (80 mM Pipes, 1 mM $MgCl_2$, 1 mM EGTA, 30% glycerol, 0.5% Triton X-100) containing 3.7% formaldehyde for 5-10 min with rotation at 23°C. Fixed reaction were spun down onto coverslips through a cushion buffer (BRB80 + 40% glycerol) at 5,000 rpm for 20 min at 16°C using a Sorvall HS-4. Coverslips were postfixed for 5 min in 100% cold methanol, rinsed with PBS-0.1%NP40, blocked with PBS–3% BSA for 45 min. Primary antibodies against GFP (diluted 1:500), pT295-AurA (1: 1,000), PCNT (1:250), Eg5 (1: 2,500), or importin-α (1: 2000) were added overnight in a humidified chamber at 4°C. The following steps were carried out at room temperature. Coverslips were rinsed 3x quickly with PBS-0.1%NP40, then 3x for 5 min. Secondary antibodies (Invitrogen; Goat anti-rabbit or Goat anti-rabbit IGG conjugated to Alexa Fluor 488, 1:500) were added and incubated for 30 min. Coverslips were rinsed 3x quickly with PBS-0.1%NP40, then 3x for 5 min. 5 µg/ml Hoechst 33258 (Sigma) was added for 10 min before mounting with ProLong™ Glass Antifade Mountant (Thermo Fisher).

Imaging and Analysis

Images were acquired using an epifluorescence Olympus BX51 microscope with an Olympus PlanApo 63x oil objective and Hamamatsu ORCA-II camera. Exposure times for each channel were set for the sample with the highest fluorescence intensity and kept constants for all replicates of that experiment. Whole spindle and spindle poles were cropped from rest of image using a square ROI, 512 X 512 pixels for whole spindles and 200 x 200 pixels for spindle poles. Median intensity values were used to perform background subtractions in each channel. All fluorescence intensities were measure using FIJI software. Statistical significance was determined by one-way

ANOVA using GraphPad Prism version 10.0.0 for MacOS, GraphPad Software, Boston, Massachusetts, USA, www.graphpad.com. p values are listed in the figure legend. Calculations of raw data were performed in R (version 3.3.0)

Immunoprecipitation and Western blotting

CSF aster reactions were used to perform all immunoprecipitation experiments. Reactions were set up similarly to spindle reactions except without sperm DNA and in the presence of 500 nM recombinant protein for each condition. Proteins and 1μM MLN 8237 inhibitor or DMSO were added prior to initiation of extract reactions, which were incubated for 40 min in an 18°C water bath and flicked every 10–15 min. Each reaction was then added to Strep-Tactin®XT 4Flow® high capacity resin (IBA # 2-5030-010) pre-equilibrated with XB buffer supplemented with cOmplete™ EDTA-free Protease Inhibitor tablets (Roche #11873580001) and/or PhosSTOP™ Phosphatase Inhibitor Tablets (Roche # 04906845001). Samples incubated with rotation at 4°C were each washed with 700 μl of XB buffer. After the initial wash, samples were pelleted at max speed for 1 min in a tabletop centrifuge. Supernatant was carefully removed followed by two more washes with 700 μl XB buffer + 0.1% triton x-100. After the last wash, samples were pelleted and resuspended in 1X SDS sample buffer and boiled for 10 min. For Western blot analysis, 25% of sample was run on a SDS-PAGE gel. Wet transferers were carried out using nitrocellulose membrane (Thermo Fisher #). Blots were blocked with either 5% milk + PBS-0.1% Tween or 5% BSA + PBS-0.1% Tween for 1 hour at room temperature then washed with 1xTBST or 1xTBS 3x quickly then 3x for 5 min. Primary antibodies diluted in blocking buffer against GFP (1:1000), pT295-AurA (1:1,000), Eg5 (1:2,500), or importin-α (1:2000) were incubated overnight at 4°C with rotation. Blots were washed with 1xTBST or 1xTBS 3x quickly then 3x for 5 min before incubating with secondary antibodies Alexa Fluor 700 goat-anti-rabbit IgG (Invitrogen # A21038) or IRDye-800CW goat anti-mouse IgG (LI-COR # 926-32210) diluted in blocking buffer for 1 hour at room temperature. Blots were washed with 1xTBST or 1xTBS 3x quickly then 3x for 5 min then scanned on an Odyssey Infrared Imaging System (LI-COR Biosciences). Band intensities were quantified using Fiji.

Supplemental Figures

Supplemental Figure 2.1

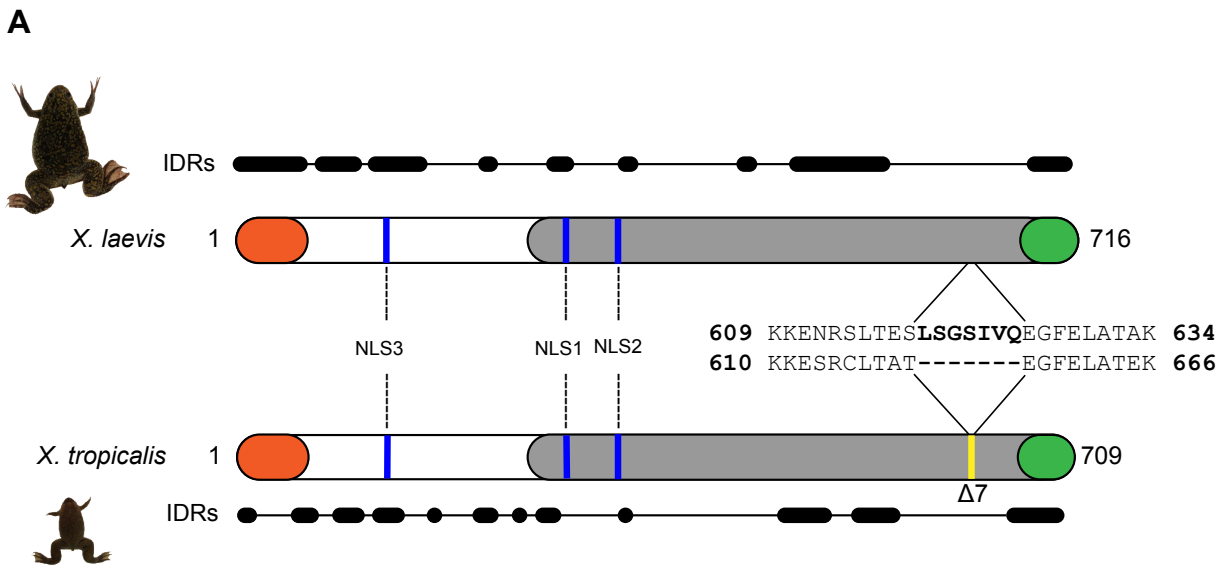

Supplementary Figure 2.1: Schematic of TPX2 domains in *X. laevis* and *X. tropicalis*
N-terminal Aurora A binding domain (orange; (Bayliss *et al.*, 2003)) and C-terminal Eg5 binding domain (green; (Bayliss *et al.*, 2003; Eckerdt *et al.*, 2008)). Mapped NLS1 (^{284}KRKH^{287}), NLS2 (^{327}KMIK^{330}) (Giesecke and Stewart, 2010) and NLS3 (^{123}KKLK^{126}) (Safari *et al.*, 2021) *X. tropicalis* NLS2 (^{328}KMVR^{331}). Region known to interact with MT and stimulate nucleation *in vitro* (gray; (Roostalu *et al.*, 2015; Zhang *et al.*, 2017)). Zoomed in view of sequence alignment between *X. laevis* and *X. tropicalis* highlighting 7-aa deletion (Δ7) in *X. tropicalis* (yellow; (Helmke and Heald, 2014)). Disordered regions are predicted using flDPnn program (Hu *et al.*, 2021).

Supplemental Figure 2.2

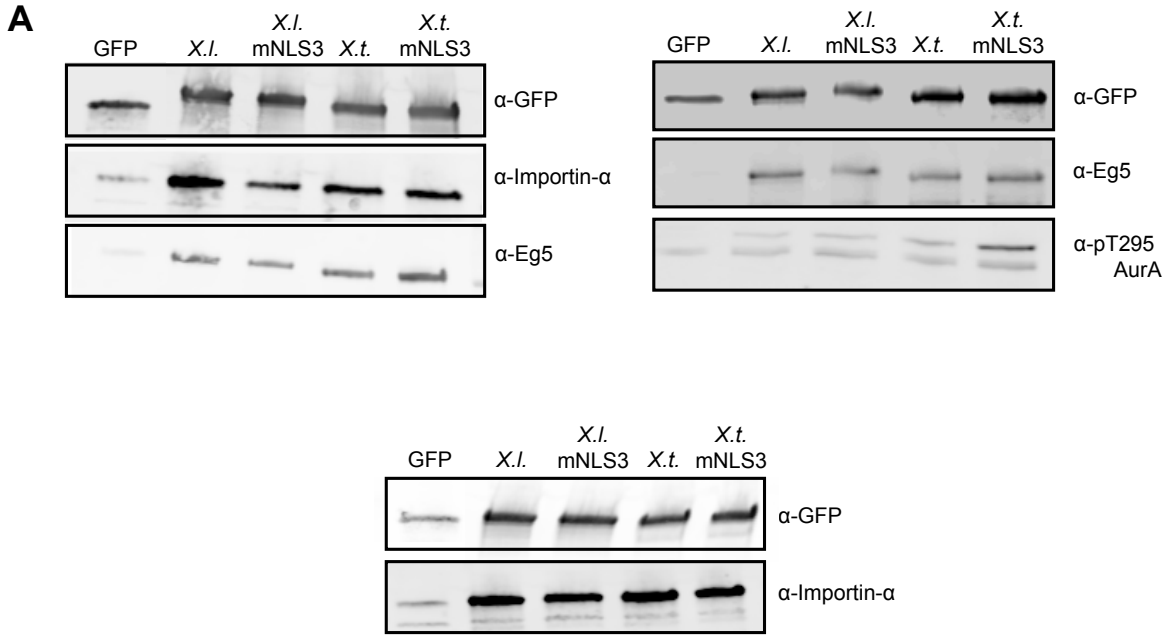

Supplementary Figure 2.2: Additional immunoprecipitation western blots in *Xenopus* egg extract

(A) Immunoprecipitation of GFP and GFP-TPX2 from CSF aster reactions supplemented with 500 nM recombinant protein followed by immunoblot analysis using indicated antibodies.

Supplemental Figure 2.3

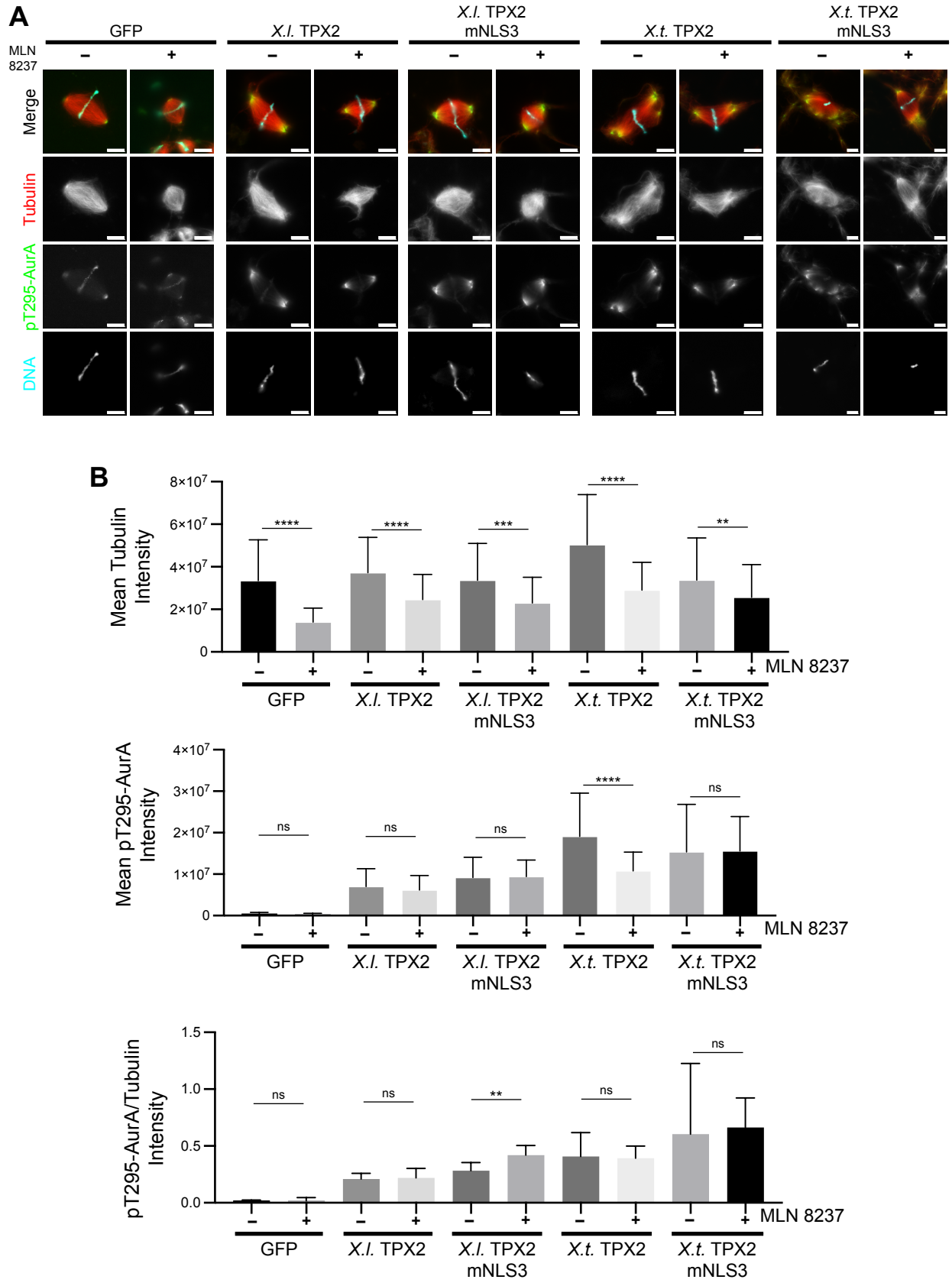

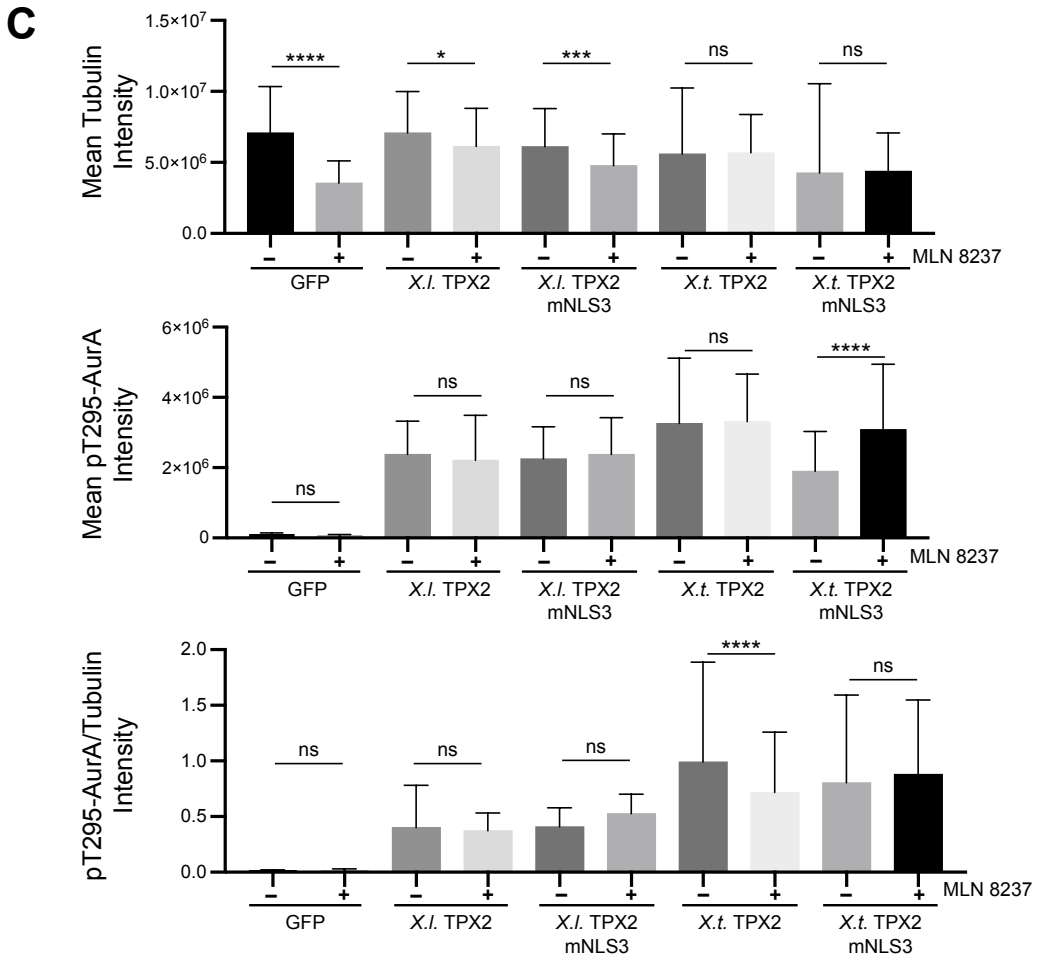

Supplementary Figure 2.3: Inhibition of Aurora A by MLN 8235 inhibitor decreases tubulin intensity in spindles in the presence of *X. laevis* and *X. tropicalis* TPX2 NLS3 motif mutants

(A) Immunostaining of spindle assembly reactions in *X. laevis* egg extracts with 100 nm recombinant GFP and GFP-tagged TPX2 proteins and DMSO or 1 μM MLN 8237. Spindle reactions were sedimented onto coverslips before immunostaining. Scale bar = 10 μm. *X.t*. TPX2 mNLS3 image is taken from a larger field of view. (B) Mean intensity measurements from bipolar spindles of GFP fluorescence (Top), Tubulin fluorescence (middle), and GFP/Tubulin intensity ratio (bottom). n = 3 different extracts, >23 spindles per biological replicate for DMSO and >33 spindles per biological replicate for MLN 8237. Error bars indicate SD. One-way ANOVA results indicate significant differences between conditions, ****p<0.0001, ***= p<0.001, ** = p<0.01, ns = not significant. (C) Mean intensity measurements from spindle poles of GFP fluorescence (Top), Tubulin fluorescence (middle), and GFP/Tubulin intensity ratio (bottom). n = 3 different extracts, >39 spindle poles per biological replicate for DMSO and >52 spindle poles per biological replicate for MLN 8237. Error bars indicate SD. One-way ANOVA results indicate significant differences between conditions, **** = p<0.0001, *** = p<0.001, ** = p<0.01, * = p<0.1, ns = not significant.

Supplemental Figure 2.4

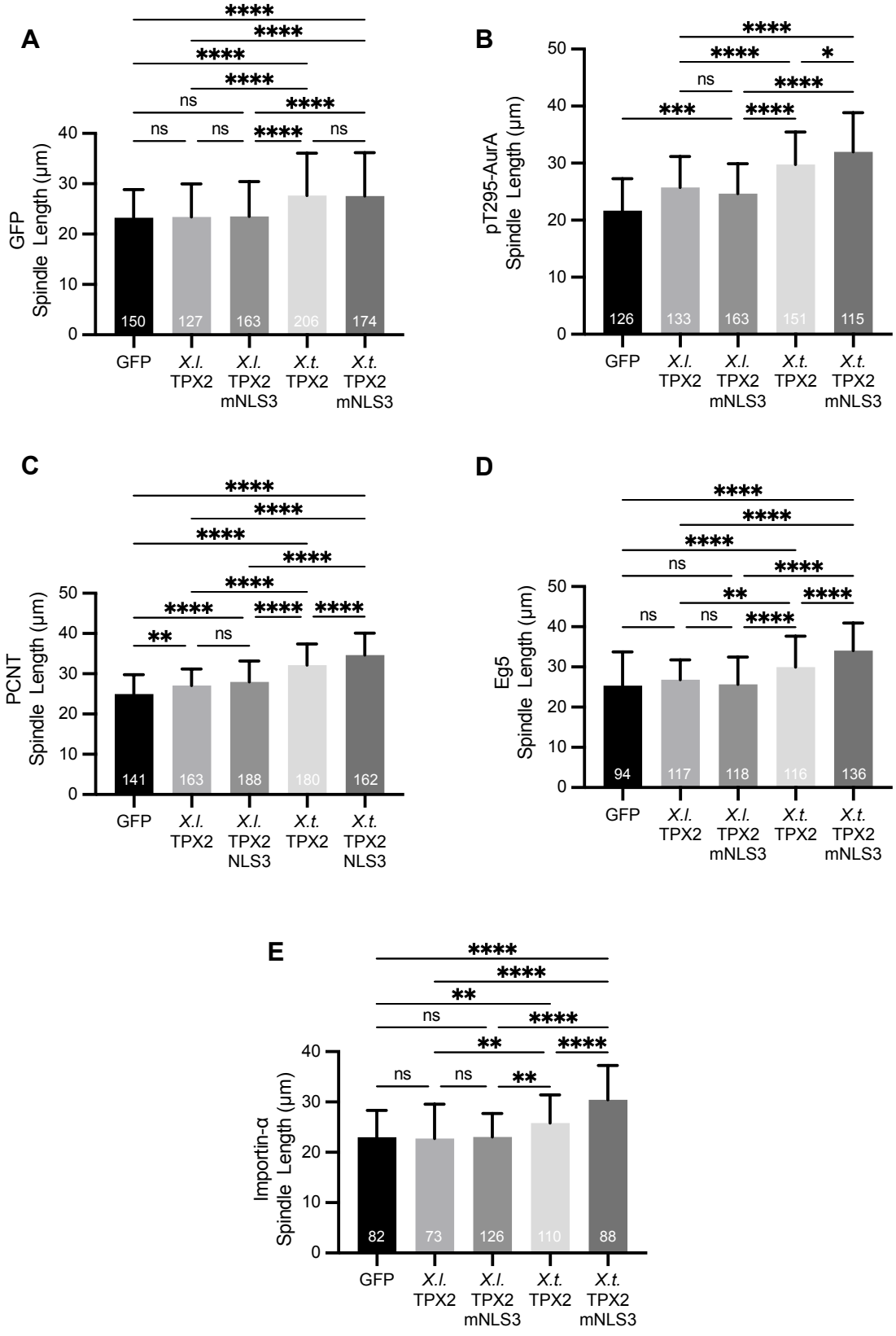

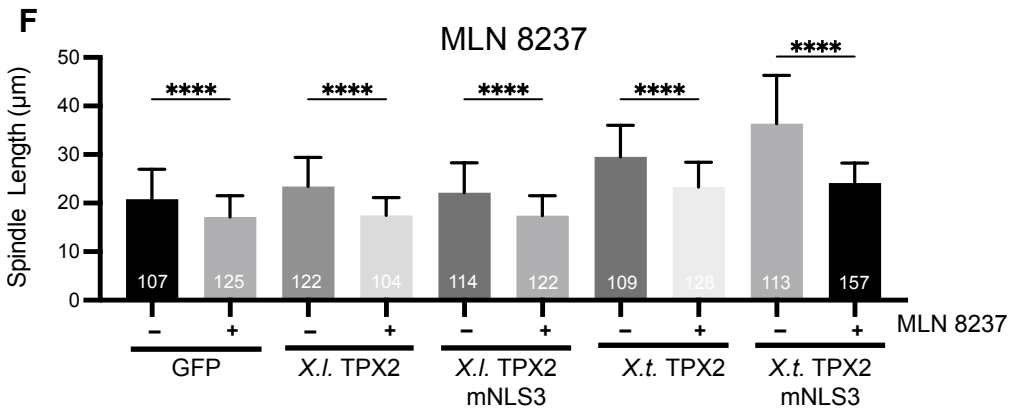

Supplementary Figure 2.4: Spindle length analysis
(A-F) Spindle length quantification using line scan data from each figure. One-way ANOVA results indicate significant differences between conditions, **** = p<0.0001, *** = p<0.001, ** = p<0.01, * = p<0.1, ns = not significant. n = 3 biological replicates, sample size per experiment noted on columns for each condition.

Unpublished Findings

Further characterization of the NLS3 motif of *Xenopus laevis* TPX2

The NL3 motif of TPX2 contains three lysine residues that are positively charged and can undergo a variety of post-translational modifications (PTMs) that regulate protein activities and interactions (Wang and Cole, 2020). When mutating this motif from 123KKLK126 to 123AALA126, we neutralized the charge of the lysine residues and eliminated the possibility of PTMs. To discern whether a PTM or the positive charge of NLS3 regulated the activity of TPX2, we generated *X. laevis* TPX2 NLS3 mutants containing arginine (R) residues, 123RRLR126. Arginine is similar in structure and charge to lysine but is not similarly modified post-translationally. When added to *Xenopus laevis* CSF egg extract, NLS3 RRLR mutant generated ectopic MT asters similar to the NLS3 AALA mutant in spindle and MT aster reactions (Figure 2.6A and B). Further analysis and experiments are required to determine if NLS3 RRLR mutants can actively recruit PCM, activate Aurora A, and bind more Eg5 like NLS3 AALA mutants, and if this is due to a lack of PTMs on these residues.

Figure 2.6

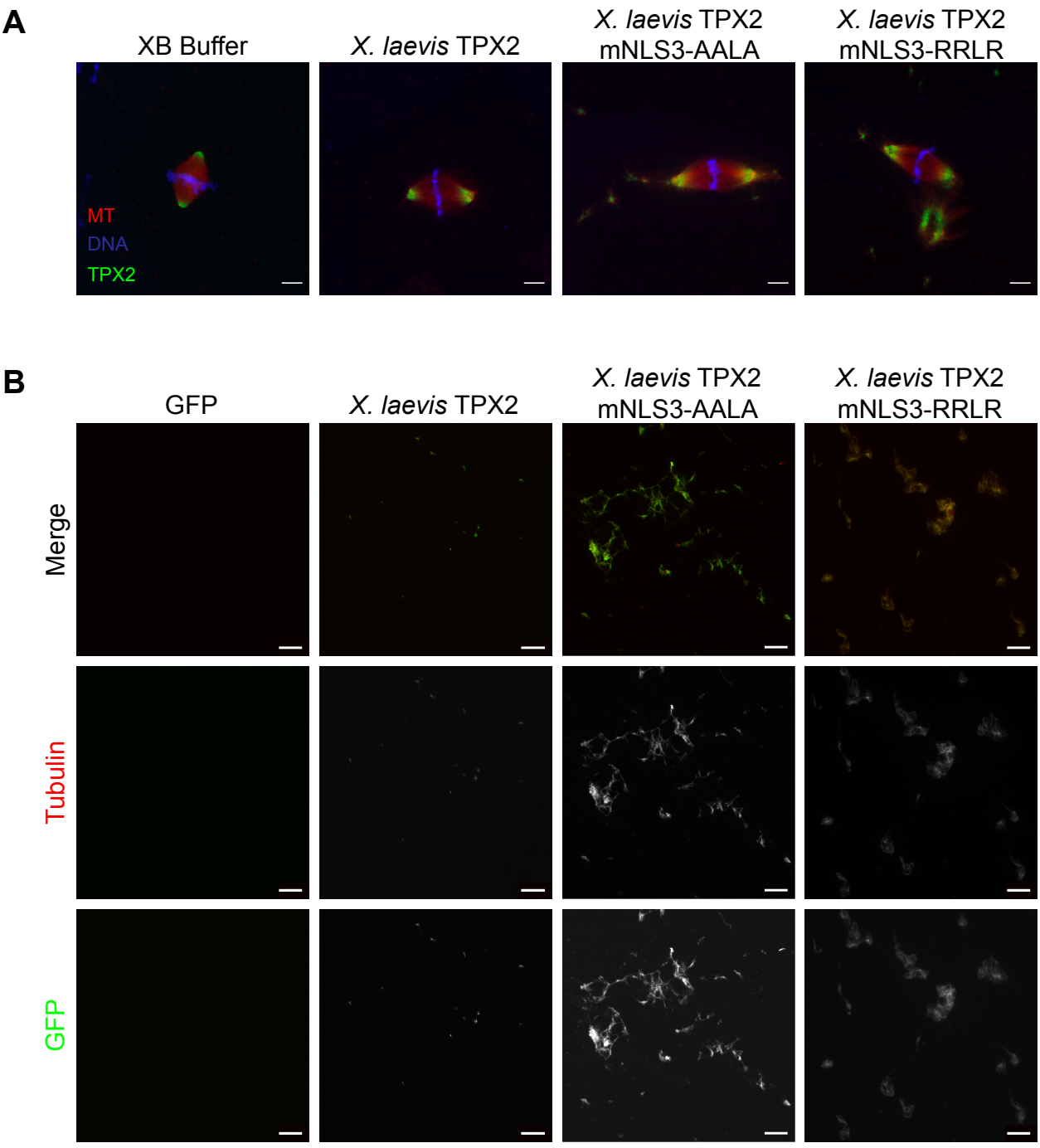

Figure 2.6: NLS3 RRLR motif mutant produces ectopic MT asters
(A) Immunostaining of spindle assembly reactions in *X. laevis* egg extracts with 100 nM recombinant GFP and GFP-tagged TPX2 proteins added. Scale bars = 10 μm. (B) Immunostaining of MT aster reactions in *X. laevis* egg extracts with 200 nM recombinant GFP and GFP-tagged TPX2 proteins (No DNA). Scale bars = 10 μm.

Phylogenetic comparison of TPX2

Although TPX2 is essential for spindle assembly, its protein sequence is not well conserved across many species. There is no yeast homolog of TPX2 and several organisms have dramatically altered protein sequences and contain only a subset of conserved domains. For example, *C. elegans* TPX2 ortholog TPXL-1 is significantly shorter than *X. laevis* and human TPX2 and shares homology only with N-terminal residues responsible for Aurora A binding and activation (Özlü *et al.*, 2005). The *Drosophila* ortholog, D-TPX2, is also significantly smaller than TPX2 found in vertebrates. D-TPX2 not only lacks the C-terminal Eg5 binding domain but also the N-terminal Aurora A binding domain and contains only the three conserved central domains important for MT binding (Goshima, 2011). Given the sequence diversity of TPX2 across various organisms, we performed a broader phylogenetic comparison across various TPX2 homologs. This comparison identified several marine invertebrate species, including the purple sea urchin *Strongylocentrotus purpuratus* and the sea squirt *Ciona intestinalis,* which possess a significantly longer N-terminal domain. The longer N-terminal regions were overall not well conserved like *Xenopus* TPX2 and were also highly disordered and unstructured (Figure 2.7 and 2.10). However, NLS1 and NLS3 motif were highly conserved and located within the disordered N-terminus as in *Xenopus* TPX2 (Figure 2.10).

Figure 2.7

X. laevis TPX2

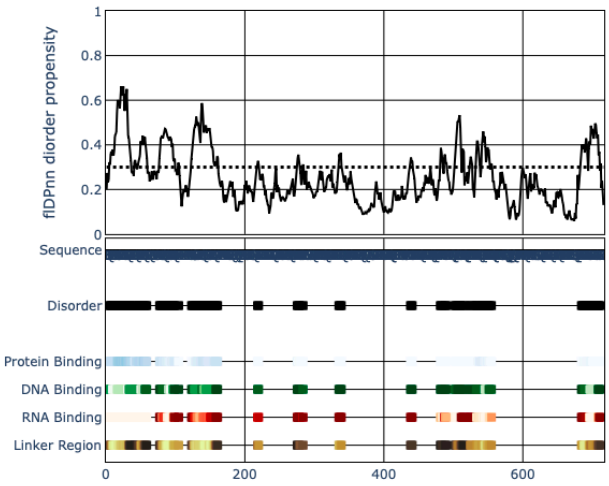

S. purpuratus TPX2

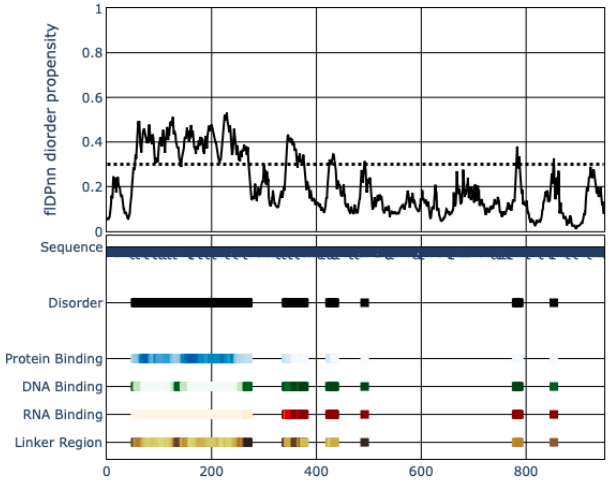

C. intestinalis TPX2

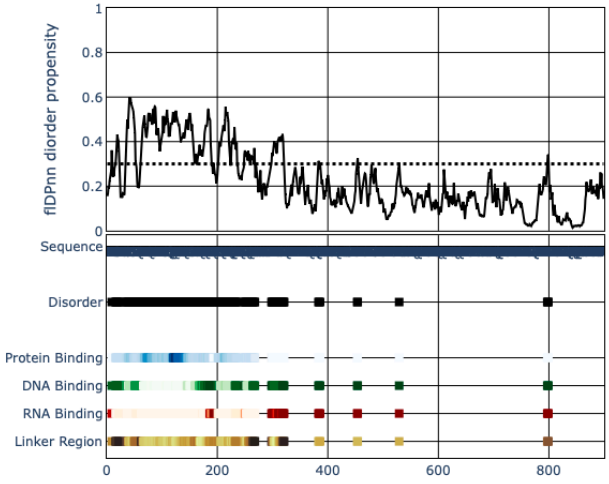

Figure 2.7: Sequence analysis of TPX2 homologs
Disordered regions were predicted using fIDPnn program (Hu *et al.*, 2021) for *Xenopus laevis* TPX2, *Strongylocentrotus purpuratus* TPX2 and *Ciona intestinalis* TPX2.

Characterization of wild type and NLS3 mutant TPX2 proteins of *Strongylocentrotus purpuratus*

We next wanted to understand if mutating the NLS3 motif in these TPX2 homologs would produce the same effects observed with *X. laevis* and *X. tropicalis* NLS3 mutants. Due to issues with protein expression, we only successfully produced GFP0tagged wildtype *S. purpuratus* TPX2 and *S. purpuratus* TPX2 NLS3 (352AAAA355) mutant proteins. When added to spindle assembly reactions in *Xenopus* CSF extract at 100 nM, both wildtype and NLS3 mutant *S. purpuratus* TPX2 proteins generated spindle-like structures surrounded by vast networks of MTs (Figure 2.8A). Notably, in the MT meshwork there were many tubulin-rich foci that often appeared in pairs (Figure 2.8B). Interestingly, both wildtype and NL3 mutant *S. purpuratus* TPX2 proteins recruited p295T-Aurora A to these foci and the NLS3 mutant appeared to increase levels of activated Aurora A across the vast MT meshwork (Figure 2.9A). Increased activation of Aurora A was also confirmed biochemically in *Xenopus* egg extracts by immunoprecipitation of S. purpuratus TPX2 protein in MT aster reaction (Figure 2.9B). Further quantitative analysis is required to determine if *S. purpuratus* TPX2 is increasing MT nucleation and activation of Aurora A and if this leads to the formation of focal MTOCs such as centrioles.

Figure 2.8

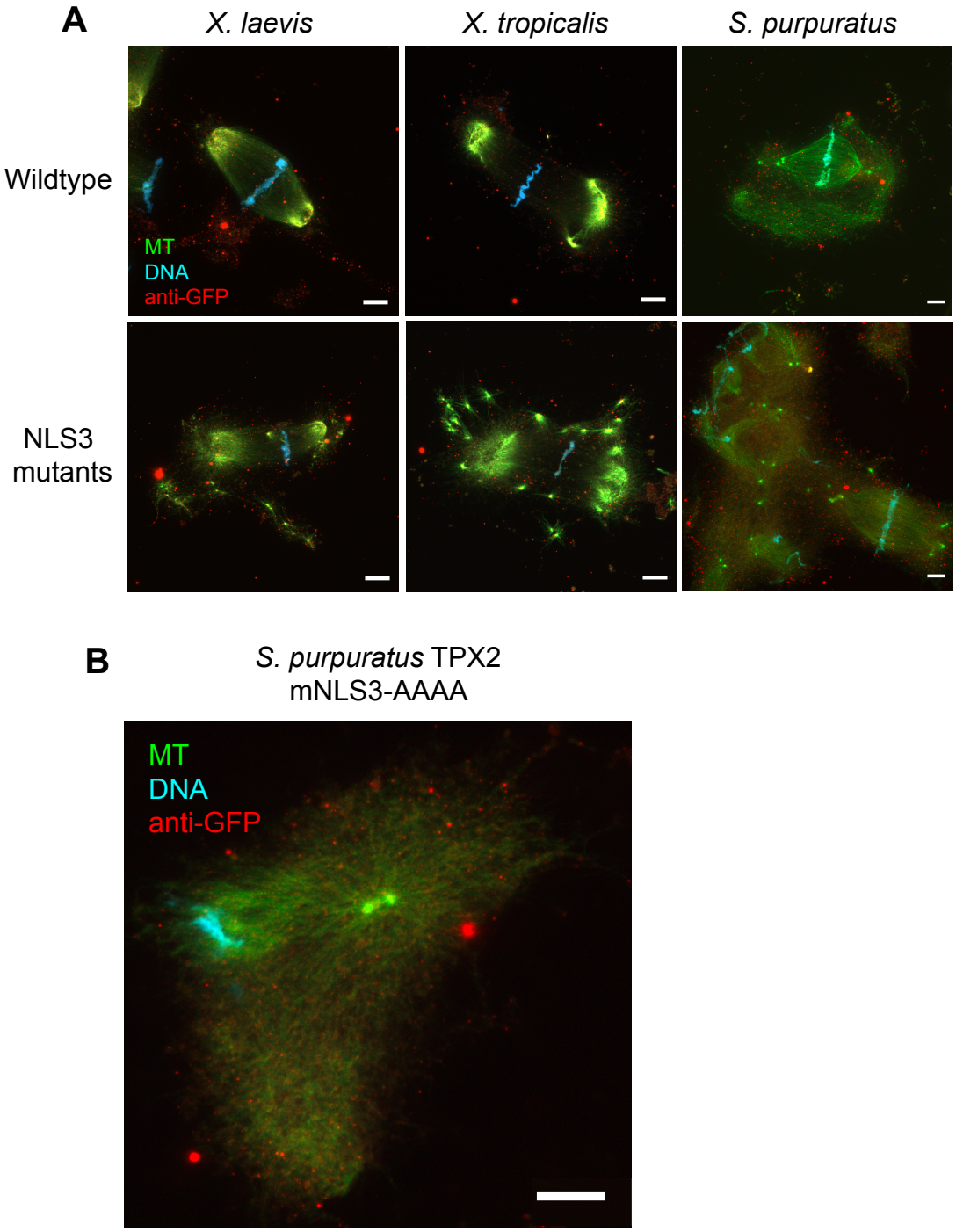

Figure 2.8: Both wildtype and NLS3 mutant S. purpuratus TPX2 proteins produce large MT networks with MT rich foci in CSF extract
(A) Immunostaining of spindle assembly reactions in *X. laevis* egg extracts with 100 nM recombinant GFP and GFP-tagged TPX2 proteins. Scale bars = 10 μm. (B) Zoomed in view of MT rich foci in spindle reaction with *S. purpuratus* NLS3 TPX2 mutant, Scale bar

= 10 μm. Fluorescent HiLyte 488 Tubulin from Cytoskeleton was used for only this experiment.

Figure 2.9

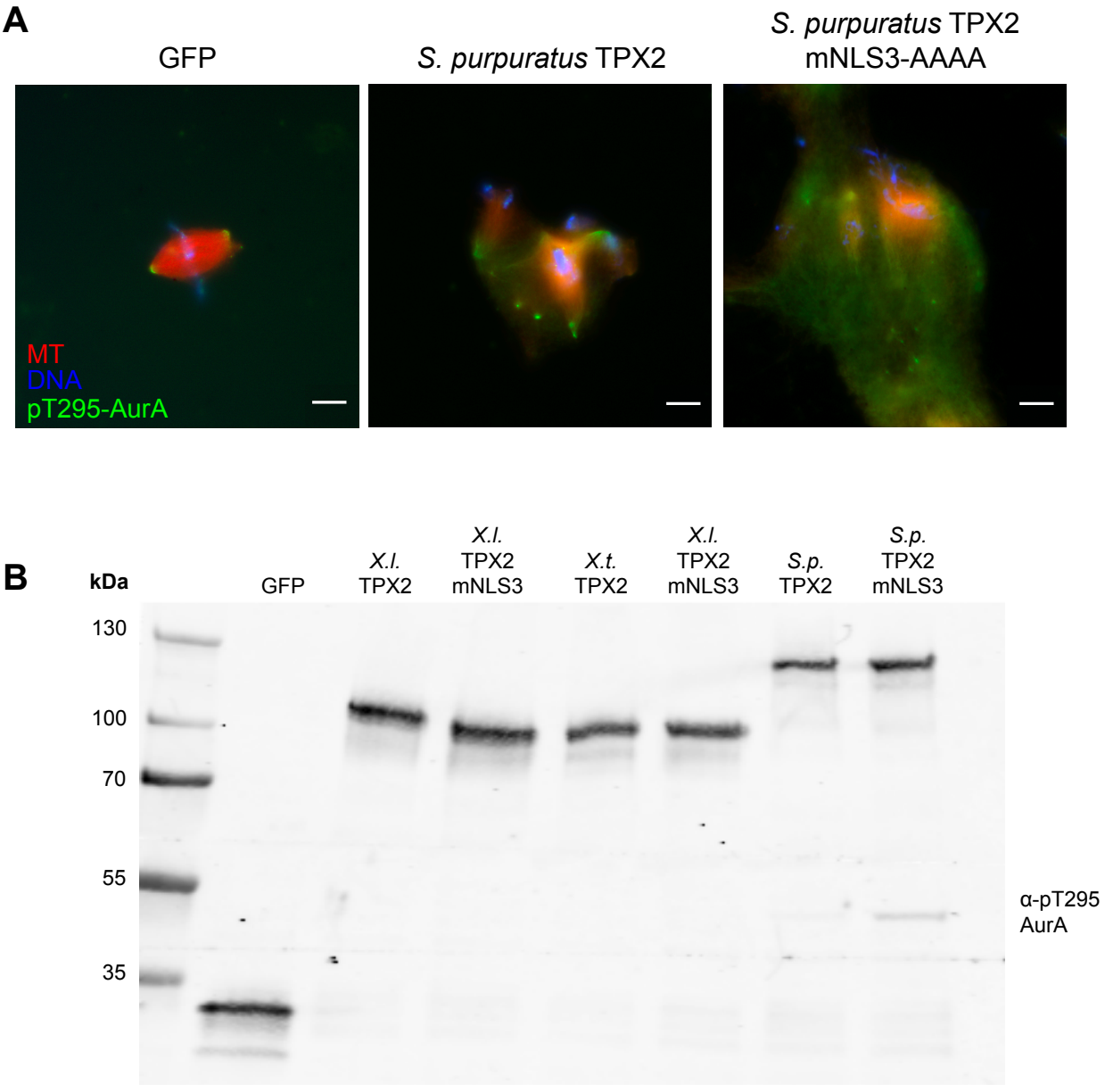

Figure 2.9: *S. purpuratus* NLS3 mutant TPX2 protein activates Aurora A in *Xenopus* egg extract
(A) Immunostaining of spindle assembly reactions in *X. laevis* egg extracts with 100 nM recombinant GFP and 75 nM GFP-tagged *S. purpuratus* TPX2 proteins. Scale bars = 10 μm. (B) Immunoprecipitation of GFP and GFP-TPX2 from CSF aster reactions

supplemented with 200 nM recombinant protein followed by immunoblot analysis using indicated antibodies.

S. purpuratus only has one Aurora kinase compared to other organisms that contain Aurora A and Aurora B (Consortium *et al.*, 2006; Fernandez-Guerra *et al.*, 2006). Several other invertebrate organisms such as the starfish *Asterina pectinifera* and the sea squirt *Ciona intestinalis* also contain one Aurora gene, which is predicted to be an ancestral gene which gave rise to the vertebrate Aurora A and B (Dehal *et al.*, 2002; Abe *et al.*, 2010). Sequence alignment of *X. laevis* Aurora A with *S. purpuratus* Aurora show 64% identity and have many conserved serine/threonine sites including T295 (Figure 2.11). Yet, how *S. purpuratus* TPX2 can activate and bind *X. laevis* Aurora A is not very clear.

Conclusion

Overall, our findings suggest that lysines comprising NLS3 play a crucial role in maintaining the proper regulation of TPX2. Phosphorylation predictors indicate that in humans, the first lysine, K158, is acetylated (PV *et al.*, 2015). Future experiments in Xenopus egg extract could help elucidate whether Xenopus TPX2 harbors any post-translational modifications (PTMs) in NLS3.

The lack of conservation in the primary sequence of TPX2 leads to many disordered and unstructured domains across several TPX2 homologs. These unstructured domains, such as the N-terminal half of Xenopus laevis TPX2, have been shown to be crucial in driving TPX2's ability to co-condense with tubulin and nucleate microtubules (King and Petry, 2020). However, it remains unclear how variations in the length of this N-terminal domain might affect the phase separation properties of TPX2 proteins and their ability to mediate microtubule nucleation. Could a longer disordered region enhance MT nucleation activity? Further experiments with TPX2 homologs harboring a longer disordered N-terminus could provide additional evidence explaining why certain organisms have distinct spindle architectures.

Figure 2.10

CLUSTAL O(1.2.4) multiple sequence alignment

```
C.intestinalis      -------MAAWEYDAPNFVDFDASCDSVDDAEAYFNRRHSHEYGGIPINYEDESESIPVE        53
S.purpuratus        MEPEKAFDENYEYNCPRFVDFSVPHVIDDNADEYFDIAHEGKDGQYDFMAEADG-QIP--        57
D.rerio             ------------------------------------------------------------        0
H.sapien            ------------------------------------------------------------        0
X.laevis            ------------------------------------------------------------        0
X.tropicalis        ------------------------------------------------------------        0

C.intestinalis      PEMTQILSNPDPVDNPTEEKDICDQNKELEE---NIPSTNHEAAEEVNIVNKADSTSLIK        110
S.purpuratus        ----EEFENPGPPSD------CRSQESRGEERISEVPPPCQKETESVEHLQETTTNSIQD        107
D.rerio             ------------------------------------------------------------        0
H.sapien            ------------------------------------------------------------        0
X.laevis            ------------------------------------------------------------        0
X.tropicalis        ------------------------------------------------------------        0

C.intestinalis      PDQSQSIQVLENQE----IAVEHTGEKDHHDENNQVKSEINTTSECDNGEVD-PVDKVDS        165
S.purpuratus        TEGEHEYQTKNNETGHIDQNVEHITD----NENTVVEAA-APMREEDDDRIDQPVQDETP        162
D.rerio             ------------------------------------------------------------        0
H.sapien            ------------------------------------------------------------        0
X.laevis            ------------------------------------------------------------        0
X.tropicalis        ------------------------------------------------------------        0

C.intestinalis      AADEQVTLKKDLKQNTVKESKKPDEDIKQKVAEEPIKSEDLNQN--AVEESIIHEEDLKQ        223
S.purpuratus        -GPEVKEMMEHV-QEPVCEDSPMNTEVQNPMTEAPEESTDQEMPVLELNTAPSVE--EEE        218
D.rerio             -------MDGGS-TYSYAWDAPTH---------------------VLESIDDFALDPQD        30
H.sapien            --------MSQV-KSSYSYDAPSD---------------------FINFSSLDDEGDTQ        29
X.laevis            --------MEDT-QDTYSYDAPSI---------------------FNFSSFHED---H        25
X.tropicalis        --------MAEA-QDLYTFDAPST---------------------FINFTAFHED---H        26
                                     .                           .:          .

C.intestinalis      KLQMQHESGEVAISEVTIKQECIKLS---IPAVQDIKLQ--SDNINTKEESVTP---SEV        275
S.purpuratus        ESEMMFTQEKPSVEEEETHVEEKQMEVVNETSVTRDSPESPQME--THDAEIPP------        270
D.rerio             NADKWFGLQ--------AASESGVMEQLTTPLRT--KPFDEPVDTNKPKAMVSPLVRQEP        80
H.sapien            NIDSWFEEK--------ANLENKLLGKNGTGGLF--QGKTPLRKANLQQAIVTPLKPVDN        79
X.laevis            NADSWFDQV--------TNAENIPPDQRRLSET--------SVN-TEQNSKVEP---VQT        65
X.tropicalis        GADSWFDKV--------TNAENIPPDQRRLSEI-------PAVN-AEQNGMVEP---EET        67
                      :  .             *                     .    .  : *

C.intestinalis      DTSEK---KAYSNIM-TPSRLASWNTAKPKVVPKAKL--VKSAPKKSATPNAPK---PQL        326
S.purpuratus        ----AVIPSNIAPVVKPKNLVTSWGNSNTDKTTSAKETRSRRSTRRSTRSLNSD--VSQL        324
D.rerio             TSSES------TSTDIPSNIVTSWGNSRTTGAPGQGPKSVPAQPRRVSKRPLPK------        128
H.sapien            TYYKEAEKENLVEQSIPSNACSSLEVE------AAISRKTPAQPQRRSLRLSAQKDLEQK        133
X.laevis            TPSKD----DVSNS--ATHVCD----------------VKSQSKRSSRRMSK----KHR        98
X.tropicalis        SPSKE----TVSES--AAHFSD----------------GKSQARRSSRRMSR----KHR        100
                                                          :: :
                                          NLS3
C.intestinalis      RRSI--------RNTDNIYKTPEPPIKKKK------------------------------        348
S.purpuratus        KRASAGSNTQRRSLRVYNKSSQSPALKKRRVSDRAQSGGK---------KNT--PVTTAK        373
D.rerio             -------------NEKPTVVTTPPSVKKRRVLLAASSRRVFDQRRRSSTSRTMRRSGAGV        175
H.sapien            EKHHVKM--KAKRCATPVIIDEILPSKKMK---VSNNKKK--PEEEG--SAHQDTAEKNA        184
X.laevis            QKLLVKM--KDTHLEKETAPPEYPPCKKLK---GSSSKGRHAPVIKS--QS---TSSHHS        148
X.tropicalis        QKLLVKM--RETRLEKETAQSDCPPTKKLK---GSSTKGARTPVIRG--QP---RSGHGS        150
                                          ** :
```

```
C.intestinalis      ----------LNNEPKK---NN-H--KRILTSEERQLEEVKCAKEKAQQIKHDSEMSLK      391
S.purpuratus        LVSKSFIPKLTLPSTPTFMKRNNTKPGAQFKTAEQIEMEKIAGFRKQLAARKKQSQASYK      433
D.rerio             RSSVRLKAKPAI---SKTTDIASNT--THHKSTEQQELERIEALQKEVAEQRRKNEASYR      230
H.sapien            SSPEKAKGRHTVPCMPPAK-----Q--KFLKSTEEQELEKSMKMQQEVVEMRKKNEEFKK      237
X.laevis            MTSPKPKAQLTMPSTPTVLKRRNVL--VKAKNSEEQELEKMQELQKEMLENLKKNEHSMK      206
X.tropicalis        NTSPRPKAPLTLPSTPTVLKRKNVM--VKPKSSEEQELERMQELQKEMLENLKKNEHSMK      208
                              :                  .:*: ::*.    :::     :..:   :

C.intestinalis      KIRSRRMPSWNMKTKPSLTVPKEFQFKTTDRATKAHPMSTRSDSAASSSNDFMKDLRKHN      451
S.purpuratus        MVQG-SSAYHAVKAVVPTTKPVGFTFETDQR-IKEHPMATR-----QDAKTFESDLRGK-      485
D.rerio             AALA-GS-QLVKKQVLSTTIPKEFNFRTDSR-LKNYKDGVSAVDNSYKETTFTSQLRKHP      287
H.sapien            LALA-GIGQPVKKSVSQVTKSVDFHFRTDER-IKQHP----KNQEEYKEVNFTSELRKHP      291
X.laevis            VAIT-GAGQPVK-TFIPVTKPVDFHFKTDDR-LKRTANQ--PEGDGYKAVDFASELRKHP      261
X.tropicalis        AAIS-GTGPSVKKSAVPITKPVDFHFKTDDR-PKRVADQ--PKGEEYKEVDFAAALRKHP      264
                                    *    * *.* .*  *             .   *   ** :
                                          NLS1
C.intestinalis      PSPHKLK---PTVVKPFHFSDDNKKAKRKLERDADHGSAFVPMAAVIRDFHKSTPKRFRA      508
S.purpuratus        ISPAKVPHG-PTVPKPFKLTDNRKRKLG-EGGEGSKNSPYCSMATRIQQFHNKTPQRFHT      543
D.rerio             SSPLKAPKG-TTIPKPFNLSRGKRKH---D-----ETGVYVPMAQQVEQFQKRTPTRYHL      338
H.sapien            SSPARVTKG-CTIVKPFNLSQGKKRTFD-E-----TVSTYVPLAQQVEDFHKRTPNRYHL      344
X.laevis            PSPVQVTKGGHTVPKPFNLSKGKRKH---E-----EASDYVSTAEQVIAFYKRTPARYHL      313
X.tropicalis        PSPVS--KAALTVPKPFNLSKGKRKH---E-----EASEFVSTAEQVISFSKKTPARYHL      314
                     **       *: ***::: ..::            . :   *  :  * : ** *::

C.intestinalis      RNENVPLAK---NGPMKALKVTIPKTPHF-SKIRSRPIATMSAKEKEELEVQEMKNYQFK      564
S.purpuratus        RRSGDHRDNSMHKEEVPKPRLTHPKTPNLECRNRKRVITVQSTAEREEQELQEMQSYKFK      603
D.rerio             RSRQSQER-GPSPLKADKSKITHPKTPQLLTQQRHRPTTVKSTAELEAEEVEKLQQFKFK      397
H.sapien            RSKKDDIN-LLPSKSSVTKICRDPQTPVLQTKHRARAVTCKSTAELEAEELEKLQQYKFK      403
X.laevis            RSRQREME-GPSPVKMIKTKLTNPKTPLLQTKGRHRPVTCKSAAELEAEELEMINQYKFK      372
X.tropicalis        RSRQRELE-GPSPVKMVRPKLTNPKTPLLQTKQRLRPVMCKSAAELEAEELERIQQYKFK      373
                    *                    *:** :  : * *     *: * *  *:: ::.::**

C.intestinalis      AKEVSN-----TEVTLKKVEKKPSTVPVEFNLHTENRTSKQED--------HEIKQKPFK      611
S.purpuratus        AKPVNPKVMSNLNIGLKMPTHKEPTKAIGFNLESERLMKERATKKAQEEEQKEEEHYEFH      663
D.rerio             ALELNRKILEGA-LVPKKPACKEKTKPEGFHLEIEKRLQERQTSKK----PEEKEDHTFH      452
H.sapien            ARELDPRILEGGPILPKKPPVKPPTEPIGFDLEIEKRIQERESKKK-----TEDEHFEFH      458
X.laevis            AQELDTRILEGGPVLLKKPLVKEPTKAIGFDLEIEKRIQQREKKEE-----IEEETFTFH      427
X.tropicalis        AQELDSRILEGAQVLPRKPPVKEPTKAIGFDLEIEKRIQQREKRDE-----GEEEAFTFH      428
                    *  :.        :  :    *  *    *.*. *.  .::           * :   *:

C.intestinalis      ARPVPVAILEKPTGIKEKQVAEVTIPQSPAFALKHRIKPPPVVPD---KNSTKPTYYHPP      668
S.purpuratus        ARPVSTKMLEGPVGIGAAKPRSLTCPKSPAFALKNRVRVKEDVIVEPEEPKSRIIHAKPI      723
D.rerio             SRPLPTRILEEVVGVPEKKMINPTVPESPAFALKSRVRIEKKKEE--E-KPPAPIKALAV      509
H.sapien            SRPCPTKILEDVVGVPEKKVLPITVPKSPAFALKNRIRMPTKEDE--EEDEPVVIKAQPV      516
X.laevis            SRPCPSKMLTDVVGVPLKKLLPVTVPQSPAFALKNRVRIPAQEEK--QEEMVPVIKATRM      485
X.tropicalis        SRPCPSKLLTEVVGVPLKKLLPVTVPHSPSFALKNRVRLPAREEK--E-EEVPAIKATAM      485
                    :**    :*   .*:   :    * *.**:**** *::

C.intestinalis      PIFGVPFMPKVVS-TKLEVKPFSFDKSDKERFAKKQEKIKQQKEKEAEVAVFTANPVPST      727
S.purpuratus        LHVGVPFKPQTTH-KTTEIQPFSFEQRDKETQARKEAKIQEIYQE--EEKARLFKAKPIL      780
D.rerio             PHY-LPFQPKPPVKSQVEMCPFSFEERDRERKMMKEKKLEELRNE--EVPKFKAQPLPDF      566
H.sapien            PHYGVPFKPQIPEARTVEICPFSFDSRDKERQLQKEKKIKELQKG--EVPKFKALPLPHF      574
X.laevis            PHYGVPFKPKLVEQRQVDVCPFSFCDRDKERQLQKEKRLDELRKD--EVPKFKAQPLPQF      543
X.tropicalis        PHYGVPFRPKLVQQRQVEVCPFSFSDQDRERLLRKEKRMEELRKE--EVHKFKAQPLPEF      543
                        :** *:       :: **** . *:*    *: ::.:  :   *         *
```

```
C.intestinalis      ITHAEPVLANKKSKEPTKAKPFNLETDHRAANRAEKWSKNVEDEVQQLRDK-TLFKANTD       786
S.purpuratus        E---PVSMPEKKVKPVTKLEPFQLGNEEKGAKRAEMWSKKIEEELNEQRAMANAFKAK-P       836
D.rerio             H---EVHLPEKKVQEATKPAPFKLMIDERGAARSERWEQMMKEELKHQAEA-ACFKAR-P       621
H.sapien            D---TINLPEKKVKNVTQIEPFCLETDRRGALKAQTWKHQLEEELRQQKEA-ACFKAR-P       629
X.laevis            D---NIRLPEKKVKMPTQQEPFDLEIEKRGASKLQRWQQQIQEELKQQKEM-VVFKAR-P       598
X.tropicalis        G---HVSLPEKRVKMPTQQEPFVLEIDKRGAPRLQRWQQQVKEEQKQQKEM-AVFKAR-P       598
                           : :*: :  *:  ** *  :.:.* : : *.: :::* ..       ***.

C.intestinalis      IDVVLKKPWKPKKLSRDPVDTI-----AMDPHLHSDERAKERRLFDEKLAFEKQQMAKLL       841
S.purpuratus        ADVVYNQPFVPQKPNKPLT-------EIDAFDLNTDRRAVEREGFEQWKMKKDLDERESR       889
D.rerio             NTVSYKEPFVPKKENRSILANTTNSAVPEGFQLATERRAKERLEFEKELSEREALRARME       681
H.sapien            NTVISQEPFVPKKEKKSVAEGLSGSLVQEPFQLATEKRAKERQELEKRMAEVEAQKAQQL       689
X.laevis            NTVVHQEPFVPKKENRSLTESLSGSIVQEGFELATAKRAKERQEFDKCLAETEAQKSLLE       658
X.tropicalis        NTVVHQEPFLPKKESRCLT-------ATEGFELATEKRAKERQEFEKSLAEMEAQKSLLE       651
                      *  ::*: *:* .:              .* : .** **  :::     .

C.intestinalis      EEQKKKQELQDKEEIARLRK-SMEHKASEIKHYKTVTVALSEKKLTEPHSPHFSTRFKK 899
S.purpuratus        CQLEKLKEEEERKEIERMRREDMHHKAQPVKHYKPVHVMPSLKPLTDACSPNFSDRFQK 948
D.rerio             EERARE REQQEKEEIARLRQ-EQVCKAQPIRHYKPVELKKSDVSLTVPQSPNFSDRFRM 739
H.sapien            EEARLQEEEQKKEELARLRR-ELVHKANPIRKYQGLEIKSSDQPLTVPVSPKFSTRFHC 747
X.laevis            EEIRKRREEEEKEEISQLRQ-ELVHKAKPIRKYRAVEVKASDVPLTVPRSPNFSDRFKC 716
X.tropicalis        EETRQRQEEEEREEISHLRK-ELVHKAQPIRKYKAVDVKASDTPLTIPESPNFSDRFKC 709
                     :    .* :.::*: ::*: .   **. :::*: : :  *   **   **:** **:
```

Figure 2.10: Multiple sequence alignment of TPX2 homologs
Protein sequence alignment of TPX2 homologs using Clustal Omega Multiple Sequence Alignment (MSA) tool (Madeira *et al.*, 2022)

Figure 2.11

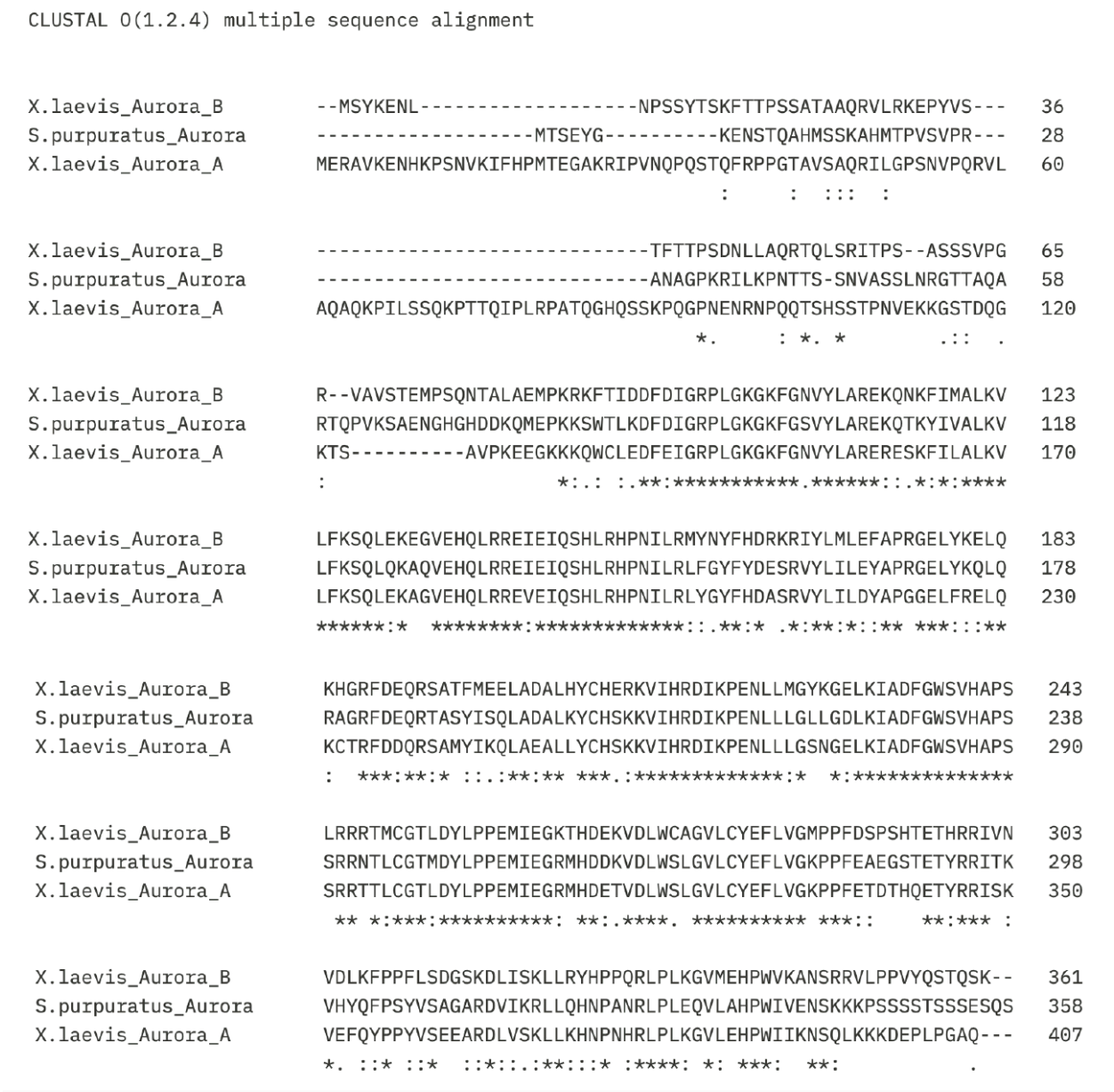

```
CLUSTAL O(1.2.4) multiple sequence alignment


X.laevis_Aurora_B       --MSYKENL-------------------NPSSYTSKFTTPSSATAAQRVLRKEPYVS---   36
S.purpuratus_Aurora     -------------------MTSEYG----------KENSTQAHMSSKAHMTPVSVPR---   28
X.laevis_Aurora_A       MERAVKENHKPSNVKIFHPMTEGAKRIPVNQPQSTQFRPPGTAVSAQRILGPSNVPQRVL   60
                                                      :     :  :::  :


X.laevis_Aurora_B       ----------------------------TFTTPSDNLLAQRTQLSRITPS--ASSSVPG   65
S.purpuratus_Aurora     ----------------------------ANAGPKRILKPNTTS-SNVASSLNRGTTAQA   58
X.laevis_Aurora_A       AQAQKPILSSQKPTTQIPLRPATQGHQSSKPQGPNENRNPQQTSHSSTPNVEKKGSTDQG   120
                                                   *.     : *. *        .::  .


X.laevis_Aurora_B       R--VAVSTEMPSQNTALAEMPKRKFTIDDFDIGRPLGKGKFGNVYLAREKQNKFIMALKV   123
S.purpuratus_Aurora     RTQPVKSAENGHGHDDKQMEPKKSWTLKDFDIGRPLGKGKFGSVYLAREKQTKYIVALKV   118
X.laevis_Aurora_A       KTS----------AVPKEEGKKKQWCLEDFEIGRPLGKGKFGNVYLARERESKFILALKV   170
                        :                   *:.: :.**:***********.******::.*:*:****


X.laevis_Aurora_B       LFKSQLEKEGVEHQLRREIEIQSHLRHPNILRMYNYFHDRKRIYLMLEFAPRGELYKELQ   183
S.purpuratus_Aurora     LFKSQLQKAQVEHQLRREIEIQSHLRHPNILRLFGYFYDESRVYLILEYAPRGELYKQLQ   178
X.laevis_Aurora_A       LFKSQLEKAGVEHQLRREVEIQSHLRHPNILRLYGYFHDASRVYLILDYAPGGELFRELQ   230
                        ******:*  ********:**************::.**:* .*:**:*::** ***:::**


 X.laevis_Aurora_B      KHGRFDEQRSATFMEELADALHYCHERKVIHRDIKPENLLMGYKGELKIADFGWSVHAPS   243
 S.purpuratus_Aurora    RAGRFDEQRTASYISQLADALKYCHSKKVIHRDIKPENLLLGLLGDLKIADFGWSVHAPS   238
 X.laevis_Aurora_A      KCTRFDDQRSAMYIKQLAEALLYCHSKKVIHRDIKPENLLLGSNGELKIADFGWSVHAPS   290
                        :  ***:**:* ::.:**:** ***.:**************:*  *:***************


 X.laevis_Aurora_B      LRRRTMCGTLDYLPPEMIEGKTHDEKVDLWCAGVLCYEFLVGMPPFDSPSHTETHRRIVN   303
 S.purpuratus_Aurora    SRRNTLCGTMDYLPPEMIEGRMHDDKVDLWSLGVLCYEFLVGKPPFEAEGSTETYRRITK   298
 X.laevis_Aurora_A      SRRTTLCGTLDYLPPEMIEGRMHDETVDLWSLGVLCYEFLVGKPPFETDTHQETYRRISK   350
                         ** *:***:**********: **:.****. ********** ***::    **:*** :


 X.laevis_Aurora_B      VDLKFPPFLSDGSKDLISKLLRYHPPQRLPLKGVMEHPWVKANSRRVLPPVYQSTQSK--   361
 S.purpuratus_Aurora    VHYQFPSYVSAGARDVIKRLLQHNPANRLPLEQVLAHPWIVENSKKKPSSSSTSSSESQS   358
 X.laevis_Aurora_A      VEFQYPPYVSEEARDLVSKLLKHNPNHRLPLKGVLEHPWIIKNSQLKKKDEPLPGAQ---   407
                        *. ::* ::*  ::*::.:**:::* :****: *: ***:  **:           .
```

Figure 2.11: Multiple sequence alignment of Aurora proteins in *X. laevis* and *S. purpuratus*

Protein sequence alignment of *X. laevis* Aurora A and B protein with *S. purpuratus* Aurora using Clustal Omega Multiple Sequence Alignment (MSA) tool (Madeira *et al.*, 2022)

Chapter 3: Changes in spindle morphology driven by TPX2 over expression in MYC-driven breast cancer cells

Introduction

The MYC oncogene was previously shown to induce mitotic spindle defects, chromosome instability, and reliance on the microtubule-associated protein TPX2 to survive, but how TPX2 levels affect spindle morphology in cancer cells has not previously been examined in detail. We show that breast cancer cell lines expressing high levels of MYC and TPX2 possess shorter spindles with increased TPX2 localization at spindle poles. A similar effect was observed in non-transformed human RPE-1 cells compared to a tumor cell line (HeLa) which overexpresses MYC. These results demonstrate that TPX2 alters spindle length and morphology in cancer cells, which may contribute their ability to divide despite MYC-induced mitotic stress.

Results and Discussion

MYC is an oncogene that is overexpressed in many aggressive human cancers (Felsher and Bishop, 1999; Soucek and Evan, 2010). It was shown previously that overexpression of MYC leads to error-prone mitosis and spindle assembly defects accompanied by up-regulation several spindle-associated genes including the microtubule-associated protein TPX2 (Rohrberg *et al.*, 2020). Targeting Protein for Xklp2 (TPX2) is a RanGTP-regulated importin cargo that is overexpressed in many aggressive human cancers and is associated with chromosomal instability (Carter *et al.*, 2006; Castro *et al.*, 2007; Asteriti *et al.*, 2010; Hu *et al.*, 2012; Neumayer *et al.*, 2014). Interestingly, TPX2 depletion was shown to be synthetically lethal with MYC overexpression (Rohrberg *et al.*, 2020).

In a variety of systems, TPX2 has been shown to be essential for spindle bipolarity, microtubule nucleation, stabilization and organization at spindle poles (Schatz *et al.*, 2003; Brunet *et al.*, 2004; Tulu *et al.*, 2006). TPX2 is indispensable for microtubule branching nucleation (Brunet *et al.*, 2004; Petry *et al.*, 2013) and also binds and activates the mitotic kinase Aurora A (Bayliss *et al.*, 2003; Eyers *et al.*, 2003; Tsai *et al.*, 2003). Using *Xenopus* egg extracts, we showed previously that addition of recombinant TPX2 results in significantly shorter spindles and a change in microtubule organization

(Helmke and Heald, 2014). However, it is poorly understood how overexpression of TPX2 affects spindle architecture in human cancer cells.

To examine the effect of TPX2 overexpression on spindle morphology, we analyzed three breast cancer cell lines with either high or low MYC and TPX2 levels (Figure 3.1A). Tubulin and TPX2 immunofluorescence of BT549 cells expressing high levels of MYC/TPX2 revealed significantly shorter spindles than the low MYC/TPX2 expressing lines T47D and MCF7. The high MYC/TPX2 cell line showed greater recruitment of TPX2 along the length of the spindle, with a greater accumulation at the spindle poles compared to the low MYC/TPX2 cell lines (Figure 3.1B&C). We next compared a non-tumorigenic human retinal pigment epithelium (RPE-1) cell line versus Hela cells that overexpresses MYC. Immunofluorescence and spindle length analysis again showed that cells expressing higher levels of TPX2 displayed significantly shorter spindles than the control (Figure 3.1D&E). Similar to the high TPX2 expressing breast cancer cells, line scan analysis of TPX2/tubulin intensity ratio showed that MYC high Hela cells recruited higher levels of TPX2 along the length of the spindle (Figure 3.1F). Line scan analysis of breast cancer cell lines showed a more dramatic difference in TPX2/tubulin intensity between cells expressing low and high TPX2 compared to the RPE-1 cells, which likely reflects more significant heterogeneity of spindle microtubule distribution in the cancer cells (Figure 3.1A).

In summary, this analysis revealed that cell lines with high levels of TPX2 and MYC overexpression possess morphologically distinct spindles compared to cells expressing low MYC/TPX2. Future experiments could elucidate how TPX2 mediates this effect by recruiting other spindle factors such as Aurora A or by altering microtubule branching nucleation and organization. TPX2 upregulation and dependency across various aggressive cancers make it an attractive target for cancer therapies. Understating how TPX2 contributes to spindle architecture would provide insightful understanding of how this linchpin spindle assembly protein protects genomically unstable cancer cells.

Figure 3.1

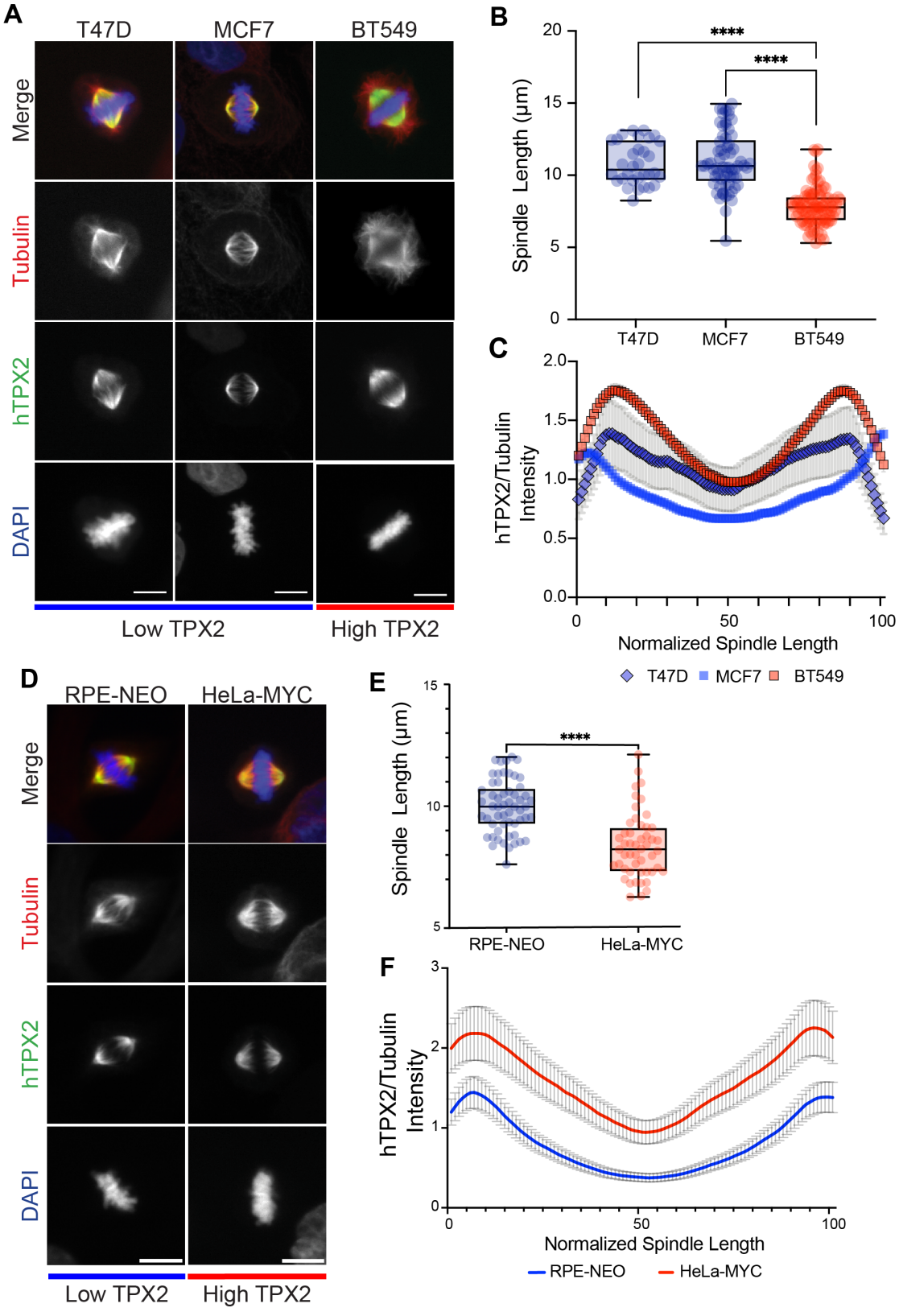
A
T47D
MCF7
BT549
Merge
Tubulin
hTPX2
DAPI
Low TPX2
High TPX2
B
Spindle Length (µm)
****
****
T47D
MCF7
BT549
C
hTPX2/Tubulin Intensity
Normalized Spindle Length
T47D
MCF7
BT549
D
RPE-NEO
HeLa-MYC
Merge
Tubulin
hTPX2
DAPI
Low TPX2
High TPX2
E
Spindle Length (µm)
****
RPE-NEO
HeLa-MYC
F
hTPX2/Tubulin Intensity
Normalized Spindle Length
RPE-NEO
HeLa-MYC

Figure 3.1: Higher TPX2 expression in MYC-driven breast cancer cell lines decreases spindle length and increases TPX2 intensity, especially at spindle poles
(A) Immunostaining of fixed metaphase spindles of low and high TPX2 expressing breast cancer cell lines. Scale bar = 10 μm. (B) Quantification of spindle length, T47D n = 32, MCF7 n = 65, BT549 n = 95. Boxplot shows median marked at center and data maxima and minima indicated by whiskers. Box shows 25th to 75th percentiles. **** = P < 0.0001 from two-tailed unpaired t tests. (C) Line scan analysis of hTPX2/Tubulin fluorescence intensity, Mean ± SEM, T47D n = 25, LY2 n = 45, BT549 n = 115 (D) Immunostaining of fixed metaphase RPE-NEO and HeLa-MYC cells. (E) Quantification of spindle lengths, RPE-NEO n = 56, HeLa-MYC n = 50. Boxplot shows median marked at center and data maxima and minima indicated by whiskers. Box shows 25th to 75th percentiles, **** = P < 0.0001 from two-tailed unpaired t test. (F) Line scan analysis of hTPX2/Tubulin fluorescence intensity, Mean ± SEM, RPE-NEO n = 53, HeLa-MYC n = 52.

Methods

Cell culture

BT549 and T47D breast cancer cell lines were grown in RPMI supplemented with 10% FBS, 10 U/ml penicillin and 10 mg/ml streptomycin at 37°C. MCF7 breast cancer cells, RPE-1 and Hela were grown in DMEM supplemented with 10% FBS and 10 U/ml penicillin, 10 mg/ml streptomycin at 37°C.

Immunofluorescence

Cells were seeded overnight on 12 mm coverslips, fixed for 2 minutes in with -20°C methanol in freezer, washed three times with 1x PBS and permeabilized with 0.5% Triton X-100 in 1x PBS for 5 minutes at room temperature. Cells were incubated with blocking buffer (1% goat serum, 0.1% Triton X-100, and 9.8 mg/ml of bovine serum albumin in 1x PBS) for 1 hour at room temperature. Primary antibodies were diluted with 3% BSA in 1x PBS and added to cells for 1 hour at room temperature. Cells were washed three times quickly followed by three 5 minutes washes of 1x PBS. Secondary antibodies were diluted with 3% BSA in 1x PBS and added to cells for 30 minutes at room temperature. Cells were washed three times quickly followed by three 5 minutes washes of 1x PBS. Final PBS wash contained 0.05 μg/ml of DAPI. Cells were washed two times quickly with 1x PBS before being mounted with ProLong Diamond reagent (Invitrogen). Listed antibodies were used as indicated: Rabbit anti-TPX2 (1:1000, HPA005487, Sigma), mouse anti-beta tubulin (E7; Developmental Studies Hybridoma Bank, Iowa City, IA), rabbit secondary antibody conjugated to Alexa Fluor 488 (1:500, A21206, Invitrogen), and mouse secondary antibody conjugated to Alexa Fluor 568 (1:500, A21124, Invitrogen).

Microscopy

Metaphase cells were imaged using micromanager software (Edelstein *et al.*, 2014) with an Olympus BX51 microscope using an ORCA-ER camera (Hamamatsu Photonics) and with an Olympus UPlan FL 40× air objective.

Quantification and Statistical Analysis

Spindle length quantification: Individual spindle lengths measurements were taken using Fiji. Pole-to-pole measurements are represented by boxplots in figures. For all boxplots, the thick line inside the box indicates the average length, and the upper and lower box boundaries indicate 25th to 75th percentiles. For each figure, the minimum number of spindles measured (n) are listed in the figure legend. Statistical significance was determined by unpaired two sample t test using GraphPad Prism version 10.0.0 for MacOS, GraphPad Software, Boston, Massachusetts USA, www.graphpad.com. p values are listed in the figure legend.

Fluorescence intensity line scans quantification: Line scans were generated using an automated Java ImageJ plugin developed by X. Zhou (https://github.com/XiaoMutt/AiSpindle, (Gibeaux *et al.*, 2018). Line scans quantify the average ratio of hTPX2 to tubulin fluorescence intensity across the spindle length from pole to pole. Spindle length is normalized across the range from 1-100. The number of spindles measured in each condition (n) is listed in the figure legend. Error bars indicate ± standard error over the mean (SEM).

Chapter 4: Conclusions

Xenopus egg extracts provide a powerful research model and an ideal system to investigate mechanisms regulating spindle architecture. The biochemical tractability of this system and its ability to recapitulate cell cycle events including spindle assembly, allows for in-depth characterization of protein function in this process. Through the research presented in this thesis, we have investigated the regulation of the spindle assembly factor TPX2. TPX2 plays a central role during spindle assembly by mediating MT nucleation and organization through various protein interactions, making it a significant contributor to spindle architecture.

In Chapter 2 we investigated the regulation of TPX2 activity by perturbing a conserved NLS motif which had not been characterized in the context of spindle assembly. Mutation of TPX2 NLS3 motif in in both *X. laevis* and *X. tropicalis* produced distinct spindle pole morphologies when recombinant proteins were added to *Xenopus laevis* egg extract, increasing the recruitment of TPX2 binding proteins including Aurora A, Eg5 and importin-α.The *X. tropicalis* NLS3 mutant had the most dramatic effect on spindle pole morphology and recruitment of other interacting proteins. Previously we identified a 7 a.a. deletion in *X. tropicalis* TPX2, which when deleted *in X. laevis* TPX2, increased the formation of ectopic MT asters and MT aster formation at the spindle poles (Helmke and Heald, 2014). This work shows that the NLS3 mutation and the 7 a.a deletion in *X. tropicalis* TPX2 have an additive effect on TPX2 function. The lack of secondary structure and overall disorder in TPX2 sequence makes it difficult to understand how these two sites, located on opposite ends of the protein, produce this additive function. Elucidating how the distinct functional domains of TPX2 influence each will further our understanding of its regulation and protein interactions.

Additionally, in Chapter 2, unpublished findings describe TPX2 homologs that contain a significantly longer N-terminal intrinsically disordered region (IDR). Organisms with these longer N-terminal IDRs, such as *S. purpuratus* and *C. intestinalis* also happen to undergo some of the most dramatic spindle architectural rearrangements of MT when transitioning from a meiotic spindle to a mitotic spindle upon fertilization (Crowder *et al.*, 2015). These changes in spindle architecture during this transition are likely crucial for proper spindle function, but how they are brought about is unknown. Could this longer IDR in TPX2 be affecting MT nucleation*? In vitro* experiments show that *Xenopus* TPX2 can undergo LLPS and co-condense with tubulin due to its N-terminal IDR (King and Petry, 2020). Could increasing the length of the IDR lower the effective concentration of TPX2 to drive co-condensation with tubulin? Future experiments with purified tubulin and MT branching assays could address whether increasing the length of the N-terminal IDR region also enhances TPX2-driven MT nucleation. TPX2s diverse domains and functionality could be the adaptive mechanism organisms have evolved to promote diverse spindle architecture.

In Chapter 3, cancer cells overexpressing TPX2 displayed morphologically different spindles, which were shorter than those of cells expressing lower levels of TPX2. Further experiments could investigate microtubule (MT) organization differences in

cancer cells with varying TPX2 expression levels. Techniques such as expansion microscopy could help demonstrate whether higher TPX2 expression leads to differences in MT organization within the spindle. Additionally, it would be intriguing to examine how spindle morphology varies among different cancers overexpressing TPX2.

Many cancers with TPX2 overexpression also overexpress the mitotic kinase Aurora A. Overexpression of this TPX2/Aurora A complex has been speculated as a novel oncogenic holoenzyme (Asteriti *et al.*, 2010; Joukov and Nicolo, 2018; Orth *et al.*, 2018). Recently, an inhibitor, CAM2602, was developed to target the protein interaction between Aurora A and TPX2 (Stockwell *et al.*, 2024). Understanding the molecular mechanisms by which TPX2 functions and interacts with other proteins can provide deeper insights into its role in cancer progression and metastasis, potentially leading to more effective targeted therapies.

With the characterization of TPX2 proteins from various species in this study and future advancements in high-resolution microscopy, we can help enhance our understanding of how this enigmatic protein shapes and organizes the spindle.

References

Abe, Y, Okumura, E, Hosoya, T, Hirota, T, and Kishimoto, T (2010). A single starfish Aurora kinase performs the combined functions of Aurora-A and Aurora-B in human cells. J Cell Sci 123, 3978–3988.

Alberti, S, Gladfelter, A, and Mittag, T (2019). Considerations and Challenges in Studying Liquid-Liquid Phase Separation and Biomolecular Condensates. Cell 176, 419–434.

Alfaro-Aco, R, Thawani, A, and Petry, S (2017). Structural analysis of the role of TPX2 in branching microtubule nucleation. J Cell Biol 216, 983–997.

Alfaro-Aco, R, Thawani, A, and Petry, S (2020). Biochemical reconstitution of branching microtubule nucleation. ELife 9, e49797.

Asteriti, IA, Cesare, ED, Mattia, FD, Hilsenstein, V, Neumann, B, Cundari, E, Lavia, P, and Guarguaglini, G (2014). The Aurora-A inhibitor MLN8237 affects multiple mitotic processes and induces dose-dependent mitotic abnormalities and aneuploidy. Oncotarget 5, 6229–6242.

Asteriti, IA, Rensen, WM, Lindon, C, Lavia, P, and Guarguaglini, G (2010). The Aurora-A/TPX2 complex: A novel oncogenic holoenzyme? Biochim Biophys Acta (BBA) - Rev Cancer 1806, 230–239.

Banani, SF, Lee, HO, Hyman, AA, and Rosen, MK (2017). Biomolecular condensates: organizers of cellular biochemistry. Nat Rev Mol Cell Biol 18, 285–298.

Barr, AR, and Gergely, F (2007). Aurora-A: the maker and breaker of spindle poles. J Cell Sci 120, 2987–2996.

Basto, R, Lau, J, Vinogradova, T, Gardiol, A, Woods, CG, Khodjakov, A, and Raff, JW (2006). Flies without Centrioles. Cell 125, 1375–1386.

Bayliss, R, Sardon, T, Vernos, I, and Conti, E (2003). Structural Basis of Aurora-A Activation by TPX2 at the Mitotic Spindle. Mol Cell 12, 851–862.

Berdnik, D, and Knoblich, JA (2002). Drosophila Aurora-A Is Required for Centrosome Maturation and Actin-Dependent Asymmetric Protein Localization during Mitosis. Curr Biol 12, 640–647.

Biggins, S, and Walczak, CE (2003). Captivating Capture: How Microtubules Attach to Kinetochores. Curr Biol 13, R449–R460.

Bird, AW, and Hyman, AA (2008). Building a spindle of the correct length in human cells requires the interaction between TPX2 and Aurora A. J Cell Biol 182, 289–300.

Bischoff, FR, and Ponstingl, H (1991). Catalysis of guanine nucleotide exchange on Ran by the mitotic regulator RCC1. Nature 354, 80–82.

Brouhard, GJ, and Rice, LM (2018). Microtubule dynamics: an interplay of biochemistry and mechanics. Nat Rev Mol Cell Biol 19, 451–463.

Brown, KS, Blower, MD, Maresca, TJ, Grammer, TC, Harland, RM, and Heald, R (2007). Xenopus tropicalis egg extracts provide insight into scaling of the mitotic spindle. J Cell Biol 176, 765–770.

Brunet, S, Sardon, T, Zimmerman, T, Wittmann, T, Pepperkok, R, Karsenti, E, and Vernos, I (2004). Characterization of the TPX2 Domains Involved in Microtubule Nucleation and Spindle Assembly in Xenopus Egg Extracts. Mol Biol Cell 15, 5318–5328.

Budde, PP, Kumagai, A, Dunphy, WG, and Heald, R (2001). Regulation of Op18 during Spindle Assembly in Xenopus Egg Extracts. J Cell Biol 153, 149–158.

Carazo-Salas, RE, Guarguaglini, G, Gruss, OJ, Segref, A, Karsenti, E, and Mattaj, IW (1999). Generation of GTP-bound Ran by RCC1 is required for chromatin-induced mitotic spindle formation. Nature 400, 178–181.

Carlier, M-F (1982). Guanosine-5′-triphosphate hydrolysis and tubulin polymerization. Mol Cell Biochem 47, 97–113.

Carmena, M, Wheelock, M, Funabiki, H, and Earnshaw, WC (2012). The chromosomal passenger complex (CPC): from easy rider to the godfather of mitosis. Nat Rev Mol Cell Biol 13, 789–803.

Carter, SL, Eklund, AC, Kohane, IS, Harris, LN, and Szallasi, Z (2006). A signature of chromosomal instability inferred from gene expression profiles predicts clinical outcome in multiple human cancers. Nat Genet 38, 1043–1048.

Castro, IP de, Cárcer, G de, and Malumbres, M (2007). A census of mitotic cancer genes: new insights into tumor cell biology and cancer therapy. Carcinogenesis 28, 899–912.

Cavazza, T, and Vernos, I (2016). The RanGTP Pathway: From Nucleo-Cytoplasmic Transport to Spindle Assembly and Beyond. Front Cell Dev Biol 3, 82.

Chrétien, D, Metoz, F, Verde, F, Karsenti, E, and Wade, R (1992). Lattice defects in microtubules: protofilament numbers vary within individual microtubules. J Cell Biol 117, 1031–1040.

Cleveland, DW, Mao, Y, and Sullivan, KF (2003). Centromeres and Kinetochores From Epigenetics to Mitotic Checkpoint Signaling. Cell 112, 407–421.

Cole, DG, Saxton, WM, Sheehan, KB, and Scholey, JM (1994). A “slow” homotetrameric kinesin-related motor protein purified from Drosophila embryos. J Biol Chem 269, 22913–22916.

Conduit, PT, Feng, Z, Richens, JH, Baumbach, J, Wainman, A, Bakshi, SD, Dobbelaere, J, Johnson, S, Lea, SM, and Raff, JW (2014). The Centrosome-Specific Phosphorylation of Cnn by Polo/Plk1 Drives Cnn Scaffold Assembly and Centrosome Maturation. Dev Cell 28, 659–669.

Consortium, SUGS, Sodergren, E, Weinstock, GM, Davidson, EH, Cameron, RA, Gibbs, RA, Angerer, RC, Angerer, LM, Arnone, MI, Burgess, DR, *et al.* (2006). The Genome of the Sea Urchin Strongylocentrotus purpuratus. Science 314, 941–952.

Crowder, ME, Strzelecka, M, Wilbur, JD, Good, MC, von Dassow, G, and Heald, R (2015). A Comparative Analysis of Spindle Morphometrics across Metazoans. Curr Biol 25, 1542–1550.

Dehal, P, Satou, Y, Campbell, RK, Chapman, J, Degnan, B, Tomaso, AD, Davidson, B, Gregorio, AD, Gelpke, M, Goodstein, DM, *et al.* (2002). The Draft Genome of Ciona intestinalis: Insights into Chordate and Vertebrate Origins. Science 298, 2157–2167.

Desai, A, and Mitchison*, TJ (1997). MICROTUBULE POLYMERIZATION DYNAMICS. Annu Rev Cell Dev Biol 13, 83–117.

Desai, A, Murray, A, Mitchison, TJ, and Walczak, CE (1998). Chapter 20 The Use of Xenopus Egg Extracts to Study Mitotic Spindle Assembly and Function in Vitro. Methods Cell Biol 61, 385–412.

Dignon, GL, Best, RB, and Mittal, J (2020). Biomolecular Phase Separation: From Molecular Driving Forces to Macroscopic Properties. Annu Rev Phys Chem 71, 53–75.

Downing, KH, and Nogales, E (1998). Tubulin and microtubule structure. Curr Opin Cell Biol 10, 16–22.

Doxsey, SJ, Stein, P, Evans, L, Calarco, PD, and Kirschner, M (1994). Pericentrin, a highly conserved centrosome protein involved in microtubule organization. Cell 76, 639–650.

Dumont, S, and Mitchison, TJ (2009). Force and Length in the Mitotic Spindle. Curr Biol 19, R749–R761.

Eckerdt, F, Eyers, PA, Lewellyn, AL, Prigent, C, and Maller, JL (2008). Spindle Pole Regulation by a Discrete Eg5-Interacting Domain in TPX2. Curr Biol 18, 519–525.

Edelstein, AD, Tsuchida, MA, Amodaj, N, Pinkard, H, Vale, RD, and Stuurman, N (2014). Advanced methods of microscope control using μManager software. J Biol Methods 1, e10.

Ems-McClung, SC, Zheng, Y, and Walczak, CE (2004). Importin α/β and Ran-GTP Regulate XCTK2 Microtubule Binding through a Bipartite Nuclear Localization Signal. Mol Biol Cell 15, 46–57.

Endow, SA, Chandra, R, Komma, DJ, Yamamoto, AH, and Salmon, ED (1994). Mutants of the Drosophila ncd microtubule motor protein cause centrosomal and spindle pole defects in mitosis. J Cell Sci 107, 859–867.

Endow, SA, and Komma, DJ (1997). Spindle Dynamics during Meiosis in Drosophila Oocytes. J Cell Biol 137, 1321–1336.

Erickson, HP, and O'Brien, ET (1992). Microtubule Dynamic Instability and GTP Hydrolysis. Annu Rev Biophys Biomol Struct 21, 145–166.

Eyers, PA, Erikson, E, Chen, LG, and Maller, JL (2003). A Novel Mechanism for Activation of the Protein Kinase Aurora A. Curr Biol 13, 691–697.

Eyers, PA, and Maller, JL (2004). Regulation of Xenopus Aurora A Activation by TPX2*. J Biol Chem 279, 9008–9015.

Felsher, DW, and Bishop, JM (1999). Transient excess of MYC activity can elicit genomic instability and tumorigenesis. Proc Natl Acad Sci 96, 3940–3944.

Fernandez-Guerra, A, Aze, A, Morales, J, Mulner-Lorillon, O, Cosson, B, Cormier, P, Bradham, C, Adams, N, Robertson, AJ, Marzluff, WF, *et al.* (2006). The genomic repertoire for cell cycle control and DNA metabolism in S. purpuratus. Dev Biol 300, 238–251.

Fong, K-W, Choi, Y-K, Rattner, JB, and Qi, RZ (2008). CDK5RAP2 Is a Pericentriolar Protein That Functions in Centrosomal Attachment of the γ-Tubulin Ring Complex. Mol Biol Cell 19, 115–125.

Forth, S, and Kapoor, TM (2017). The mechanics of microtubule networks in cell division. J Cell Biol 216, 1525–1531.

Fried, H, and Kutay, U (2003). Nucleocytoplasmic transport: taking an inventory. Cell Mol Life Sci CMLS 60, 1659–1688.

Gable, A, Qiu, M, Titus, J, Balchand, S, Ferenz, NP, Ma, N, Collins, ES, Fagerstrom, C, Ross, JL, Yang, G, *et al.* (2012). Dynamic reorganization of Eg5 in the

mammalian spindle throughout mitosis requires dynein and TPX2. Mol Biol Cell 23, 1254–1266.

Garrett, S, Auer, K, Compton, DA, and Kapoor, TM (2002). hTPX2 Is Required for Normal Spindle Morphology and Centrosome Integrity during Vertebrate Cell Division. Curr Biol 12, 2055–2059.

Gibeaux, R, Acker, R, Kitaoka, M, Georgiou, G, Kruijsbergen, I van, Ford, B, Marcotte, EM, Nomura, DK, Kwon, T, Veenstra, GJC, *et al.* (2018). Paternal chromosome loss and metabolic crisis contribute to hybrid inviability in Xenopus. Nature 553, 337–341.

Giesecke, A, and Stewart, M (2010). Novel Binding of the Mitotic Regulator TPX2 (Target Protein for Xenopus Kinesin-like Protein 2) to Importin-α*. J Biol Chem 285, 17628–17635.

Goshima, G (2011). Identification of a TPX2-Like Microtubule-Associated Protein in Drosophila. PLoS ONE 6, e28120.

Goshima, G, Mayer, M, Zhang, N, Stuurman, N, and Vale, RD (2008). Augmin: a protein complex required for centrosome-independent microtubule generation within the spindle. J Cell Biol 181, 421–429.

Goshima, G, Wollman, R, Goodwin, SS, Zhang, N, Scholey, JM, Vale, RD, and Stuurman, N (2007). Genes Required for Mitotic Spindle Assembly in Drosophila S2 Cells. Science 316, 417–421.

Gould, RR, and Borisy, GG (1978). Quantitative initiation of microtubule assembly by chromosomes from Chinese hamster ovary cells. Exp Cell Res 113, 369–374.

Greenan, G, Brangwynne, CP, Jaensch, S, Gharakhani, J, Jülicher, F, and Hyman, AA (2010). Centrosome Size Sets Mitotic Spindle Length in Caenorhabditis elegans Embryos. Curr Biol 20, 353–358.

Gruss, OJ, Carazo-Salas, RE, Schatz, CA, Guarguaglini, G, Kast, J, Wilm, M, Bot, NL, Vernos, I, Karsenti, E, and Mattaj, IW (2001). Ran Induces Spindle Assembly by Reversing the Inhibitory Effect of Importin α on TPX2 Activity. Cell 104, 83–93.

Gruss, OJ, and Vernos, I (2004). The mechanism of spindle assembly. J Cell Biol 166, 949–955.

Gruss, OJ, Wittmann, M, Yokoyama, H, Pepperkok, R, Kufer, T, Silljé, H, Karsenti, E, Mattaj, IW, and Vernos, I (2002). Chromosome-induced microtubule assembly mediated by TPX2 is required for spindle formation in HeLa cells. Nat Cell Biol 4, 871–879.

Halpin, D, Kalab, P, Wang, J, Weis, K, and Heald, R (2011). Mitotic Spindle Assembly around RCC1-Coated Beads in Xenopus Egg Extracts. PLoS Biol 9, e1001225.

Hannak, E, and Heald, R (2006). Investigating mitotic spindle assembly and function in vitro using Xenopus laevis egg extracts. Nat Protoc 1, 2305–2314.

Hannak, E, Kirkham, M, Hyman, AA, and Oegema, K (2001). Aurora-A kinase is required for centrosome maturation in Caenorhabditis elegans. J Cell Biol 155, 1109–1116.

Hatsumi, M, and Endow, SA (1992). Mutants of the microtubule motor protein, nonclaret disjunctional, affect spindle structure and chromosome movement in meiosis and mitosis. J Cell Sci 101, 547–559.

Hayden, JH, Bowser, SS, and Rieder, CL (1990). Kinetochores capture astral microtubules during chromosome attachment to the mitotic spindle: direct visualization in live newt lung cells. J Cell Biol 111, 1039–1045.

Heald, R, Tournebize, R, Blank, T, Sandaltzopoulos, R, Becker, P, Hyman, A, and Karsenti, E (1996). Self-organization of microtubules into bipolar spindles around artificial chromosomes in Xenopus egg extracts. Nature 382, 420–425.

Heald, R, Tournebize, R, Habermann, A, Karsenti, E, and Hyman, A (1997). Spindle Assembly in Xenopus Egg Extracts: Respective Roles of Centrosomes and Microtubule Self-Organization. J Cell Biol 138, 615–628.

Heidebrecht, HJ, Buck, F, Steinmann, J, Sprenger, R, Wacker, HH, and Parwaresch, R (1997). p100: A Novel Proliferation-Associated Nuclear Protein Specifically Restricted to Cell Cycle Phases S, G2 , and M. Blood 90, 226–233.

Helmke, KJ, and Heald, R (2014). TPX2 levels modulate meiotic spindle size and architecture in Xenopus egg extracts. J Cell Biol 206, 385–393.

Helmke, KJ, Heald, R, and Wilbur, JD (2013). Chapter Three Interplay Between Spindle Architecture and Function. Int Rev Cell Mol Biol 306, 83–125.

Hodel, MR, Corbett, AH, and Hodel, AE (2001). Dissection of a Nuclear Localization Signal*. J Biol Chem 276, 1317–1325.

Holehouse, AS, and Pappu, RV (2018). Functional Implications of Intracellular Phase Transitions. Biochemistry 57, 2415–2423.

Holy, TE, and Leibler, S (1994). Dynamic instability of microtubules as an efficient way to search in space. Proc Natl Acad Sci 91, 5682–5685.

Howard, J, and Hyman, AA (2009). Growth, fluctuation and switching at microtubule plus ends. Nat Rev Mol Cell Biol 10, 569–574.

Hu, G, Katuwawala, A, Wang, K, Wu, Z, Ghadermarzi, S, Gao, J, and Kurgan, L (2021). flDPnn: Accurate intrinsic disorder prediction with putative propensities of disorder functions. Nat Commun 12, 4438.

Hu, Y, Wu, G, Rusch, M, Lukes, L, Buetow, KH, Zhang, J, and Hunter, KW (2012). Integrated cross-species transcriptional network analysis of metastatic susceptibility. Proc Natl Acad Sci 109, 3184–3189.

Huang, Y, Li, T, Ems-McClung, SC, Walczak, CE, Prigent, C, Zhu, X, Zhang, X, and Zheng, Y (2018). Aurora A activation in mitosis promoted by BuGZ. J Cell Biol 217, 107–116.

Hyman, AA, Weber, CA, and Jülicher, F (2014). Liquid-Liquid Phase Separation in Biology. Annu Rev Cell Dev Biol 30, 39–58.

Jiang, H, Wang, S, Huang, Y, He, X, Cui, H, Zhu, X, and Zheng, Y (2015). Phase Transition of Spindle-Associated Protein Regulate Spindle Apparatus Assembly. Cell 163, 108–122.

Jiang, X, Ho, DBT, Mahe, K, Mia, J, Sepulveda, G, Antkowiak, M, Jiang, L, Yamada, S, and Jao, L-E (2021). Condensation of pericentrin proteins in human cells illuminates phase separation in centrosome assembly. J Cell Sci 134, jcs258897.

Jiang, Y, Liu, Y, Tan, X, Yu, S, and Luo, J (2019). TPX2 as a Novel Prognostic Indicator and Promising Therapeutic Target in Triple-negative Breast Cancer. Clin Breast Cancer 19, 450–455.

Joukov, V, and Nicolo, AD (2018). Aurora-PLK1 cascades as key signaling modules in the regulation of mitosis. Sci Signal 11.

Joukov, V, Walter, JC, and De Nicolo, A (2014). The Cep192-Organized Aurora A-Plk1 Cascade Is Essential for Centrosome Cycle and Bipolar Spindle Assembly. Mol Cell 55, 578–591.

Kalab, P, and Heald, R (2008). The RanGTP gradient – a GPS for the mitotic spindle. J Cell Sci 121, 1577–1586.

Kalab, P, Pu, RT, and Dasso, M (1999). The Ran GTPase regulates mitotic spindle assembly. Curr Biol 9, 481–484.

Kalab, P, Weis, K, and Heald, R (2002). Visualization of a Ran-GTP Gradient in Interphase and Mitotic Xenopus Egg Extracts. Science 295, 2452–2456.

Kapitein, LC, Peterman, EJG, Kwok, BH, Kim, JH, Kapoor, TM, and Schmidt, CF (2005). The bipolar mitotic kinesin Eg5 moves on both microtubules that it crosslinks. Nature 435, 114–118.

Kapoor, TM, Mayer, TU, Coughlin, ML, and Mitchison, TJ (2000). Probing Spindle Assembly Mechanisms with Monastrol, a Small Molecule Inhibitor of the Mitotic Kinesin, Eg5. J Cell Biol 150, 975–988.

Karsenti, E, and Vernos, I (2001). The Mitotic Spindle: A Self-Made Machine. Science 294, 543–547.

Kashlna, AS, Baskin, RJ, Cole, DG, Wedaman, KP, Saxton, WM, and Scholey, JM (1996). A bipolar kinesin. Nature 379, 270–272.

Khodjakov, A, Cole, RW, Oakley, BR, and Rieder, CL (2000). Centrosome-independent mitotic spindle formation in vertebrates. Curr Biol 10, 59–67.

King, MR, and Petry, S (2020). Phase separation of TPX2 enhances and spatially coordinates microtubule nucleation. Nat Commun 11, 270.

Kinoshita, K, Noetzel, TL, Pelletier, L, Mechtler, K, Drechsel, DN, Schwager, A, Lee, M, Raff, JW, and Hyman, AA (2005). Aurora A phosphorylation of TACC3/maskin is required for centrosome-dependent microtubule assembly in mitosis. J Cell Biol 170, 1047–1055.

Kitamura, E, Tanaka, K, Komoto, S, Kitamura, Y, Antony, C, and Tanaka, TU (2010). Kinetochores Generate Microtubules with Distal Plus Ends: Their Roles and Limited Lifetime in Mitosis. Dev Cell 18, 248–259.

Koike, Y, Yin, C, Sato, Y, Nagano, Y, Yamamoto, A, Kitajima, T, Shimura, T, Kawamura, M, Matsushita, K, Okugawa, Y, *et al.* (2022). TPX2 is a prognostic marker and promotes cell proliferation in neuroblastoma. Oncol Lett 23, 136.

Kollman, JM, Merdes, A, Mourey, L, and Agard, DA (2011). Microtubule nucleation by γ-tubulin complexes. Nat Rev Mol Cell Biol 12, 709–721.

Kollman, JM, Polka, JK, Zelter, A, Davis, TN, and Agard, DA (2010). Microtubule nucleating γ-TuSC assembles structures with 13-fold microtubule-like symmetry. Nature 466, 879–882.

Kollu, S, Bakhoum, SF, and Compton, DA (2009). Interplay of Microtubule Dynamics and Sliding during Bipolar Spindle Formation in Mammalian Cells. Curr Biol 19, 2108–2113.

Kraus, J, Alfaro-Aco, R, Gouveia, B, and Petry, S (2023a). Microtubule nucleation for spindle assembly: one molecule at a time. Trends Biochem Sci 48, 761–775.

Kraus, J, Travis, SM, King, MR, and Petry, S (2023b). Augmin is a Ran-regulated spindle assembly factor. J Biol Chem 299, 104736.

Kufer, TA, Silljé, HHW, Körner, R, Gruss, OJ, Meraldi, P, and Nigg, EA (2002). Human TPX2 is required for targeting Aurora-A kinase to the spindle. J Cell Biol 158, 617–623.

Lajoie-Mazenc, I, Tollon, Y, Detraves, C, Julian, M, Moisand, A, Gueth-Hallonet, C, Debec, A, Salles-Passador, I, Puget, A, Mazarguil, H, *et al.* (1994). Recruitment of antigenic gamma-tubulin during mitosis in animal cells: presence of gamma-tubulin in the mitotic spindle. J Cell Sci 107, 2825–2837.

Lawo, S, Bashkurov, M, Mullin, M, Ferreria, MG, Kittler, R, Habermann, B, Tagliaferro, A, Poser, I, Hutchins, JRA, Hegemann, B, *et al.* (2009). HAUS, the 8-Subunit Human Augmin Complex, Regulates Centrosome and Spindle Integrity. Curr Biol 19, 816–826.

Lee, K, and Rhee, K (2011). PLK1 phosphorylation of pericentrin initiates centrosome maturation at the onset of mitosis. J Cell Biol 195, 1093–1101.

Li, B, Qi, X-Q, Chen, X, Huang, X, Liu, G-Y, Chen, H-R, Huang, C-G, Luo, C, and Lu, Y-C (2010). Expression of targeting protein for Xenopus kinesin-like protein 2 is associated with progression of human malignant astrocytoma. Brain Res 1352, 200–207.

Lindqvist, A, Rodríguez-Bravo, V, and Medema, RH (2009). The decision to enter mitosis: feedback and redundancy in the mitotic entry network. J Cell Biol 185, 193–202.

Loughlin, R, Wilbur, JD, McNally, FJ, Nédélec, FJ, and Heald, R (2011). Katanin Contributes to Interspecies Spindle Length Scaling in Xenopus. Cell 147, 1397–1407.

Lüders, J, Patel, UK, and Stearns, T (2006). GCP-WD is a γ-tubulin targeting factor required for centrosomal and chromatin-mediated microtubule nucleation. Nat Cell Biol 8, 137–147.

Ma, N, Titus, J, Gable, A, Ross, JL, and Wadsworth, P (2011). TPX2 regulates the localization and activity of Eg5 in the mammalian mitotic spindle. J Cell Biol 195, 87–98.

Ma, N, Tulu, US, Ferenz, NP, Fagerstrom, C, Wilde, A, and Wadsworth, P (2010). Poleward Transport of TPX2 in the Mammalian Mitotic Spindle Requires Dynein, Eg5, and Microtubule Flux. Mol Biol Cell 21, 979–988.

Ma, Y, Lin, D, Sun, W, Xiao, T, Yuan, J, Han, N, Guo, S, Feng, X, Su, K, Mao, Y, *et al.* (2006). Expression of targeting protein for xklp2 associated with both malignant transformation of respiratory epithelium and progression of squamous cell lung cancer. Clin Cancer Res 12, 1121–1127.

Madeira, F, Pearce, M, Tivey, ARN, Basutkar, P, Lee, J, Edbali, O, Madhusoodanan, N, Kolesnikov, A, and Lopez, R (2022). Search and sequence analysis tools services from EMBL-EBI in 2022. Nucleic Acids Res 50, W276–W279.

Magnaghi-Jaulin, L, Eot-Houllier, G, Gallaud, E, and Giet, R (2019). Aurora A Protein Kinase: To the Centrosome and Beyond. Biomolecules 9, 28.

Mahoney, NM, Goshima, G, Douglass, AD, and Vale, RD (2006). Making Microtubules and Mitotic Spindles in Cells without Functional Centrosomes. Curr Biol 16, 564–569.

Manda, R, Kohno, T, Matsuno, Y, Takenoshita, S, Kuwano, H, and Yokota, J (1999). Identification of Genes (SPON2 and C20orf2) Differentially Expressed between

Cancerous and Noncancerous Lung Cells by mRNA Differential Display. Genomics 61, 5–14.
Maresca, TJ, Groen, AC, Gatlin, JC, Ohi, R, Mitchison, TJ, and Salmon, ED (2009). Spindle Assembly in the Absence of a RanGTP Gradient Requires Localized CPC Activity. Curr Biol 19, 1210–1215.
Maresca, TJ, and Heald, R (2006). Xenopus Protocols, Cell Biology and Signal Transduction. Methods Mol Biol 322, 459–474.
Matsuura, Y (2023). Crystallographic data of an importin-α3 dimer in which the two protomers are bridged by a bipartite nuclear localization signal. Data Brief 47, 108988.
Matthies, HJ, McDonald, HB, Goldstein, LS, and Theurkauf, WE (1996). Anastral meiotic spindle morphogenesis: role of the non-claret disjunctional kinesin-like protein. J Cell Biol 134, 455–464.
McGill, M, and Brinkley, BR (1975). Human chromosomes and centrioles as nucleating sites for the in vitro assembly of microtubules from bovine brain tubulin. J Cell Biol 67, 189–199.
Merdes, A, Heald, R, Samejima, K, Earnshaw, WC, and Cleveland, DW (2000). Formation of Spindle Poles by Dynein/Dynactin-Dependent Transport of Numa. J Cell Biol 149, 851–862.
Mitchison, T, and Kirschner, M (1984a). Dynamic instability of microtubule growth. Nature 312, 237–242.
Mitchison, T, and Kirschner, M (1984b). Microtubule assembly nucleated by isolated centrosomes. Nature 312, 232–237.
Miyamoto, Y, and Oka, M (2016). Data on dimer formation between importin α subtypes. Data Brief 7, 1248–1253.
Moritz, M, Braunfeld, MB, Sedat, JW, Alberts, B, and Agard, DA (1995). Microtubule nucleation by γ-tubulin-containing rings in the centrosome. Nature 378, 638–640.
Nadkarni, AV, and Heald, R (2021). Reconstitution of muscle cell microtubule organization in vitro. Cytoskeleton 78, 492–502.
Neumayer, G, Belzil, C, Gruss, OJ, and Nguyen, MD (2014). TPX2: of spindle assembly, DNA damage response, and cancer. Cell Mol Life Sci 71, 3027–3047.
Nigg, EA (2001). Mitotic kinases as regulators of cell division and its checkpoints. Nat Rev Mol Cell Biol 2, 21–32.
Ohba, T, Nakamura, M, Nishitani, H, and Nishimoto, T (1999). Self-organization of microtubule asters induced in Xenopus egg extracts by GTP-bound Ran. Science 284, 1356–1358.
Ohi, R, Sapra, T, Howard, J, and Mitchison, TJ (2004). Differentiation of Cytoplasmic and Meiotic Spindle Assembly MCAK Functions by Aurora B-dependent Phosphorylation. Mol Biol Cell 15, 2895–2906.
Orth, M, Unger, K, Schoetz, U, Belka, C, and Lauber, K (2018). Taxane-mediated radiosensitization derives from chromosomal missegregation on tripolar mitotic spindles orchestrated by AURKA and TPX2. Oncogene 37, 52–62.
Özlü, N, Srayko, M, Kinoshita, K, Habermann, B, O'Toole, ET, Müller-Reichert, T, Schmalz, N, Desai, A, and Hyman, AA (2005). An Essential Function of the C. elegans Ortholog of TPX2 Is to Localize Activated Aurora A Kinase to Mitotic Spindles. Dev Cell 9, 237–248.

Palazzo, RE, Vogel, JM, Schnackenberg, BJ, Hull, DR, and Wu, X (1999). Centrosome maturation. Curr Top Dev Biol 49, 449–470.

Petry, S, Groen, AC, Ishihara, K, Mitchison, TJ, and Vale, RD (2013). Branching Microtubule Nucleation in Xenopus Egg Extracts Mediated by Augmin and TPX2. Cell 152, 768–777.

Pinyol, R, Scrofani, J, and Vernos, I (2013). The Role of NEDD1 Phosphorylation by Aurora A in Chromosomal Microtubule Nucleation and Spindle Function. Curr Biol 23, 143–149.

PV, H, B, Z, B, M, JM, K, V, L, and E, S (2015). PhosphoSitePlus, 2014: mutations, PTMs and recalibrations. Nucleic Acids Res. 2015 43:D512-20. Available at: https://www.phosphosite.org/staticCiteUs.action. Accessed March 6, 2024.

Reid, TA, Schuster, BM, Mann, BJ, Balchand, SK, Plooster, M, McClellan, M, Coombes, CE, Wadsworth, P, and Gardner, MK (2016). Suppression of microtubule assembly kinetics by the mitotic protein TPX2. J Cell Sci 129, 1319–1328.

Renda, F, and Khodjakov, A (2023). Cell biology: Kinetochores nucleate their own microtubules. Curr Biol 33, R187–R190.

Rieder, CL (2005). Kinetochore fiber formation in animal somatic cells: dueling mechanisms come to a draw. Chromosoma 114, 310–318.

Rohrberg, J, Mark, DV de, Amouzgar, M, Lee, JV, Taileb, M, Corella, A, Kilinc, S, Williams, J, Jokisch, M-L, Camarda, R, *et al.* (2020). MYC Dysregulates Mitosis, Revealing Cancer Vulnerabilities. Cell Rep 30, 3368-3382.e7.

Roostalu, J, Cade, NI, and Surrey, T (2015). Complementary activities of TPX2 and chTOG constitute an efficient importin-regulated microtubule nucleation module. Nat Cell Biol 17, 1422–1434.

Ruchaud, S, Carmena, M, and Earnshaw, WC (2007). Chromosomal passengers: conducting cell division. Nat Rev Mol Cell Biol 8, 798–812.

Safari, MS, King, MR, Brangwynne, CP, and Petry, S (2021). Interaction of spindle assembly factor TPX2 with importins-α/β inhibits protein phase separation. J Biol Chem 297, 100998.

Sampath, SC, Ohi, R, Leismann, O, Salic, A, Pozniakovski, A, and Funabiki, H (2004). The Chromosomal Passenger Complex Is Required for Chromatin-Induced Microtubule Stabilization and Spindle Assembly. Cell 118, 187–202.

Sardon, T, Peset, I, Petrova, B, and Vernos, I (2008). Dissecting the role of Aurora A during spindle assembly. EMBO J 27, 2567–2579.

Schatz, CA, Santarella, R, Hoenger, A, Karsenti, E, Mattaj, IW, Gruss, OJ, and Carazo-Salas, RE (2003). Importin α-regulated nucleation of microtubules by TPX2. EMBO J 22, 2060–2070.

Schuh, M, and Ellenberg, J (2007). Self-Organization of MTOCs Replaces Centrosome Function during Acentrosomal Spindle Assembly in Live Mouse Oocytes. Cell 130, 484–498.

Scrofani, J, Sardon, T, Meunier, S, and Vernos, I (2015). Microtubule Nucleation in Mitosis by a RanGTP-Dependent Protein Complex. Curr Biol 25, 131–140.

Shigeishi, H, Ohta, K, Hiraoka, M, Fujimoto, S, Minami, M, Higashikawa, K, and Kamata, N (2009). Expression of TPX2 in salivary gland carcinomas. Oncol Rep 21, 341–344.

Shin, Y, and Brangwynne, CP (2017). Liquid phase condensation in cell physiology and disease. Science 357.

Snyder, JA, and McIntosh, JR (1975). Initiation and growth of microtubules from mitotic centers in lysed mammalian cells. J Cell Biol 67, 744–760.

So, C, Seres, KB, Steyer, AM, Mönnich, E, Clift, D, Pejkovska, A, Möbius, W, and Schuh, M (2019). A liquid-like spindle domain promotes acentrosomal spindle assembly in mammalian oocytes. Science 364.

Song, J-G, King, MR, Zhang, R, Kadzik, RS, Thawani, A, and Petry, S (2018). Mechanism of how augmin directly targets the γ-tubulin ring complex to microtubules. J Cell Biol 217, 2417–2428.

Soucek, L, and Evan, GI (2010). The ups and downs of Myc biology. Curr Opin Genet Dev 20, 91–95.

Stockwell, SR, Scott, DE, Fischer, G, Guarino, E, Rooney, TPC, Feng, T-S, Moschetti, T, Srinivasan, R, Alza, E, Asteian, A, *et al.* (2024). Selective Aurora A-TPX2 interaction inhibitors have in vivo efficacy as targeted anti-mitotic agents. BioRxiv, 2023.03.22.533679.

Takahashi, M, Yamagiwa, A, Nishimura, T, Mukai, H, and Ono, Y (2002). Centrosomal Proteins CG-NAP and Kendrin Provide Microtubule Nucleation Sites by Anchoring γ-Tubulin Ring Complex. Mol Biol Cell 13, 3235–3245.

Telzer, BR, Moses, MJ, and Rosenbaum, JL (1975). Assembly of microtubules onto kinetochores of isolated mitotic chromosomes of HeLa cells. Proc Natl Acad Sci 72, 4023–4027.

Thawani, A, Kadzik, RS, and Petry, S (2018). XMAP215 is a microtubule nucleation factor that functions synergistically with the γ-tubulin ring complex. Nat Cell Biol 20, 575–585.

Tillery, MML, Blake-Hedges, C, Zheng, Y, Buchwalter, RA, and Megraw, TL (2018). Centrosomal and Non-Centrosomal Microtubule-Organizing Centers (MTOCs) in Drosophila melanogaster. Cells 7, 121.

Tirnauer, JS, Salmon, ED, and Mitchison, TJ (2004). Microtubule Plus-End Dynamics in Xenopus Egg Extract Spindles. Mol Biol Cell 15, 1776–1784.

Travis, SM, Mahon, BP, and Petry, S (2022). How Microtubules Build the Spindle Branch by Branch. Annu Rev Cell Dev Biol 38, 1–23.

Trivedi, P, Palomba, F, Niedzialkowska, E, Digman, MA, Gratton, E, and Stukenberg, PT (2019). The inner centromere is a biomolecular condensate scaffolded by the chromosomal passenger complex. Nat Cell Biol 21, 1127–1137.

Tsai, M-Y, Wiese, C, Cao, K, Martin, O, Donovan, P, Ruderman, J, Prigent, C, and Zheng, Y (2003). A Ran signalling pathway mediated by the mitotic kinase Aurora A in spindle assembly. Nat Cell Biol 5, 242–248.

Tulu, US, Fagerstrom, C, Ferenz, NP, and Wadsworth, P (2006). Molecular Requirements for Kinetochore-Associated Microtubule Formation in Mammalian Cells. Curr Biol 16, 536–541.

Tunquist, BJ, and Maller, JL (2003). Under arrest: cytostatic factor (CSF)-mediated metaphase arrest in vertebrate eggs. Genes Dev 17, 683–710.

Uteng, M, Hentrich, C, Miura, K, Bieling, P, and Surrey, T (2008). Poleward transport of Eg5 by dynein–dynactin in Xenopus laevis egg extract spindles. J Cell Biol 182, 715–726.

Vanneste, D, Takagi, M, Imamoto, N, and Vernos, I (2009). The Role of Hklp2 in the Stabilization and Maintenance of Spindle Bipolarity. Curr Biol 19, 1712–1717.
Walczak, CE, and Heald, R (2008). Chapter Three Mechanisms of Mitotic Spindle Assembly and Function. Int Rev Cytol 265, 111–158.
Walczak, CE, Vernos, I, Mitchison, TJ, Karsenti, E, and Heald, R (1998). A model for the proposed roles of different microtubule-based motor proteins in establishing spindle bipolarity. Curr Biol 8, 903–913.
Wang, ZA, and Cole, PA (2020). The Chemical Biology of Reversible Lysine Post-translational Modifications. Cell Chem Biol 27, 953–969.
Weaver, LN, Ems-McClung, SC, Chen, S-HR, Yang, G, Shaw, SL, and Walczak, CE (2015). The Ran-GTP Gradient Spatially Regulates XCTK2 in the Spindle. Curr Biol 25, 1509–1514.
Wieczorek, M, Bechstedt, S, Chaaban, S, and Brouhard, GJ (2015). Microtubule-associated proteins control the kinetics of microtubule nucleation. Nat Cell Biol 17, 907–916.
Wilde, A, and Zheng, Y (1999). Stimulation of Microtubule Aster Formation and Spindle Assembly by the Small GTPase Ran. Science 284, 1359–1362.
Wittmann, T, Boleti, H, Antony, C, Karsenti, E, and Vernos, I (1998). Localization of the Kinesin-like Protein Xklp2 to Spindle Poles Requires a Leucine Zipper, a Microtubule-associated Protein, and Dynein. J Cell Biol 143, 673–685.
Wittmann, T, Wilm, M, Karsenti, E, and Vernos, I (2000). Tpx2, a Novel Xenopus Map Involved in Spindle Pole Organization. J Cell Biol 149, 1405–1418.
Wollman, R, Cytrynbaum, EN, Jones, JT, Meyer, T, Scholey, JM, and Mogilner, A (2005). Efficient Chromosome Capture Requires a Bias in the ‘Search-and-Capture’ Process during Mitotic-Spindle Assembly. Curr Biol 15, 828–832.
Woodruff, JB, Gomes, BF, Widlund, PO, Mahamid, J, Honigmann, A, and Hyman, AA (2017). The Centrosome Is a Selective Condensate that Nucleates Microtubules by Concentrating Tubulin. Cell 169, 1066-1077.e10.
Woodruff, JB, Wueseke, O, and Hyman, AA (2014). Pericentriolar material structure and dynamics. Philos Trans R Soc B: Biol Sci 369, 20130459.
Wu, J, Larreategui-Aparicio, A, Lambers, MLA, Bodor, DL, Klaasen, SJ, Tollenaar, E, Ruijter-Villani, M de, and Kops, GJPL (2023). Microtubule nucleation from the fibrous corona by LIC1-pericentrin promotes chromosome congression. Curr Biol 33, 912-925.e6.
Zhang, C, Hughes, M, and Clarke, PR (1999). Ran-GTP stabilizes microtubule asters and inhibits nuclear assembly in Xenopus egg extracts. J Cell Sci 112, 2453–2461.
Zhang, R, Roostalu, J, Surrey, T, and Nogales, E (2017). Structural insight into TPX2-stimulated microtubule assembly. ELife 6, e30959.
Zheng, Y (2010). A membranous spindle matrix orchestrates cell division. Nat Rev Mol Cell Biol 11, 529–535.
Zheng, Y, Wong, ML, Alberts, B, and Mitchison, T (1995). Nucleation of microtubule assembly by a γ-tubulin-containing ring complex. Nature 378, 578–583.
Zhu, F, Lawo, S, Bird, A, Pinchev, D, Ralph, A, Richter, C, Müller-Reichert, T, Kittler, R, Hyman, AA, and Pelletier, L (2008). The Mammalian SPD-2 Ortholog Cep192 Regulates Centrosome Biogenesis. Curr Biol 18, 136–141.

Zimmerman, WC, Sillibourne, J, Rosa, J, and Doxsey, SJ (2004). Mitosis-specific Anchoring of γ Tubulin Complexes by Pericentrin Controls Spindle Organization and Mitotic Entry. Mol Biol Cell 15, 3642–3657.

Zorba, A, Buosi, V, Kutter, S, Kern, N, Pontiggia, F, Cho, Y-J, and Kern, D (2014). Molecular mechanism of Aurora A kinase autophosphorylation and its allosteric activation by TPX2. ELife 3, e02667.

Zou, J, Huang, R-Y, Jiang, F-N, Chen, D-X, Wang, C, Han, Z-D, Liang, Y-X, and Zhong, W-D (2018). Overexpression of TPX2 is associated with progression and prognosis of prostate cancer. Oncol Lett 16, 2823–2832.

Zwicker, D, Decker, M, Jaensch, S, Hyman, AA, and Jülicher, F (2014). Centrosomes are autocatalytic droplets of pericentriolar material organized by centrioles. Proc Natl Acad Sci 111, E2636–E2645.